SERDP

FINAL REPORT

In Situ Sequestration of PFAS from Contaminated Groundwater using Injectable High Affinity Cationic Hydrophobic Polymers

Jon Chorover
Leif Abrell
Jim Field
Reyes Sierra-Alvarez
Neeraja Setlur
Anton Gomeniuc
James Hatton
Robert Root
University of Arizona

James Hatton
Jacobs

August 2024

SERDP Project ER22-3155

REPORT DOCUMENTATION PAGE

Form Approved
OMB No. 0704-0188

1. REPORT DATE *(DD-MM-YYYY)*	**2. REPORT TYPE**	**3. DATES COVERED** *(From - To)*
23/08/2024	SERDP Final Report	9/30/2021 - 9/30/2024

4. TITLE AND SUBTITLE

In Situ Sequestration of PFAS from Contaminated Groundwater using Injectable High Affinity Cationic Hydrophobic Polymers

5a. CONTRACT NUMBER
21-P-0100

5b. GRANT NUMBER

5c. PROGRAM ELEMENT NUMBER

6. AUTHOR(S)

Jon Chorover, Leif Abrell, Jim Field, Reyes Sierra-Alvarez, Neeraja Setlur, Anton Gomeniuc, James Hatton, and Robert Root
University of Arizona

James Hatton
Jacobs

5d. PROJECT NUMBER
ER22-3155

5e. TASK NUMBER

5f. WORK UNIT NUMBER

7. PERFORMING ORGANIZATION NAME(S) AND ADDRESS(ES)
University of Arizona
1177 E. Fourth Street
Tucson, AZ 85721-0038

8. PERFORMING ORGANIZATION REPORT NUMBER
ER22-3155

9. SPONSORING/MONITORING AGENCY NAME(S) AND ADDRESS(ES)
Office of the Deputy Assistant Secretary of Defense (Energy Resilience & Optimization)
3500 Defense Pentagon, RM 5C646
Washington, DC 20301-3500

10. SPONSOR/MONITOR'S ACRONYM(S)
SERDP

11. SPONSOR/MONITOR'S REPORT NUMBER(S)
ER22-3155

12. DISTRIBUTION/AVAILABILITY STATEMENT

DISTRIBUTION STATEMENT A. Approved for public release: distribution unlimited.

13. SUPPLEMENTARY NOTES

14. ABSTRACT

The goal of this research was to develop a proof-of-concept for in situ remediation of PFAS-impacted sand and gravel aquifers. In this one-year study, bench-scale experiments were completed to evaluate high-PFAS-affinity cationic colloidal polymer behavior in saturated sands and their PFAS removal capacity under simulated aquifer conditions. Injectable high-affinity polymers (IHAPs) synthesized by our team using a cross-linking approach exhibited strong PFAS removal affinity. This proof-of-concept study completed the necessary bench-scale experiments for follow-on column and mesocosm experiments with additional SERDP support, ultimately working towards field deployment of the technology.

15. SUBJECT TERMS

PFAS, injectable colloidal sorbents, PANI

16. SECURITY CLASSIFICATION OF:			**17. LIMITATION OF ABSTRACT**	**18. NUMBER OF PAGES**	**19a. NAME OF RESPONSIBLE PERSON**
a. REPORT	**b. ABSTRACT**	**c. THIS PAGE**			Jon Chorover
UNCLASS	UNCLASS	UNCLASS	UNCLASS	90	**19b. TELEPHONE NUMBER** *(Include area code)* 520-626-5635

`

Table of Contents

`

`

List of Tables

List of Figures

`

`

Figure 2. Impacts on PFOA adsorption of competition from natural organic matter (NOM). Dissolved NOM represents a significant hindrance to PFAS adsorption on GAC and other sorbents used for PFAS remediation because NOM competes with PFAS for adsorption sites (ER18-1052, Sierra-Alvarez et al. 2019).

Figure 3. Structure of A.) polyaniline and B.) poly-o-toluidine.

Figure 4. Dynamic light scattering data for a) zeta potential and b) hydrodynamic diameter of c_{PANI} as a function of pH. The pH at which the zeta potential equals 0 is the isoelectric point (IEP= 6.76).

Figure 5. Dynamic light scattering data for a) zeta potential and b) hydrodynamic diameter of c_{POT} as a function of pH. The IEP is at 4.85.

Figure 6. SEM micrographs of c_{PANI} with a reaction time of a) 10hr, b) 5hr, c) 4hr, and d) 3hr

Figure 7. SEM micrograph images of c_{POT} with a reaction time of e) 10hr, f) 4hr, and g) 3 hr.

Figure 8. SEM micrographs with different molar ratios of $CuCl_2$ to Aniline and APS at the same reaction time. a) 8 aniline: 8 APS: 0.25 $CuCl_2$; b) 8 aniline: 8 APS : 2 CuCl2; c) 8 aniline: 8 APS : 4 $CuCl_2$.

Figure 9. a) The effect of increasing sonication time on zeta potential of c_{PANI} as a function of pH. b) The effect of sonication on hydrodynamic diameter of c_{PANI} as a function of pH

Figure 10. Comparison of Kd and Qe values for PFOA between products of different synthesis reaction times for c_{PANI} and c_{POT} compared to PANI synthesized in Olshansky et. al 2022 and SERDP project ER 18-1052.

Figure 11. a) Hydrodynamic diameter of c_{PANI} over time at different pH's. Linearized aggregation rate as a function of b) pH and c) zeta potential.

Figure 12. c_{PANI} average breakthrough for each group of columns. Group 1 columns were infused with a pH 4 influent solution. Group 2 columns were infused with a pH 6 influent solution, and group 3 columns were infused with a pH 6 influent solution.

Figure 13. c_{PANI} loading on Sand at 1cm increments along the length of the column.

Figure 14. Loading of c_{PANI} per g of sand calculated by the average effluent breakthrough mass balance for each group and the solid phase dissection of one of the triplicates in each group.

Figure 15: PFAS breakthrough following infusion into the a) group 1, b) group 2, and c) group 3 columns from experiment 1A.

Figure 16. Comparison of c_{PANI} average breakthrough from duplicate columns of two types of sand infused at a) pH 4, b) pH 6, and c) pH 9.

`

`

Figure 17. Comparison of the average loading of c_{PANI} on a) uncoated sand and b) aluminum hydroxide coated sand with distance for the three influent suspension pH values.

Figure 18. Average c_{PANI} loading calculated from effluent mass balance and solid dissection.

Figure 19. SEM micrographs of the surface of sand particles on the a) aluminum hydroxide coated sand and b) uncoated sand. As compared to the surface of the plain sand (b) the aluminum hydroxide coated sand (a) has the added nodular texture of the aluminum hydroxide. The darker areas in a) are due to the charging of the sand surface caused by the aluminum hydroxide coating.

Figure 20: c_{PANI} loading distribution across a 1m distance in horizontal and down flow regimes.

Figure 21. Column breakthrough data normalized to the influent concentrations for 20 mg of (a, d) CAC, (c, f) c_{PANI}, and (b, e) PANI to g of aluminum hydroxide coated (a-c) and uncoated sand (d -f).

Figure 22. Column breakthrough data normalized to the influent concentrations for 2 mg of (a, e) CAC, (c, g) c_{PANI}, and (b, f) PANI to g of aluminum hydroxide coated (a to c) and uncoated sand (e, f). The two sands were used as controls for PFAS through aluminum hydroxide coated (d) and uncoated sand (h).

Figure 23. PFAS loading onto c_{PANI}, PANI, and CAC from the 20 mgg-1 loading experiment without accounting for CAC loss.

Figure 24. PFAS loading onto c_{PANI}, PANI, and CAC from the 20 mg g^{-1} loading experiment with accounting for CAC loss (same data from Fig 22 but CAC loss included).

Figure 25. PFAS loading onto c_{PANI}, PANI, and CAC from the 2 mgg-1 loading experiment without accounting for CAC loss.

Figure 26. PFAS loading onto c_{PANI}, PANI, and CAC from the 2 mg g^{-1} loading experiment without accounting for CAC loss (same data in Fig 24 shown as a log).

Figure 27: Breakthrough curves for c_{PANI} columns treating groundwater samples from Willow Grove (Site 5 and Hangar B 680) and Tucson Water (ADEQ)

Acknowledgements: This research was supported by the Strategic Environmental Research and Development Program (SERDP) Grant Number ER22-3155.

`

List of Acronyms

AC	Activated Carbon
ADEQ	Arizona Department of Environmental Quality
AFFF	Aqueous Film Forming Foam
ALEC	Arizona Laboratory for Emerging Contaminants
Al-Qtz	Aluminum Hydroxide-Coated Quartz Sand
CAC	Colloidal Activated Carbon
CTPP	Central Tucson PFAS Project
DLVO	Derjaguin Landau Verwey and Overbeek
DMAFB	Davis Monthan Air Force Base
DoD	Department of Defense
DOM	Dissolved Organic Matter
EISA	Extracted Internal Standard Analytes
EPA	U.S. Environmental Protection Agency
GAC	Granular Activated Carbon
IEP	Isoelectric Point
IHAP	Injectable High-PFAS-Affinity Polymer
IISA	Injection Internal Standard Analytes
LC-MS/MS	Liquid Chromatography Tandem Mass Spectrometry
LOD	Limit of Detection
LVI	Large Volume Injection
MS/MS	Mass Spectrometry, Tandem Mass Spectrometry
NASJRB	Naval Air Station Joint Reserve Base
PAC	Powdered Activated Carbon
PANI	Polyanilines
PFAA	Perfluoroalkyl- and Polyfluoroalkyl Acids
PFCA	Perfluoroalkyl carboxylic acids
PFSA	Perfluoroalkyl sulfonic acids
PFAS	Perfluoroalkyl- and Polyfluoroalkyl Substances
PFOA	Perfluorooctanoic Acid
PFOS	Perfluorooctane Sulfonate
POT	Poly-*o*-Toluidine
QTOF	Quadrupole Time of Flight Mass
Qtz	Quartz Sand
SON	Statement of Need
UA	University of Arizona
XDLVO	Extended DLVO

Abstract

Objective: The goal of this research was to develop a proof-of-concept for in-situ remediation of PFAS-impacted sand and gravel aquifers. In this one-year study, bench-scale experiments were completed to evaluate high-PFAS-affinity cationic colloidal polymer behavior in saturated sands and their PFAS removal capacity under simulated aquifer conditions. Injectable high-affinity polymers (IHAPs) synthesized by our team using a cross-linking approach exhibited strong PFAS removal affinity. This proof-of-concept study completed the necessary bench-scale experiments for follow-on column and mesocosm experiments with additional SERDP support, ultimately working towards field deployment of the technology.

1. Technical Approach

The research was divided into four main tasks: **Task 1** was to conduct a detailed characterization of polymer colloid chemistry, focusing on hydrodynamic size and surface charge properties, using dynamic and static light scattering methods. In **Task 2** involved a series of saturated column experiments with polymer colloid injection under a range of aqueous geochemical conditions (pH, ionic strength, and polymer concentrations) to quantify the transport and adhesion behavior of the IHAPs in quartz sand (Qtz) and Al-hydroxide-coated quartz sand (Al-Qtz). **Task 3** involved experiments focused to quantify the uptake of PFAS species onto polymer-coated sands. In **Task 4**, we will examined the column-scale removal of PFAS species from contaminated groundwater samples deriving from the Central Tucson PFAS Project, which is impacted by PFAS from the Davis Monthan Air Force Base (DFAMB), and Site 5 and Hangar B from Former Naval Air Station Joint Reserve Base (NASJRB) Willow Grove.

2. Results and Benefits

This project shows that colloidal PANI (cPANI) can be developed as a sub micrometer cationic polymer that can be injected from a stable aqueous suspension into porous media. cPANI at pH 4 has as high positive zeta potential and remains suspended with minimal aggregation and settling before injection. cPANI functions as an injectable sorbent that adheres at high surface concentration in both negative- and positive-charged sand matrices with minimal detachment. cPANI has a high affinity and capacity for PFAS, removing *ca*. 90% of the PFAS concentration from a lab generated mixed water system for over thousands of PVs. It performs similarly to non-colloidal PANI at environmentally relevant concentrations (ng L^{-1}). This research indicates that cPANI is an effective injectable that, after some follow-on research, can be tested at larger scales including the field (Fig. A).

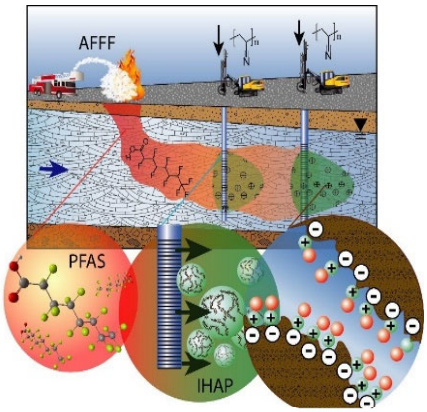

Figure A: Schematic representation of field scale application of cPANI as an in situ injectable.

Keywords: PFAS, injectable colloidal sorbents, PANI

Executive Summary

1. Introduction

PFAS such as perfluorooctanoic acid (PFOA) and perfluorooctanesulfonic acid (PFOS), as well as a wide range of shorter and longer chain analogues, are persistent pollutants present in the subsurface at many DoD facilities due to the past use of fire-fighting foams. Because of their mobility and recalcitrance, these compounds can form long, dilute plumes that require allocation of substantial resources in their cleanup. At present, remediation of PFAS is limited to pumping the groundwater and *ex- situ* treatment by adsorption, or *in-situ* treatment by commercially available activated carbon (McGregor 2018, McGregor 2020) and an experimental combination of water treatment polymers and activated carbon (Simcik et al. 2019, Liu et al. 2020). Particles are difficult to inject into an aquifer because they can be either filtered by well materials (if used) and by aquifer sediments, concentrating amendments in the vicinity of the boring, or mobilized in aquifer solutions as a result of poor retention on geo-media surfaces. Injection by aquifer fracturing to avoid filtration and improve dispersion can result in uneven distribution of treatment materials. In addition, activated carbon removes some PFAS species, e.g., PFOS, quite well, but it is less effective at removing PFOA and shorter length PFAS analogues, leading to uneven sequestration of contaminants. These issues can potentially be addressed by employing high-affinity colloidal sorbents engineered to achieve long-lasting and selective PFAS sequestration, such as those developed under our previous project (ER18-1052, Sierra-Alvarez et al. 2019). The goal of this proof-of-concept study is to determine the feasibility of utilizing these high affinity sorptive polymers for injection into highly productive sand and gravel aquifers for the *in-situ* sequestration of PFAS from contaminated groundwater at environmentally relevant concentrations.

2. Objectives

a. **Task 1. Assess surface chemistry and colloidal stability of polymers as a function of aqueous geochemistry.** *Hypothesis 1: Colloidal stability and hydrodynamic diameter of polymer particles depend on a functional relation between polymer surface charge and aqueous chemistry.*

b. **Task 2. Measure retention of polymer in saturated sand.** *Hypothesis 2: The breakthrough curve behavior of polymers in a given saturated sand matrix is a function of (i) geomedia surface chemistry, (ii) polymer colloid properties (studied under Task 1), and (iii) aqueous geochemical conditions.*

c. **Task 3. Quantify the adsorption-desorption behavior of PFAS in polymer-sand matrices**. *Hypothesis 3: Adsorptive affinity will be similar for adhered and non-adhered polymers (the latter measured in our current study), but adsorption capacity*

`

will be modestly reduced as a result of consumption of polymer interfacial area in the grain adhesion process.

d. Task 4. Test PFAS adsorption for a contaminated groundwater sample and quantify uptake of 25 recommended PFAS compounds. *Hypothesis 4: Flow of PFAS-contaminated groundwater through geomedia comprised of polymer-sand complexes will reduce dissolved PFAS concentrations to target remedial levels.*

3. Technical Approach

a. Polymer surface charge measurements are based on electrophoretic mobility while hydrodynamic diameter and aggregation rate measurements were made using dynamic light scattering. Scanning electron microscopy was used to confirm polymer morphology.

b. A predictive understanding of the transport and deposition (physicochemical filtration) of IHAP colloids in saturated geomedia is essential for predicting the fate and long-term effectiveness of these colloids once they are injected into groundwater aquifer systems. The transport of colloids from pore fluids to the surface of mineral grains is the result of interception, gravitational sedimentation, and Brownian diffusion (Tufenkji and Elimelech 2004). Rapid scale column tests were performed under saturated conditions with polymer infusions of varying geomedia surface chemistry, pH, and polymer suspension concentration.

c. Single point adsorption batch experiments were performed at pH 6 to quantify and compare polymer adsorption capacity at equilibrium. Then, rapid scale saturated column experiments were performed, also at pH 6, to quantify polymer adsorption capacity as part of the polymer-sand matrix in a flow through regime.

d. Groundwater samples from Former Naval Air Station Joint Reserve Base (NASJRB) Willow Grove (Site 5 and Hangar B 680) and a well operated by Tucson Water (production well C007A) were infused into columns pre-loaded with polymer for testing of PFAS removal in a flow through system.

4. Results and Discussion

Measurements of zeta potential for cPANI (Fig. E1a) and cPOT (Fig. E3a) shows a circum-neutral isoelectric point (IEP) of cPANI (pH 6.76) and an acidic IEP for cPOT at pH 4.85. The hydrodynamic diameter measurements of cPANI increased with increasing pH with the smallest diameter observed at pH 4 (Fig. E1b). Hydrodynamic diameter measurements for cPOT have high standard deviations for each measurement and all are above 2 μm (Fig. E3b).

`

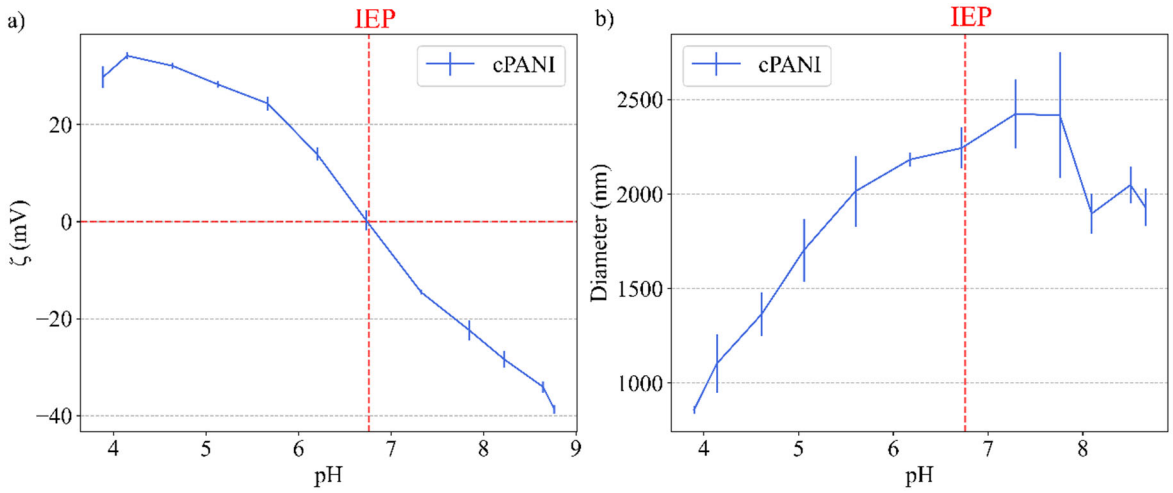

Figure E1: *Dynamic light scattering data for a) zeta potential and b) hydrodynamic diameter of cPANI as a function of pH. The pH at which the zeta potential equals 0 is the isoelectric point (IEP= 6.76).*

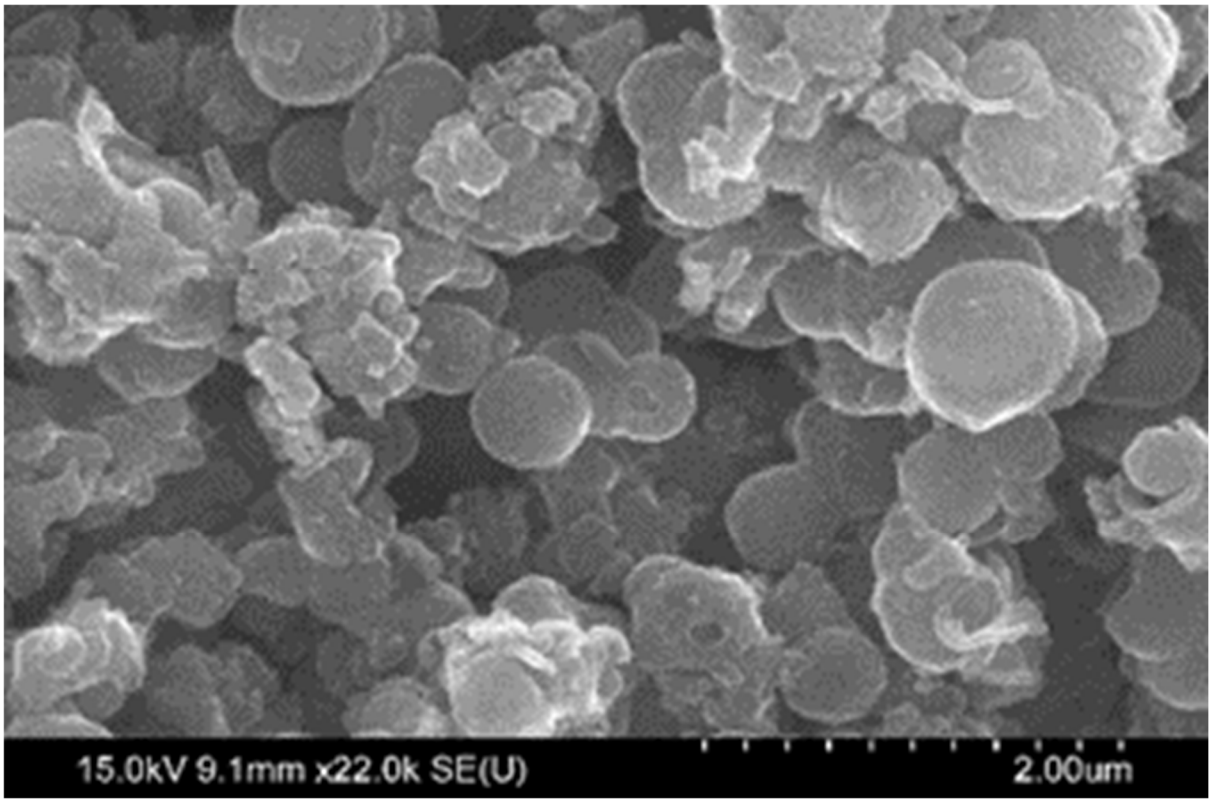

Figure E2*: SEM micrograph of cPANI showing particles are sub-micrometer spheres.*

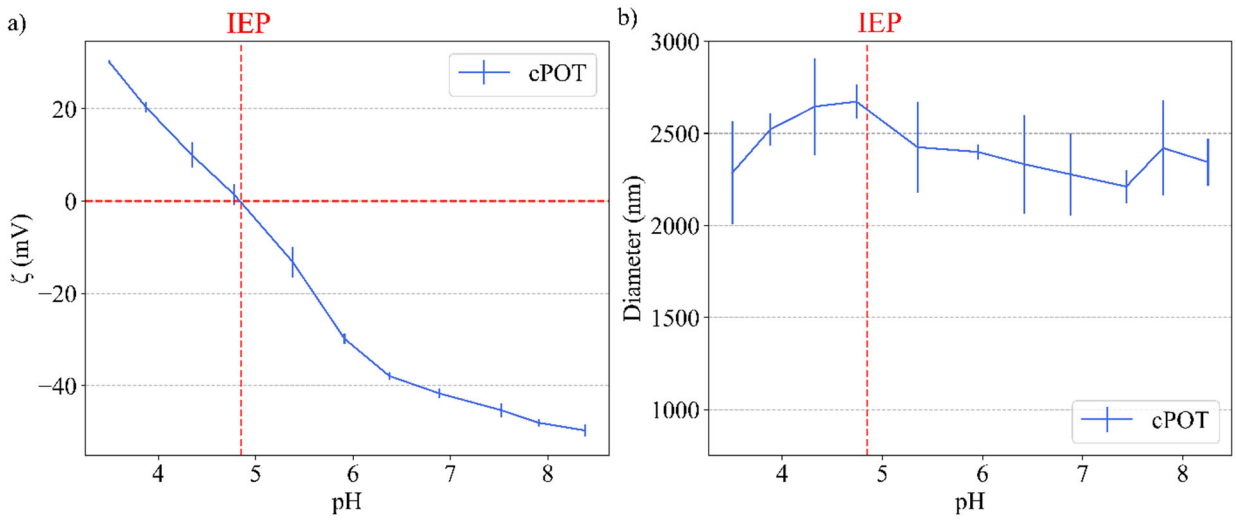

***Figure E3**: Dynamic light scattering data for a) zeta potential and b) hydrodynamic diameter of cPOT as a function of pH. The IEP is at 4.85.*

In a single point batch experiment run at pH 6 with concentrations of 10 mg L^{-1} of polymer and 1000 ng L^{-1} of PFOA, cPANI exhibited an equilibrium sorbed mass (Q_e) of 98.34 ± 0.62 ng $_{PFOA}$ mg $_{polymer}^{-1}$, a K_d of 4.11± 0.79 L mg^{-1}, and a removal efficiency of 97.59 ± 0.42 %.

When infused into columns at a suspension concentration of 10 mg L^{-1} in a 1 mM NaCl background electrolyte solution, the average loading of the cPANI is relatively high on both negatively and positively charged sand surfaces (Fig. E4).

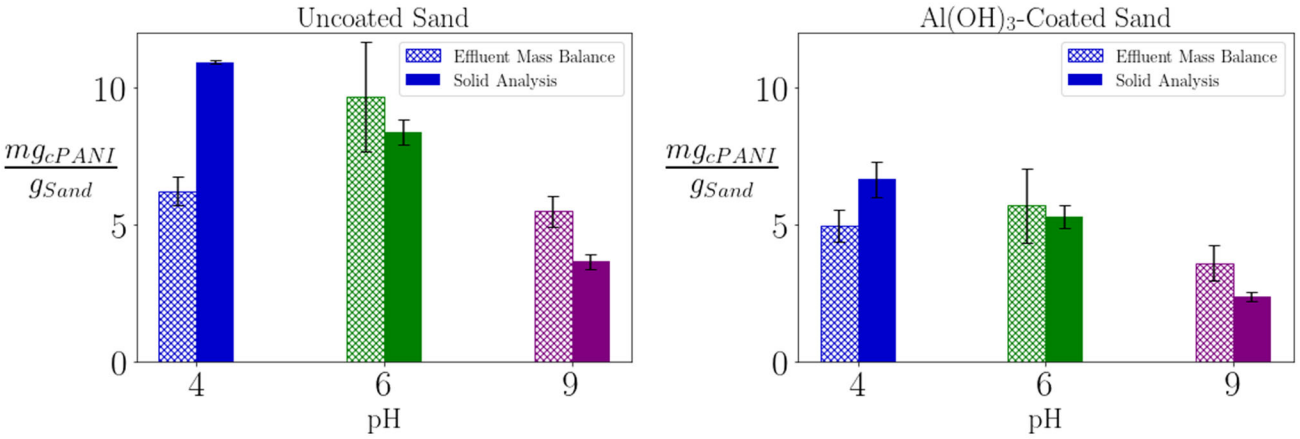

***Figure E4:** Average cPANI loading calculated from column experiment effluent mass balance and solid dissection. The black lines represent the standard deviation of duplicate samples.*

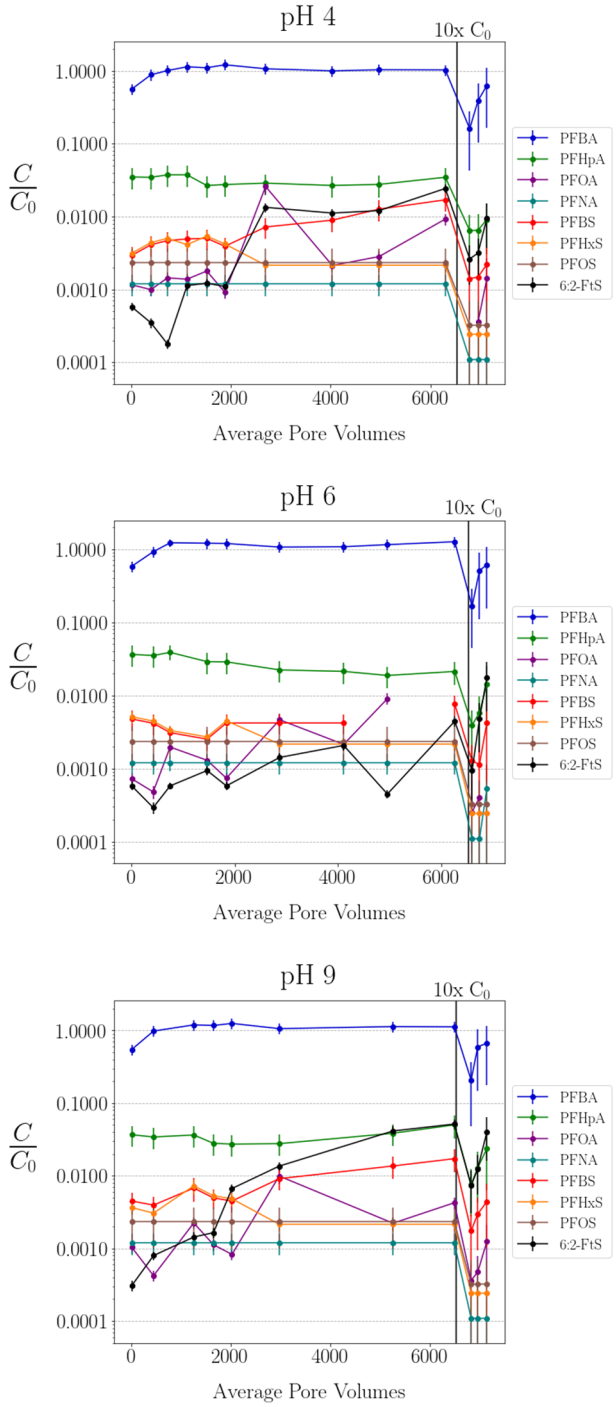

The trends with pH and sand type seen in the results of this experiment are consistent with electrostatic interaction between the charged cPANI and the charged matrices. As shown in Figure 1a and discussed in previous sections, the I–EP of cPANI is *ca*. pH 6, at which pH rapid aggregation occurs. The higher particle aggregation may explain why the maximum loading is observed at pH 6, since cPANI-cPANI adhesion may be enhanced at this pH value. Al hydroxide coating of the sand increases cPANI charge repulsion by the surface, resulting in decreased retention, particularly at pH 4.

After infusing columns with a cPANI suspensions, the average cPANI loadings of the columns were 21.63 ± 5.02, 16.62 ± 5.02 and 18.25 ± 4.61 mg g^{-1} for Groups 1, 2, and 3 respectively. Each group of columns were then infused with 1 µg L^{-1} each of the eight representative PFAS species and, after around 6,500 PV, 10x the original PFAS concentration. The columns show a reduction by 90% for majority of the PFAS over thousands of PVs at pH 6 (Fig. E5).

Figure E5: *PFAS breakthrough following infusion into the a) group 1, b) group 2, and c) group 3 columns from experiment 1A. The error bars at each point represent the standard deviation of triplicate samples. The vertical line labeled "10x C_0" represents the pore volume when the columns were infused with influent spiked to ten times the original concentration at time zero (shifted from 8 ng L^{-1} to 80 ng L^{-1} of total PFAS).*

The performance of cPANI was then tested with three different groundwaters with a loading of 20 $mg_{cPANI}\ g_{Sand}^{-1}$. The pertinent chemical compositions of the groundwater measured by a DoD certified lab are included in Table E1.

`

Table E1: *Chemical composition of PFAS contaminated groundwater tested (mean ± standard deviation shown).*

	Willow Grove		ADEQ		
	Site 5 composite	**Hanger B composite**	**C007A composite**	**Units**	**LOD**
Measured TOF	5.6 ± 0.21	42.4 ± 0.04	12.500 ± 0.003	ug L^{-1}	5.1
Calculated TOF	3.6 ± 0.1	13.83 ± 0.04	6.66 ± 0.13	ug L^{-1}	
Analyte					
PFBA	500 ± 12	1700 ± 127	2260 ± 77	ng L^{-1}	97.5
PFHpA	102 ± 2	300 ± 28	210 ± 17	ng L^{-1}	2.5
PFOA	3300 ± 65	2300 ± 290	638 ± 9.3	ng L^{-1}	2.5
6:2 FTS	50 ± 1.7	3200 ± 110	2200 ± 100	ng L^{-1}	2.5
PFBS	80 ± 10	1109 ± 116.2	186 ± 1	ng L^{-1}	5.0
PFHxS	600 ± 200	5400 ± 620	1300 ± 110	ng L^{-1}	99.7
PFNA	18 ± 1.1	31 ± 2.9	2.7 ± 0.2	ng L^{-1}	5.1
PFOS	250 ± 5	4010 ± 50	1850 ± 38	ng L^{-1}	2.5
PFPeA	138 ± 9.1	680 ± 14	540 ± 22	ng L^{-1}	7.6
PFHxA	199 ± 8.4	1480 ± 14	760 ± 26	ng L^{-1}	2.5
PFDA	11 ± 3.8	9 ± 1.9	< LOD	ng L^{-1}	1
PFUnA	4.5	3.3	< LOD	ng L^{-1}	2.5
PFDoA	< LOD	< LOD	< LOD	ng L^{-1}	2.5
PFTriDA	< LOD	< LOD	< LOD	ng L^{-1}	5.1
PFTreA	< LOD	< LOD	< LOD	ng L^{-1}	5.1
4:2 FTS	< LOD	26.7 ± 0.6	6 ± 1	ng L^{-1}	2.5
8:2FTS	34 ± 2.5	146.600 ± 0.004	< LOD	ng L^{-1}	5.1
NEtFOSAA	< LOD	< LOD	< LOD	ng L^{-1}	
PFPeS	90 ± 71	850 ± 52	120 ± 30	ng L^{-1}	1.0
PFHpS	13 ± 2.3	700 ± 130	75 ± 5	ng L^{-1}	1.0
PFNS	< LOD	50 ± 4.7	< LOD	ng L^{-1}	5.0
PFDS	< LOD	< LOD	< LOD	ng L^{-1}	5.1
FOSA	< LOD	70 ± 16	500 ± 110	ng L^{-1}	2.5
N-MeFOSA	< LOD	< LOD	< LOD	ng L^{-1}	2.4
NMeFOSAA	< LOD	< LOD	< LOD	ng L^{-1}	10.1
Total:	5400± 200	22100± 700	11000± 200	ng L^{-1}	

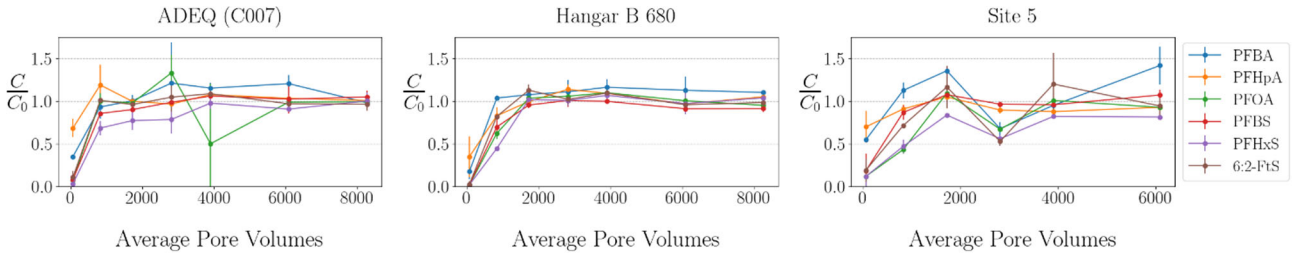

Figure E6*: Breakthrough curves for cPANI columns treating groundwater samples from Willow Grove (Site 5 and Hangar B 680) and Tucson Water (ADEQ). The error bars at each point represent the standard deviation of duplicate samples.*

`

`

The effluent samples were normalized to the average measured concentrations for the pre-filtered groundwaters during infusion. The effluent samples reached the C_o concentration quickly (within ~2000 PV) relative to the synthetic groundwater most likely due to the complexity of the PFAS mixture and the presence of native dissolved organic matter (DOM) that can compete for adsorption sites. Assuming the average faster paced ground water can move around ~ .3048 m day^{-1} (1ft day^{-1}), 2000 PV translates to ~18 years for each m^3 of treated aquifer.

5. Implications for Future Research and Benefits

This one-year proof-of-concept study has the intent of bridging the gap between our polymer synthesis and PFAS adsorption studies conducted under SERDP project (ER18-1052, *Remediation of Per- and Polyfluoroalkyl Contaminated Groundwater Using Cationic Hydrophobic Polymers as Ultra-High Affinity Sorbents,* PI Sierra-Alvarez) and assessment of *in-situ* applications of polymer-based PFAS removal from contaminated geomedia systems.

Research that could be addressed following 1-year proof-of-concept study: Based on the results of the current proof-of-concept study, several tasks could be pursued in a subsequent 2-year project:

- Flow-through column data fitting to the advection-dispersion equation with chemical retardation enabling direct quantitative comparison to distribution coefficients determined from the batch experiments conducted in the current work and field scale prediction.
- Further optimization of cPOT synthesis to increase effectiveness toward its non-colloidal counterpart, which would enable tailoring injection mixtures for site-specific conditions.
- Assessment of the long-term fate of the colloidal polymers in the subsurface, including their susceptibility to microbial biodegradation and potential generation of hazardous byproducts as amine based polymers.
- Mesocosm scale injection into a lab built aquifer model to test larger-scale injection, mobility, and retention patterns of cPANI as well as PFAS remediation
- Field scale efficacy testing in a contaminated site by injecting the cPANI downstream of a PFAS plume similar to Figure E7.

`

`

1. Objectives

1.1 Approach

In this project, we focused on sand and gravel media, which are particularly vulnerable to contamination (Aller et al. 1987) and comprise a major source of drinking water in the US (Reilly et al. 2008). PFAS migration is enhanced in low-surface area media such as sand and gravel aquifers (Ferrey et al. 2012). Groundwater velocity can be high in such systems, especially if the aquifer is subjected to pumping; these high-capacity aquifers are often the target of potable water production. Sand and gravel aquifers vary in their surface chemistry. When quartz and feldspars grains occupy most of the interfacial area, the surface is negatively charged across the pH range of natural waters, as it is composed of Si-bridging oxygen atoms and relatively acidic silanol groups. In weathered sand and gravel aquifers, quartz surfaces become coated with a metal-hydroxide mineral veneer, often dominated by $Al(OH)_3$ (Coston et al. 1995) which confers net positive charge and weakly-acidic, but highly-reactive surface aluminol groups. Treatment technology that works in sand and gravel aquifers of the quartz and hydroxide-coated quartz types will be broadly applicable and particularly useful for controlling PFAS migration.

The treatment amendment developed, tested and optimized in this project was based on innovated sorbents developed under ER18-1052 (Sierra-Alvarez et al. 2019), *Remediation of Per- and Polyfluoroalkyl Contaminated Groundwater Using Cationic Hydrophobic Polymers as Ultra-High Affinity Sorbents*. Under that project, cationic polymers were synthesized using various methods to combine cationic and hydrophobic moieties that interact with PFAS head and tail groups, respectively, effectively binding them to the polymer. Our cationic polymers have a high affinity for PFAS, with a sorptive capacity similar to GAC on a mass basis, and far superior to GAC on a surface area basis. Two polymers that emerged from our prior work (PANI and POT) were identified as most promising, and were employed for the current study. This work adapted and tested these PANI and POT materials, for injection and treatment.

1.2 SERDP relevance

This project addressed ERSON-22-C4 entitled "*Treatment of Per- and Polyfluoroalkyl Substance-Impacted Matrices*", which called for innovative research to develop cost-effective remedial technologies for matrices impacted by PFAS resulting from the use of aqueous film forming foam (AFFF) formulations. Consistent with the first objective listed in the SON, by assessing the efficacy of high PFAS-affinity polymeric adsorbents that are injectable into the saturated subsurface, the current project tested cost-effective, *in-situ* remedial treatment for PFAS-impacted sand and gravel

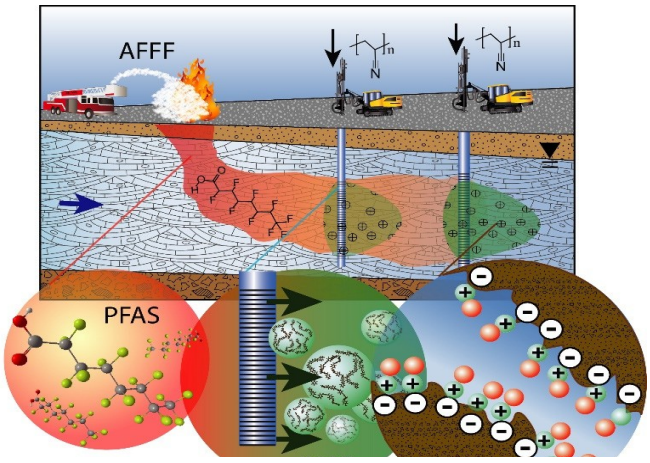

Figure O1: *Schematic representation of field scale application of cPANI as an in situ injectable.*

`

groundwater aquifers. While the proof-of-concept testing was conducted at the bench scale, the technology has prospective field-scale application. Our approach addressed this objective through the use of high affinity polymeric adsorbents that can be injected into contaminated aquifers, adhered to grain surfaces, and retained in the sediments to adsorb and sequester PFAS from the aqueous phase over long time scales. Data indicate that the polymers will be effective even when PFAS is present at environmentally-relevant concentrations (micrograms to nanograms per liter). The proposed remedial processes will immobilize PFAS into discrete zones within an aquifer, thereby contributing to the EPA goals for remediation, *i.e.,* reduction in Toxicity, Mobility or Volume (TMV).

The specific project objectives were as follows:

i. **Task 1. Assess surface chemistry and colloidal stability of polymers as a function of aqueous geochemistry.** *Hypothesis 1: Colloidal stability and hydrodynamic diameter of polymer particles depend on a functional relation between polymer surface charge and aqueous chemistry.* Polymer surface charge measurements were based on electrophoretic mobility, whereas hydrodynamic size were measured using dynamic light scattering. For non-stable colloidal suspensions, aggregation rate was measured using dynamic light scattering, which enables monitoring of the Stokes' hydrodynamic diameter as a function of time. Scanning electron microscopy was used to confirm polymer morphology.

ii. ***Task 2. Measure retention of polymer in saturated sand.*** *Hypothesis 2: The breakthrough curve behavior of polymers in a given saturated sand matrix is a function of (i) geomedia surface chemistry,(ii) polymer colloid properties (studied under Task 1), and (iii) aqueous geochemical conditions*. A predictive understanding of the transport and deposition (physicochemical filtration) of IHAP colloids in saturated geomedia is essential for predicting the fate and long-term effectiveness of these colloids once they are injected into groundwater aquifer systems. The transport of colloids from pore fluids to the surface of mineral grains is the result of interception, gravitational sedimentation, and Brownian diffusion (Tufenkji and Elimelech 2004). Rapid scale column tests were performed under saturated conditions with polymer infusions of varying geomedia surface chemistry, pH, and polymer suspension concentration.

iii. **Task 3. Quantify the adsorption-desorption behavior of PFAS in polymer-sand matrices**. *Hypothesis 3: Adsorptive affinity will be similar for adhered and non-adhered polymers (the latter measured in our current study), but adsorption capacity will be modestly reduced as a result of consumption of polymer interfacial area in the grain adhesion process.* Single point adsorption batch experiments were performed at pH 6 to quantify and compare polymer adsorption capacity at equilibrium. Then, rapid scale saturated column experiments were performed at pH 6 as well to quantify polymer adsorption capacity as part of the polymer-sand matrix in a flow through regime.

iv. **Task 4. Test PFAS adsorption for a contaminated groundwater sample and quantify uptake of 25 recommended PFAS compounds.** *Hypothesis 4: Flow of PFAS-contaminated groundwater through geomedia comprised of polymer-sand complexes will*

reduce dissolved PFAS concentrations to target remedial levels. Groundwater samples from Naval Air Station Joint Reserve Base (NASJRB) Willow Grove (Site 5 and Hangar B 680) and a well operated by Tucson Water (production well C007A) were infused into columns pre-loaded with polymer for testing of PFAS removal in a flow through system.

2. Background

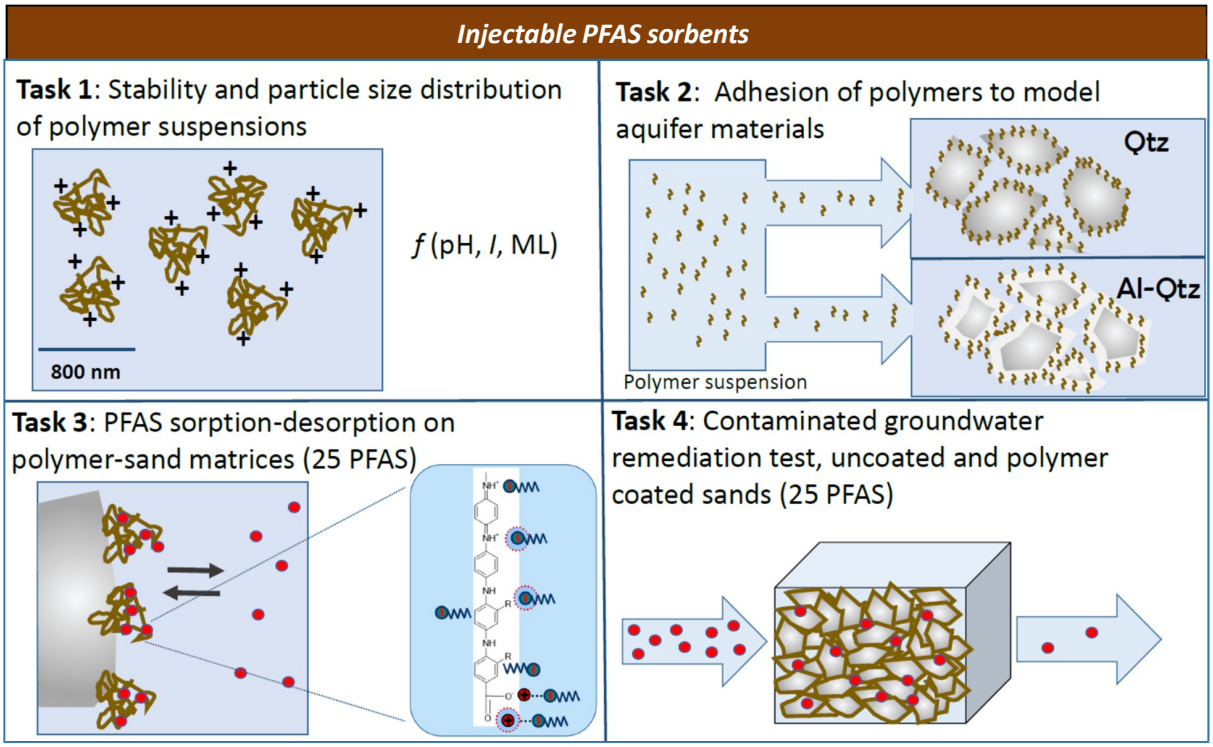

Figure 1. *This injectable polymer project comprised four inter-related tasks and culminated in a bench scale remedial test conducted on contaminated groundwater samples from priority DoD sites. In this figure, polymers are represented by brown coils and PFAS by red spheres and head/tail groups in expansion.*

2.1 Need for in situ treatment for PFAS*:* PFAS such as perfluorooctanoic acid (PFOA) and perfluorooctanesulfonic acid (PFOS), as well as a wide range of shorter and longer chain analogues, are persistent pollutants present in the subsurface at many DoD facilities due to the past use of fire-fighting foams. Because of their mobility and recalcitrance, these compounds can form long, dilute plumes that require allocation of substantial resources in their cleanup. PFAS pose a human health threat, necessitating feasible technologies for their removal or sequestration. PFAS remediation efforts are hindered by the recalcitrance of these compounds to microbial and chemical degradation under ambient conditions. At present, remediation of PFAS is limited to pumping the groundwater and *ex- situ* treatment by adsorption, or *in-situ* treatment by

commercially available activated carbon (McGregor 2018, McGregor 2020) and an experimental combination of water treatment polymers and activated carbon (Simcik et al. 2019, Liu et al. 2020).

Pumping and treating groundwater can be an effective means of controlling contaminant migration. However, it is costly and produces large volumes of water and residuals requiring disposal or re-use. It also typically fails to remove a sufficient mass fraction of contaminants for aquifer restoration. *In-situ* approaches address these concerns by avoiding pumping and by treating the contaminants in place, but such remedial approaches are not yet well developed for PFAS (McGregor 2020). Current technologies rely on particles of activated carbon suspended in an emulsion that enhances adhesion to the soil (Simcik et al. 2019).

The University of Minnesota and Brown University recently successfully tested cationic polymers used in water treatment, including poly diallyldimethylammonium chloride (polyDADMAC) and polyamine (PA), coupled with powdered activated carbon (PAC) to treat PFAS in groundwater (Simcik et al. 2019, Liu et al. 2020). Field testing of this technology is underway. The PAC was necessary because it was found that the polymers themselves were not well-retained in Ottawa sand. The PAC served as an anchor to retain the polymer while boosting overall adsorption. Results indicated hysteretic adsorption of PFAS to this material, i.e., PFAS adsorbed far more readily than it desorbed - and the material was resistant to environmental degradation. A commercially available product, referred to as "colloidal activated carbon", has also been field tested (McGregor 2018, McGregor 2020). This product suspends very fine particles of activated carbon (low μm diameters) in an emulsion to treat PFAS. Both technologies appear capable of reducing PFAS concentrations in groundwater. However, both systems have important drawbacks. The polyDADMAC-PAC system uses #100 mesh (0.149 mm) PAC to anchor the emulsion into the sand structure. This PAC is of relatively large diameter, around 100 μm, which exceeds the pore diameter of the sand. Thus, it has a limited injection radius, even when forced under pressure into sand and gravel aquifers. Both the polyDADMAC and the PAC can adsorb PFAS. The colloidal activated carbon (CAC) is small enough to penetrate into a sand formation, but it is carried in the emulsion. The emulsion, which comprises most of the injection volume, breaks down and helps the CAC adhere to the formation. But the activated carbon is prone to migrate uncontrollably, and the emulsion degrades and does not contribute to PFAS adsorption, limiting the ability of the suspension to adsorb PFAS. There is, therefore, urgent need for an injectable amendment that behaves more like a liquid or true colloidal suspension for emplacement, but is retained in aquifer sediments, and can adsorb PFAS at a high rate and high affinity.

These issues can potentially be addressed by employing high-affinity colloidal sorbents engineered to achieve long-lasting and selective PFAS sequestration, such as those developed under our previous project (ER18-1052, Sierra-Alvarez et al. 2019). These polymers, which can be tailored with surface functional groups, surface charge properties, and particle size for efficacy specific to site conditions (Olshansky et al., 2021, 2022), offer promising opportunities for application to *in-situ* remedial technologies (e.g., subsurface permeable adsorptive barriers (**PAB**) and areal treatments). The polymers have a similar adsorptive capacity to activated carbon in the μg L^{-1} PFAS concentration range but exhibit superior affinity to adsorb PFAS at low (ng L^{-1})

concentrations, and are highly selective for PFAS (e.g., less negatively impacted by dissolved NOM) (Fig 2).

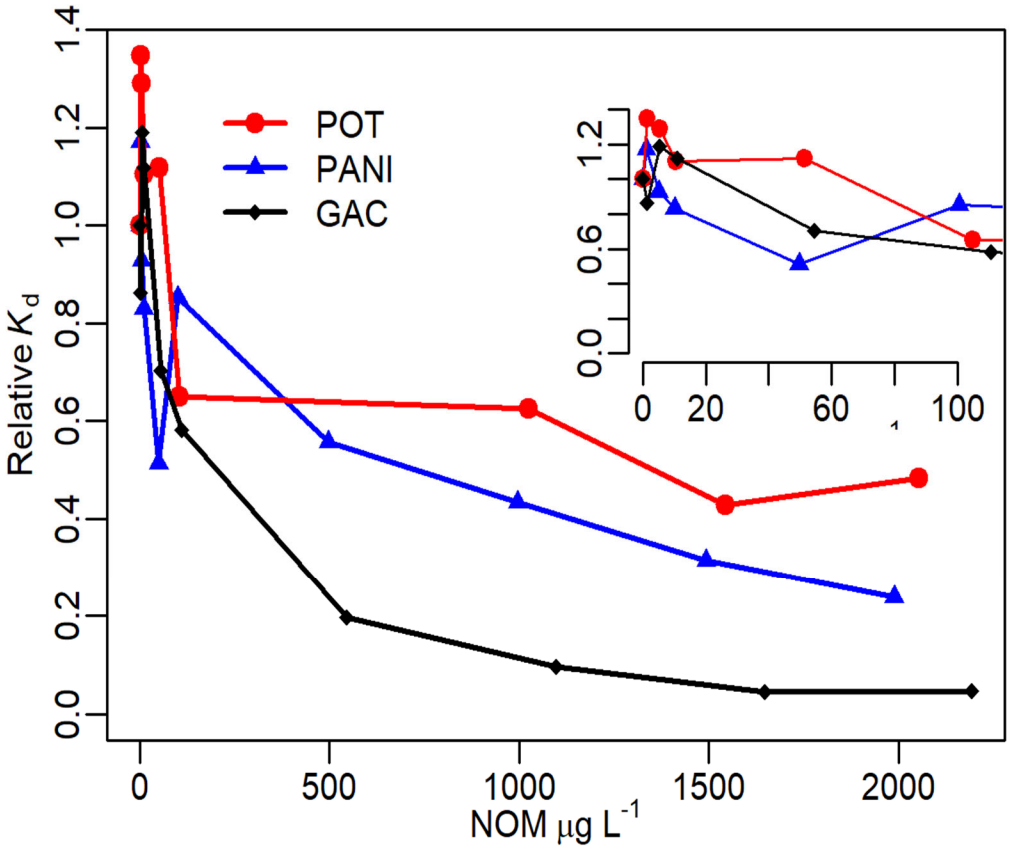

Figure 2. *Impacts on PFOA adsorption of competition from dissolved natural organic matter (NOM). Dissolved NOM represents a significant hindrance to PFAS adsorption on GAC and other sorbents used for PFAS remediation because NOM competes with PFAS for adsorption sites (Olshansky et al., 2022).*

Importantly, these polymers have the potential to be injected into aquifer sediments as a relatively pure colloidal suspension with a high capacity to adsorb PFAS *in-situ*. The goal of this proof-of-concept study is to determine the feasibility of utilizing these high affinity sorptive polymers for injection into highly productive sand and gravel aquifers for the *in-situ* sequestration of PFAS from contaminated groundwater at environmentally relevant concentrations.

2.2 PFAS migration to the saturated zone

Most PFAS of concern in this proposal were first introduced at the ground surface where they were deposited through the use of aqueous film forming foams (AFFF). Upon entry to soils, PFAS are subject to adsorption at both solid-water and air-water interfaces, which retards their subsurface transport relative to the downward percolation of water itself or relative to the gravitational

transport rate of dissolved unreactive tracers (Brusseau 2018, Lyu et al. 2018). As a result of their surfactant properties (polar head group and hydrophobic tail) many of these compounds, particularly the long- chain molecules (e.g., PFOS and PFOA) exhibit an especially high affinity for air-water interface adsorption and this contributes to the preferential retention of longer chain compounds in the vadose zone (Brusseau et al. 2020). However, the extent to which PFAS adsorption is partitioned between the air-water and solid-water interface depends on both the relative area contributed by each type of interface in a given soil volume (which varies with soil moisture) as well as the precise surface chemistry of mineral and organic particles present. For example, in vadose zone soils dominated by low surface reactivity sands and silts, PFAS adsorption is dominated by retention at air-water interfaces, whereas in soils with higher concentrations of organic matter and metal oxides, retention at solid surfaces can be dominant. Nonetheless, as a result of progressive cycles of rainfall, associated vadose zone saturation episodes, and repeated propagation of the wetting front, coupled with the extreme recalcitrance of PFAS to chemical and microbial degradation, these surface-derived contaminants eventually make their way into the saturated zone (Silva et al. 2020). Remediation of groundwater aquifers in the PFAS-receiving saturated zone, which are a primary source of drinking water to communities worldwide, is therefore the overarching goal of this research.

2.3 PFAS retention at solid surfaces

Adsorption of PFAS in the saturated zone – where air-filled porosity is negligible – is limited to solid-water interfaces. As a result of PFAS molecular structure, which combines polarity and hydrophobicity, mechanisms of adsorption are more complex than is encountered for more well-studied hydrophobic organic contaminants (HOCs). Whereas HOCs tend to exhibit low affinity for the water-wetted surface of mineral grains and high affinity for the hydrophobic micro-environments found within natural organic matter (NOM), the higher polarity and water solubility of PFAS implies that they exhibit overall lower affinity than HOCs for hydrophobic voids in NOM and higher affinity for certain types of mineral surfaces. Minerals that exhibit the highest affinity for PFAS are those that present positive surface charge throughout a wide pH range of natural waters, including iron and aluminum (oxyhydr)oxides. These metal oxides have a higher adsorptive affinity for PFAS than do layer silicate clays or primary silicate minerals like quartz and feldspars (Gao and Chorover 2012, Campos-Pereira et al. 2020). Further, the ionic composition of solution mediates adsorptive affinity through both anion competition and cation-bridging (Campos Pereira et al. 2018).

The molecular mechanisms of PFAS adsorption to solid surfaces include hydrophobic interaction, electrostatic attraction, H-bonding, cation-bridging, and even covalent bonding (Zhang et al. 2019). The specific mechanisms that are active in a given case depend on the PFAS species present, the chemistry of the surfaces, and the composition of the aqueous solution. For example, whereas both PFOA and PFOS are anionic throughout most of the pH range of natural waters, and they differ only in the polar head group of the eight-carbon chain, they differ significantly in their relative affinity for solid surfaces. PFOA forms strong inner-sphere complexes with iron oxides, whereas PFOS forms outer-sphere complexes, and this difference has a direct influence on surface affinity and adsorptive reversibility (Gao and Chorover 2012, Campos-Pereira et al. 2020).

`

2.4 Polymer Retention at Solid Surfaces

The subsurface naturally attenuates many types of contaminants *in-situ* by strong sorption to the particle-water interface or (bio)degradation reactions (Scow and Hicks 2005). Unfortunately, PFAS are highly recalcitrant to biodegradation and exhibit low affinity for most surfaces present in natural geomedia. Therefore, an effective approach to enhance adsorptive retention of contaminants in the subsurface is to modify the surface chemistry of the geomedia, increasing its affinity for the contaminants of interest. In the case of PFAS, adsorption can be promoted by modifying surface charge and hydrophobicity of the geomedia *in-situ.* Conferring both anion exchange capacity and hydrophobicity has the potential to dramatically increase uptake from solution. Our team has developed polymeric sorbents based on polyaniline (PANI) and poly-*o*-toluidine (POT) that exhibit both of these characteristics, giving them exceptionally high affinity for PFAS uptake and significant promise for *in-situ* deployment. Of particular importance in this context is the fact that these polymers can be synthesized as high specific surface area, colloid-sized particles, giving them a distinct advantage over more commonly used sorbents like granular activated carbon. The PANI and POT colloids can be injected into the subsurface where they will migrate with fluids down gradient until they are immobilized by adhesion onto collector surfaces.

Colloid Transport in Porous Media: Transport of colloids in the subsurface (including these cationic polymeric ones) is mediated by interception, gravitational sedimentation, and Brownian diffusion, all of which may bring the colloid in close proximity to a collector (e.g., sand grain) surface (Ryan and Elimelech 1996, Tufenkji and Elimelech 2004). Thereafter, colloidal adhesion at the collector surface is controlled by interactions that operate at the molecular scale, and are characterized by extended Derjaguin Landau Verwey and Overbeek (XDLVO) theory to include van der Waals, electrostatic, hydrogen bonding, hydration, and Lewis acid-base forces (Hoek and Agarwal 2006, Li et al. 2019). Given the importance of electrostatic interactions, we anticipate that transport distance and adhesion properties of cationic polymers at the surface of sand particles will exhibit strong dependence on the charge properties of the polymer colloid and the sand grains, which are, in turn, affected by surface chemistry and aqueous geochemical conditions (e.g., ionic strength and ion composition).

Once attached to a mineral surface, polymer relaxation and elongation results in the time-dependent accumulation of points of polymer-grain attachment. This decreases subsequent polymer desorption from the surface because desorption requires the simultaneous detachment of multiple points of contact. Yu et al. (2018) used density functional theory (DFT) calculations to show that the PANI polymer chain forms stable polymer-mineral complexes on a quartz substrate due, in large part, to additive hydrogen-bonding interactions between the –NH– groups on PANI and the silanol groups on the quartz surface (Yu et al. 2018). We anticipated that once the polymer colloids are immobilized on grain surfaces, they will not be subject to detachment or even remobilized by fluid shear common to that encountered in groundwater environments, but we tested this under **Task 2**.

`

`

3. Materials and Methods

3.1 Experiments

All reagents were analytical, LC-MS/MS, and trace metal grade or better; labware and equipment used for experiments and to prepare standards and reagents were properly cleaned with 100% pure ethanol to remove organic solvents, rinsed six times with nano-pure water (18.2 MΩ-cm), and air-dried prior to use. Teflon was avoided in all experiments and analyses.

Deionized (DI) water (18.2 MΩ-cm) was used in the experiments (Barnstead Thermolyne NANOpure Diamond UV water system). Common chemicals can be found in Table 1.

Table 1: Chemicals used for experiments.

Chemicals	Symbol	Purity	CAS	Company
Aniline	N/A	N/A	62-53-3	Sigma-Aldrich, St.Louis, MO, USA
O-Toluidine	N/A	N/A	95-53-3	Sigma-Aldrich, St.Louis, MO, USA
Copper (II) Chloride Dihydrate	$CuCl_2 \cdot 2H_2O$	N/A	10125-13-0	Sigma-Aldrich, St.Louis, MO, USA
Sodium Chloride	NaCl	N/A	7647-14-5	Macron Fine Chemicals
Ammonium Persulfate	APS	N/A	7727-54-0	Sigma-Aldrich, St.Louis, MO, USA
SiO_2 40-100 mesh	Sand	N/A	14808-60-7	Thermo Scientific
Aluminum Chloride hexahydrate	$AlCl_3 \cdot 6H_2O$	N/A	7784-13-6	Sigma-Aldrich, St.Louis, MO, USA
Heptafluorobutyric Acid	PFBA	98%	375-22-4	Sigma-Aldrich, St.Louis, MO, USA
Perfluorooctanoic acid	PFOA	>95%	335-67-1	Alfa Aesar, Tewksbury, MA, USA
Tridecafluoroheptanoic acid	PFHpA	>98.0%	375-85-9	TCI Portland, OR, USA
Heptadecafluorononanoic Acid	PFNA	>95%	375-95-1	TCI Portland, OR, USA
Perfluorobutane sulfonate	PFBS	>97%	375-73-5	Sigma-Aldrich, St.Louis, MO, USA
Tridecafluorohexane-1-sulfonic acid potassium salt	PFHxS	N/A	3871-99-6	Santa Cruz Biotech, Dallas,,USA
Perfluorooctane sulfonic acid	PFOS	98%	2795-39-3	Sigma-Aldrich, St.Louis, MO, USA
6:2 Fluorotelomer sulfonic acid	6:2-FTS	N/A	27619-97-2	Synquest Laboratories, Alachua

3.2 Synthesis of PANI and POT

Colloidal polyaniline (cPANI) and colloidal poly-o-toluidine (cPOT) were synthesized using a method adapted from Guo et al. (2011). Briefly, a 0.1 M APS and 0.0125 M $CuCl_2 \cdot 2H_2O$ solution was made in DI water and set to chill until the temperature reached 0-5 °C. In a separate beaker, a 0.1 M aniline/o-toluidine emulsion was prepared and chilled to 0-5 °C. The two solutions were combined and stirred using a polytetrafluoroethylene (PTFE)-free stir bar (V&P Scientific Inc., San Diego, CA, USA) for a few minutes to fully mix and then placed in an ice bath in a refrigerator to maintain the temperature at 0-5 °C for the duration of the reaction time (3, 4, 5, or 10 h). The resulting polymer and excess solution were filtered through a 0.22 µm filter under vacuum and each liter was washed with 1 L ethanol and 3 L DI water until a clear filtrate waste was achieved.

`

`

The resulting filter cake was dried at 100 °C and stored in an amber glass bottle. Successful synthesis using the same scale in Guo et al. (2011) was followed by a scaled-up method for higher yield to use in batch experiments and for detailed characterization.

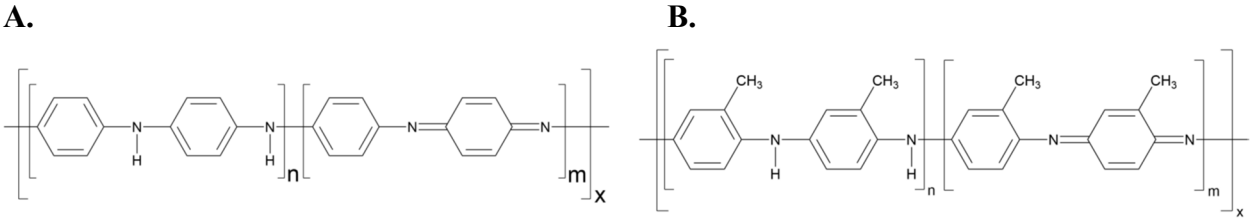

Figure 3*. Molecular structures of A.) polyaniline and B.) poly-o-toluidine (Andriianova et al. 2020; Weber et al., 2022) for dissociated forms. The pH-dependent charge properties result from progressive protonation of the imine N atoms with decreasing pH.*

3.3 Colloidal Polymer Characterization

3.3.1 *SEM Imaging*

Micrographs were collected to investigate the polymer morphology, topography, and to visualize the polymer adhesion to sand using a scanning electron microscope (SEM, Hitachi 4000) in the Kuiper Materials Imaging and Characterization Facility, at the University of Arizona.

3.3.2 *Zeta potential and hydrodynamic diameter and aggregation*

Polymer hydrodynamic diameter and zeta potential were measured on a Zetasizer Nano (Malvern, Worcestershire, UK) using dynamic light scattering. A suspension of 100 $mg_{polymer}$ L^{-1} in 5 mM NaCl background electrolyte was prepared and sonicated prior to measurements. Monitoring the effect of pH on zeta potential and hydrodynamic diameter was achieved by varying sample pH by auto-titration (MPT-2 titrator, Malvern, Worcestershire, UK) with 5 mM HCl and 5 mM NaOH as titrants. Aggregation rate measurements were conducted on aliquots of the polymer suspension pre-adjusted to the target pH quickly to control the potential for aggregation before reaching the higher pH values.

3.3.3 *K_d experiments*

Single point batch adsorption experiments were conducted according to Olshansky et al. (2022). An 80 $mg_{polymer}$ L^{-1} of 5 mM NaCl solution was brought to pH 6 using 5 mM NaOH. In a separate polypropylene (PP) bottle, a 50 ppm solution of PFOA and 5mM NaCl was brought to pH 6 with 5mM NaOH. Aliquots of 5 mL of the polymer solution, 34 mL of 5 mM NaCl, and 0.08 mL of the 50 ppm of PFAS solution were added to 40 mL polypropylene co-polymer (PPCO) tubes to reach concentrations of 10 mg L^{-1} of polymer and 1000 ng L^{-1} of PFOA. The tubes were agitated in an orbital, temperature-controlled shaker (Lab-line instruments, Melrose Park, IL, USA) at 80 rpm at room temperature (27 ±1 ºC) for over 48 h in darkness. The tubes were then centrifuged in an Evolution RC centrifuge (Kendro Laboratory Products, Reems Creek, CN, USA) at 45,000 RCF for 30 min and the supernatant solutions were filtered through a 0.22 µm polypropylene (PP)

`

syringe filters (EZFlow, Salem, NH, USA) for HPLC-MS/MS sample preparation. The remaining aliquot was used to confirm that pH remained at 6.0 ±0.4.

3.3.4 *Specific Surface Area by BET*

The specific surface areas (SSA) of polymers and sands were measured by BET N_2(g) absorption (Micromeritics, Gemini VII, Norcross, GA, USA). The polymers and sand were dried at 80 ºC under a constant stream of N_2 for >2 h to ensure sample dryness and degassed prior to measurement. Each sample was measured three times on a new aliquot each time.

3.3.5 *HPLC-QToF-MS/MS*

PFAS species quantification was conducted in the Arizona Laboratory for Emerging Contaminants (ALEC) using Liquid Chromatography Tandem Mass Spectrometry (LC-MS/MS), specifically with Quadrupole Time-of-Flight MS (Sciex TripleTOF 5600) and high pressure liquid chromatography (HPLC, Agilent 1200 Infinity) with a PTFE-free sample introduction system (5991-7863EN, Agilent, Greenville, DE, USA). Effluent samples collected from experiment columns were filtered through a 0.22µm PP syringe filters to collect a 1.5 mL aliquot in a PP microcentrifuge tube. A 30 µL aliquot of a 25 ppb internal standard mixture in 100% LCMS grade methanol (MeOH) was added to each sample tube and vortexed to ensure homogenization. The internal standards (Table 2) include isotopically labeled injection internal standards (IISA, EPA-533IS, Wellington Laboratories) and extraction internal standards (EISA, MPFAC24, Wellington Laboratories). The final target concentration of the standard in each sample aliquot was 500 ng L^{-1}.

Samples were then transferred into PP autosampler vials (Snap Ring Vial, DWK Life Sciences) for direct injection (large volume, 400 µL) through the dual needle multi-sampler. Chromatographic separation was achieved using a Gemini C18 column (100 mm × 2.0 mm, with 3 µm particle size) from Phenomenex (Torrance, AA, USA). Analytic parameters for each analyte can be found in Table 3.

The mobile phase was composed of (A) 20 mM ammonium acetate in LC−MS grade water and (B) MeOH. A constant flow of 0.5 mL min^{-1} was maintained. After 1 min, eluent A decreased from 90 to 20% over 17 min, then abruptly to 1% for 4 min to clean the column before returning to 90%, for 3 min equilibration. Negligible loss by adsorption to tubes, filters, and pipettes was confirmed using controls with known PFAS content. Mass spectrometer parameters included a capillary potential of −4500 V and a source and desolvation temperature of 550 °C.

`

Table 2. *List of LC-MS/MS QToF standards.*

CAS ID	Analyte	Extraction Internal Standards	Standard Acronym	Injection Internal Standards (IISA)
375-22-4	PFBA	Perfluoro-n-($^{13}C_4$) butanoic acid	M4PFBA	$^{13}C_3$-PFBA
375-85-9	PFHpA	Perfluoro-n-(1,2,3,4-$^{13}C_4$) heptanoic acid	M4PFHpA	$^{13}C_2$-PFOA
335-67-1	PFOA	Perfluoro-n-($^{13}C_8$) octanoic acid	M8PFOA	$^{13}C_2$-PFOA
375-95-1	PFNA	Perfluoro-n-($^{13}C_9$) nonanoic acid	M9PFNA	$^{13}C_2$-PFOA
375-73-5	PFBS	Sodium perfluoro-1-(2,3,4-$^{13}C_3$) butanesulfonate	M3PFBS	$^{13}C_4$-PFOS
355-46-4	PFHxS	Sodium perfluoro-1-(2,3,4-$^{13}C_3$) hexanesulfonate	M3PFHxS	$^{13}C_4$-PFOS
1763-23-1	PFOS	Sodium perfluoro-1-($^{13}C_8$) octanesulfonate	M8PFOS	$^{13}C_4$-PFOS
27619-97-2	6:2FTS	Sodium 1H,1H,2H,2H-perfluoro-1-(1,2$^{13}C_2$) octanesulfonate	M2-6:2FTS	$^{13}C_4$-PFOS

3.3.6 *Sonication*

Colloidal PANI was maintained in suspension by ultra sonication. Large volume PANI solutions (≥ 100 mL) were subjected to 10 min of sonication at 75% power using a 130 watt, 20 kHz ultrasonic processor. To prevent excess heating of the samples, the containers were placed in an ice bath for sonication. For smaller volume PANI solutions, including the 14 mL column effluent samples, sonication was limited to only 0.5 to 1 min at 75% power to prevent excess heating.

`

`

Table 3. Details of analytic parameters for each PFAS standards analyzed.

Analyte	Declustering Potential (V)	Collision Energy (V)	Precursor Ion (m/z)	Product Ion (m/z)
PFBA	-40	-13	212.98	168.99
PFHpA	-27	-14	362.97	318.99
PFOA	-53	-15	412.97	368.98
PFNA	-51	-16	462.96	418.97
PFBS	-12	-35	298.94	79.96
PFHxS	-35	-79	398.94	79.96
PFOS	-34	-78	498.93	79.96
6:2 FtS	-35	-33	426.97	406.96

3.3.7 *TOC measurements*

Polymeric PANI (synthesized from aniline monomers) structure consists of benzene rings linked by amine and imine moieties (Fig. 3). The total organic carbon (TOC) and total nitrogen (TN) for PANI were measured (ECS 4010 CNS Unit, Costech Analytical Technologies, Valencia, CA, USA) in triplicate and the average and standard deviation were used to quantify the presence of polymer in the solid phase and aqueous phase. Aqueous samples from column experiments were collected and sonicated prior to measurement for TOC and TN (TOC-L with TN module, Shimadzu). Samples were stirred and a wide bore needle was used to accommodate suspended polymer particles. TOC was calculated using the non-purgeable total organic carbon (NPOC) method. The injected samples were acidified with 1.5% H_3PO_4 and evolved CO_2 was purged by sparging with CO_2 free air to drive off inorganic carbon.

Solid phase measurements of TOC were performed on the ECS 4010 and the Vario Max Cube (Elementar Americas, Ronkonkoma, NY) through combustion with IR detection of combustion derived CO_2. Samples were dried over night at 100 °C and ground using a mortar and pestle to homogenize samples and ensure the grain size was < 100 μm.

3.3.8 *Aluminum hydroxide [$Al(OH)_3$] coating of sand*

Reagent silica sand was acid washed, rinsed to neutral pH and coated with $Al(OH)_3$ to create Al-Qtz using the method described in Vasquez-Ortega et al. (2014).

3.3.9 *PFAS extraction from polymer*

A 1% w/w NaCl in MeOH solution was stirred with a PTFE-free stir bar overnight in a PP bottle until dissolved. The column contents were emptied into a pre-weighed 40 mL PPCO tube with a known amount of the MeOH 1% NaCl solution. The PPCO tubes were rotated end over end at 8 rpm for ≥10 h. The PPCO tubes were then centrifuged for 30 min at 45,000 RCF. The supernatant was removed and filtered through a 0.22 μm syringe filter for LC-MS/MS analysis. Additional

`

`

MeOH 1% NaCl solution was added as a wash to the remaining contents of the PPCO tubes, rotated, and analyzed to maximize extraction of PFAS from the column contents in a second wash.

3.4 Column Experiments

Saturated flow-through experiments were performed to test cPANI's mobility, adhesion to the sand, and PFAS retention. Columns were pre-saturated with the NaCl background electrolyte concentration specific to each experiment prior to cPANI or PFAS infusion. Flow in and upward direction (against gravity) was used for the experiments unless explicitly specified (e.g., Exp. 3A and B were horizontal and down-flow, respectively). Flow was maintained with peristaltic pumps (Gilson Milspuls 3), Tygon Lab E-3603 tubing (Masterflex), PP or nylon connectors (Econo Pump Fitting Kit, BioRad Laboratories). The effluent and influent sample collection tubes were 15 mL PP non-sterile centrifuge tubes (VWR, 89049-172).

3.4.1 *Experiment 1*

Experiment 1 tested the hypotheses that cPANI adhesion on sand grains is pH dependent, whereas pH also alters species specific PFAS removal. This experiment was split into two stages (1A and 1B), starting with characterizing polymer mobility, adhesion and desorption followed by the monitoring of PFAS retention on the polymer-sand matrix. Columns for this experiment were 15 cm Flex Column™ (DWK Life Sciences, USA). The PP frit at the bottom was punctured and covered with a disc of 20 um nylon mesh to promote polymer movement while holding the sand in place. After packing with sand, another disc of nylon mesh was placed to hold the sand at the top of the column. Each column was prepared with 25.58 ± 0.01 g of sand with an average porosity of 0.40 ±0.02 and pre-saturated with DI water after packing. Each column had a total volume of 16.75 mL and an average pore volume of 6.8 ± 0.4 mL. The columns were assembled into three groups for experiments at pH 4, 6, and 9. Columns were conditioned with 5 mM NaCl to pre-saturated the media with the background electrolyte solution used throughout the experiment.

The goal of **experiment 1A** was to understand the effect of pH on polymer mobility and adhesion to sand. The cPANI was infused at 100 mg_{PANI} L^{-1} suspended in a 5 mM NaCl background electrolyte at 1 mL min^{-1} into triplicate columns for each of three pH treatments (nine columns total). The influent suspensions were sonicated and adjusted to the target pH using a 1 M NaOH or HCl. To maintain the suspension throughout the infusion process, the influent suspensions were stirred using PTFE-free stir bars. The pH of the influent and flowrate of the effluent were checked daily and adjusted as needed. Effluent samples were measured for cPANI breakthrough throughout the infusion process using the aqueous TOC/TN measurement method. The completion of experiment 1A after infusing ca. 1700 PV of the 100 mg PANI L^{-1} was determined by an unrecoverable drop in flow rate or rise in pressure. One column from each triplicate group was sacrificed for dissection at 1 cm increments using a glass cutter. The cPANI-sand at each cm increment was analyzed for TOC/TN as a function of distance. The remaining columns were infused with a 5 mM NaCl solution at each of the respective pH values to test the potential desorption of the polymer from the sand. Effluent samples were periodically collected, and TOC/TN measured.

`

In **experiment 1B**, an 8 μg L^{-1} total PFAS solution in 5 mM NaCl background electrolyte was infused into each cPANI loaded column from 1A above at a flowrate of 1 mL min^{-1}. The PFAS species in the influent solutions were PFBA, PFHpA, PFNA, PFOA, PFBS, PFHxS, 6:2-FtS, and PFOS, each at a target concentration of 1 μg L^{-1}. The PFAS solution was made from PFAS analytes included in Table 1. The PFAS mix concentrate was diluted in a 20 L HDPE tank with 5 mM NaCl solution. Effluent and influent samples were measured for PFAS concentration by LC-MS/MS. After ca. 6500 PVs the concentration of PFAS was increased by 10 x.

3.4.2 *Experiment 2*

Experiment 2 was designed to test the hypothesis that the surface charge of aquifer material and cPANI impacts adhesion of cPANI and subsequent PFAS removal. The cPANI was introduced to to cleaned sand (Qtz, negative surface charge) or Al-Qtz (positive surface charge) under a range of pH conditions (pH 4, 6, and 9) to test cPANI adhesion to aquifer material analogs and monitored PFAS removal. Borosilicate glass columns (17.5 cm) were packed and pretreated as Experiment 1. The columns had an average porosity of 0.39 ± 0.02, a total volume of 16.75 mL and an average pore volume of 6.6 ± 0.2 mL. Experiments at pH 4, 6, and 9 were performed in duplicate. The cPANI suspension concentration was 10 mg L^{-1} with a 1 mM NaCl background electrolyte to promote a stable suspension and reduce pressure within the columns. The influent suspensions were stirred as above during infusion and replaced regularly to ensure a consistent suspension concentration and that settling did not affect flow through the system. After the experiment, each column was dissected into 1 cm increments, as above, following polymer infusion for analysis of cPANI adhesion to the sand by monitoring solid state TOC/TN.

3.4.3 *Experiment 3*

Experiments 3A and 3B tested the hypothesis that cPANI advective flow over longer distances (1 m) would alter the infusion rate and polymer distribution along the flow path. The experiment used two 50 cm Kimble glass columns attached with a 1-2 cm section of Tygon® tubing to assess the cPANI mobility and loading over a 1 m distance. Columns for 3A and 3B were filled with uncoated sand and packed similarly to experiments 1 and 2. Filling the long, thin columns with dry sand proved difficult, and negatively impacted the packing homogeneity. It was determined that the best packing strategy, which minimized air pockets within the saturated column, was to fill the column with DI water and pour sand into the DI water allowing gravity settling to fill the column. As the volume of sand in the column rose, the DI water level was maintained by releasing the DI water from the column outlet until the sand reached the desired level. In both experiments the cPANI influent suspension was 10 mg L^{-1} in 1 mM NaCl background electrolyte at pH 4, which was stirred continuously. The influent suspension was placed in a borosilicate glass flask to reduce polymer adhesion to the influent vessel. Experiment 3A was run with the 1 m horizontal column to test lateral subsurface flow and minimize pressure within the column. Experiment 3B was set up vertically and the cPANI was infused from the top for downward flow through the sand matrix. Effluent samples in both experiments were collected and tested for cPANI breakthrough using the TOC/TN aqueous method. After steady state breakthrough, both columns were dissected at 2 cm increments and measured for cPANI adhesion to the sand using the TOC/TN solid state method.

`

3.4.4 *Experiment 4*

Experiments 4A and 4B tested the hypothesis that the PFAS removal capacity is dependent on the loading of cPANI to aquifer material, using Qtz and Al-Qtz. The 2 mL PP columns were layered with a nylon disc on the bottom, filled with a layer of sand with either 43 mg or 4.3 mg of polymer added, followed by another layer of sand and a 20 μm pore size PP frit at the top to prevent polymer loss. In experiment 4A, the adsorption of cPANI was compared to non-colloidal PANI (PANI) and FluxSorb IS (ADA technologies, Greenwood Village, CO) colloidal activated carbon (CAC) at a polymer loading of 20 $mg_{PANI}\ g^{-1}_{sand}$ in duplicate. The columns were infused with a 2.0 nM solution of each of the eight target PFAS (16 nM total PFAS) in a 1 mM NaCl background electrolyte at pH 6 at a flowrate of 1 mL min^{-1}. The PFAS influent solution was made from analytes included in Table 1. The packing and design of experiment 4B was similar to 4A with 10 x lower polymer loading of 2 $mg_{PANI}\ g^{-1}_{sand}$ and control Qtz and Al-Qtz columns with no PANI added. Visible loss of CAC from the beginning PVs prompted analysis of the effluent for CAC loss using the TOC/TN aqueous measurement method. The influent and effluent samples were measured for PFAS concentration.

3.4.5 *Experiment 5*

Experiment 5 tested the hypothesis that cPANI could efficiently remove PFAS from groundwater collected from three contaminated sites: 1) Site 5 and 2) Hangar B 680 in Willow Grove and 3) Tucson Water (Well C007A, ADEQ). The columns were packed as experiment 4A with only Qtz in duplicate for each of the 3 groundwaters tested. Due to the high potential for microbial growth in the natural groundwaters at room temperature, the influent water was filter sterilized through a 0.22 μm PP filter prior to infusion into columns and the system was kept dark to eschew photosynthetic growth. The effluent and influent samples were measured for PFAS concentration daily.

4. Results and Discussion

4.1 Synthesis and Characterization of polymers cPANI and cPOT

Following the method from Guo et al. (2011), spherical sub-micrometer to micrometer sized cPOT and cPANI were produced with apparent variability in size (Fig. 4-5). The reaction time and ratio of monomer, ammonium persulfate (APS, CAS 7727-54-0, Sigma Aldrich) and copper (II) chloride dihydrate ($CuCl_2 \cdot H_2O$, CAS 10125-13-0), were adjusted to optimize the polydispersity and zeta potential distribution (Table 4). Using the same monomer ratio and decreasing the reaction time had the effect of decreasing the size of the polymer particles, and the smallest hydrodynamic diameter was achieved using a 10 h reaction time for cPANI at pH 4 (Table 4).

Measurements of zeta potential for cPANI (Fig. 4a) and cPOT (Fig. 5a) show a circumneutral isoelectric point (IEP) for cPANI of pH 6.76 and an IEP for cPOT at pH 4.85. The hydrodynamic diameter of cPANI increased with increasing pH with the smallest diameter observed at pH 4 (Fig.

`

4b). Hydrodynamic diameter measurements for cPOT have high standard deviations for each measurement and all are above 2 µm (Fig. 5b).

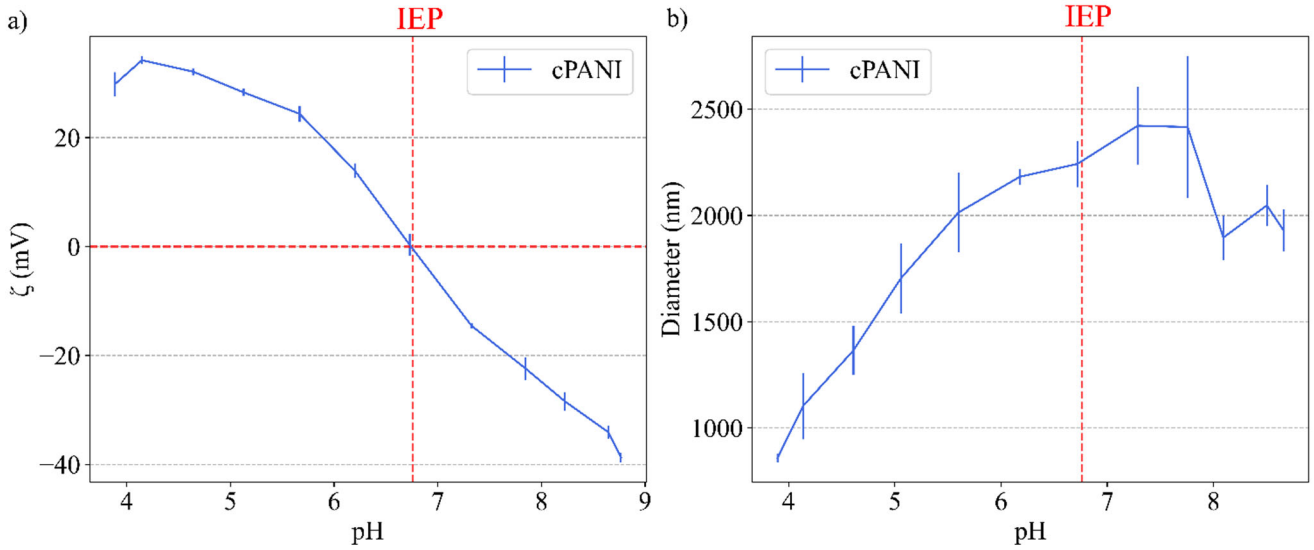

Figure 4. *Dynamic light scattering data for a) zeta potential and b) hydrodynamic diameter of cPANI as a function of pH. The pH at which the zeta potential vanishes is defined as the isoelectric point (IEP= 6.76). The error bars at each point represent the standard deviation of triplicate measurements at each pH.*

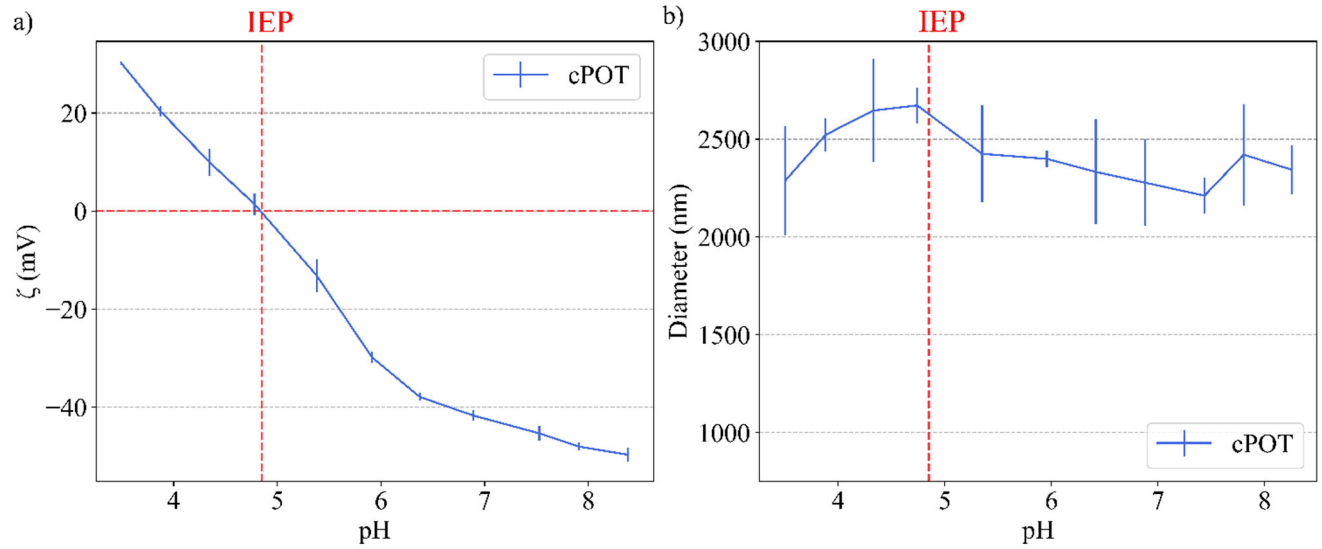

Figure 5. *Dynamic light scattering data for a) zeta potential and b) hydrodynamic diameter of cPOT as a function of pH. The IEP is 4.85. The error bars at each point represent the standard deviation of triplicate measurements at each pH.*

Table 4. *Summary of characterization data for cPANI synthesized at different reaction times.*

	Polymer	PANI	PANI	PANI	PANI
	8 An:8 APS:_ CuCl2	1	1	1	1
	Reaction Time	10 h	5 h	4 h	3 h
	Starting pH	4	4	4.5	5
Zetasizer Data	IEP	6.8	5.1	5.1	3.8
	Diameter at pH4 (nm)	600-800	2090	1225	1250
	Diameter at pH6 (nm)	1300-2200	1820	1200	1000
	Diameter at pH8.5 (nm)	1300-2200	1820	1100	1100
	ζ at pH4 (mV)	30-35	30	21	25
	ζ at pH8.5 (mV)	-38	-45	-48	-43
SEM	Size (nm)	600-800	600	400	400
	Image	5a	5b	5c	5d

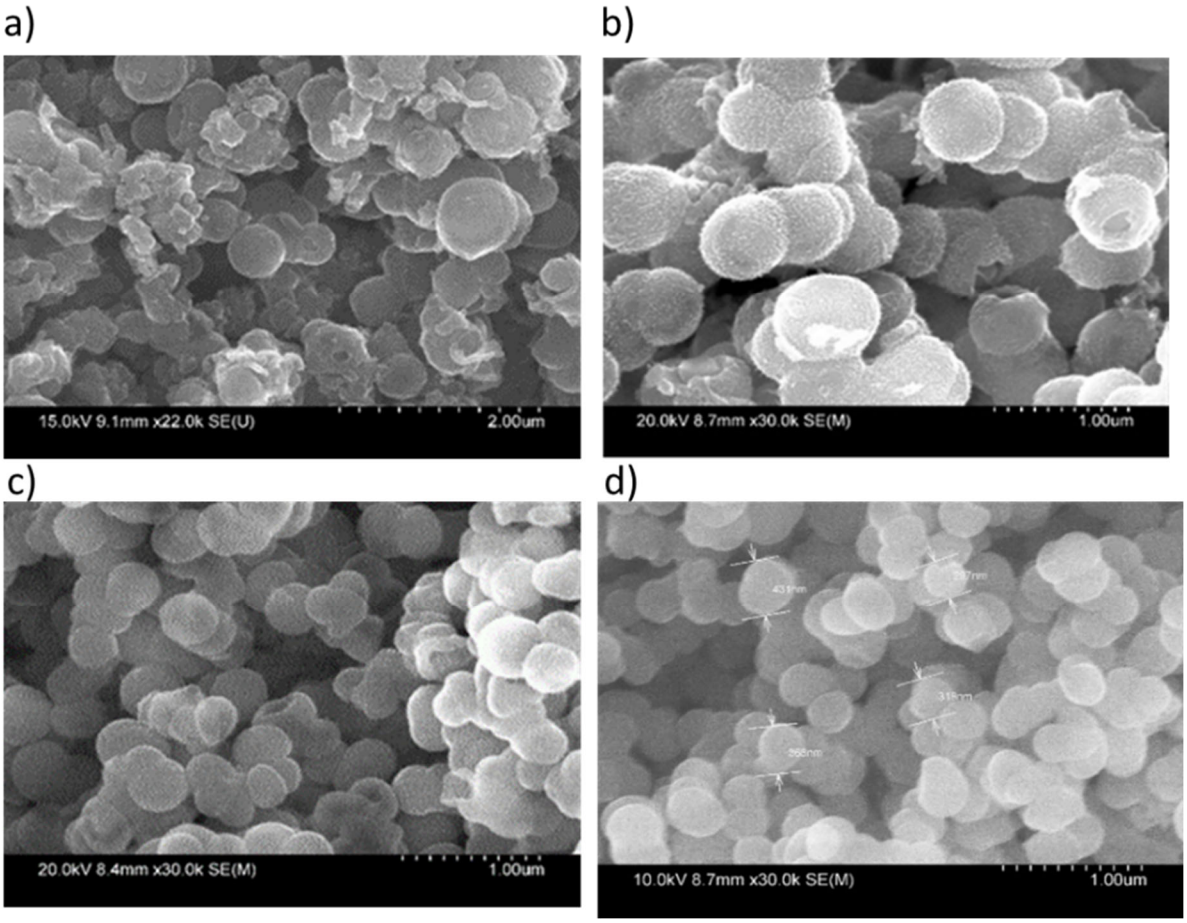

Figure 6. *SEM micrographs of cPANI with a reaction time of a) 10 h, b) 5 h, c) 4 h, and d) 3h.*

Table 5. Summary of characterization data for cPOT synthesized at different reaction times.

	Polymer	POT	POT	POT
	8 An:8 APS:_ CuCl2	1	1	1
	Reaction Time	10 h	4 h	3 h
	Starting pH	3.5	4	5
Zetasizer Data	IEP	4.9	5	3.7
	Diameter at pH4 (nm)	2550	1550	1375
	Diameter at pH6 (nm)	2375	1750	1280
	Diameter at pH8.5 (nm)	2350	3250	1255
	ζ at pH4 (mV)	18	20	-10
	ζ at pH8.5 (mV)	-50	-36	-47
SEM	Size (nm)	600-1000	300-2000	600-800
	Image	6a	6b	6c

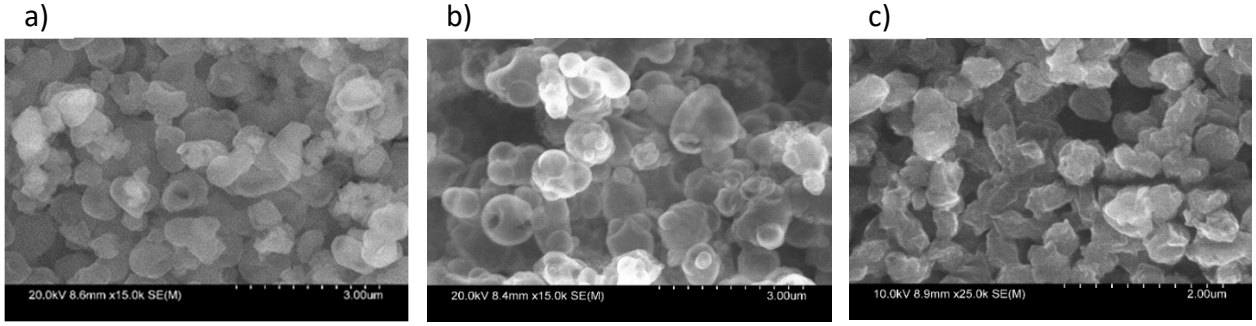

Figure 7. *SEM micrograph images of cPOT with a reaction time of e) 10 h, f) 4 h, and g) 3 h.*

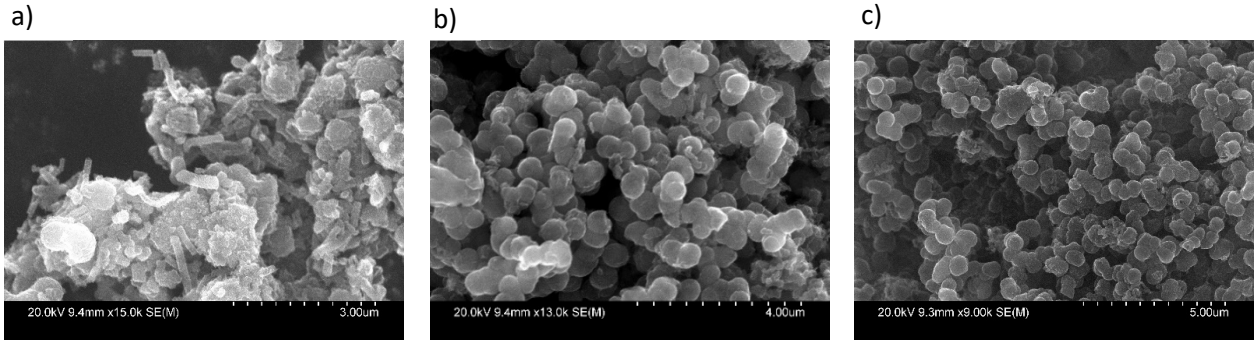

Figure 8*. SEM micrographs with different molar ratios of $CuCl_2$ to Aniline and APS at the same reaction time. a) 8 aniline: 8 APS: 0.25 $CuCl_2$; b) 8 aniline: 8 APS : 2 $CuCl_2$; c) 8 aniline: 8 APS : 4 $CuCl_2$.*

Varying the $CuCl_2 \cdot 2H_2O$ concentration affected the morphology of the cPANI (Fig. 8 a-c). Fusion of individual spherical particles increased with increased $CuCl_2 \cdot 2H_2O$. Decreasing the amount of $CuCl_2 \cdot 2H_2O$ produced multiple morphologies including tubes, sheets and unstructured particles (e.g., Fig. 8 a).

The particle hydrodynamic diameter measurements reveal the diameter of the suspended particles and aggregates as a function of pH and time. As the absolute magnitude of the zeta potential (± ζ mV) decreased and the pH approached the IEP, the interparticle electrostatic repulsion was reduced allowing aggregation to proceed due to attractive van der Waals interactions (Fig 9). The hydrodynamic diameter measurements for cPANI show an increase in diameter with increasing pH, suggesting larger particles due to aggregation (Fig 9b). The hydrodynamic diameter of the particles at pH > IEP might be expected to decline with the same slope as the rise at pH < IEP (Fig 9b) but an increase in pH is apparently not sufficient to disperse aggregates once they have formed in the absence of sufficient shear forces. This contention is supported by the need to sonicate for proper dispersion of the polymer particles in water, and an observed decrease in the hydrodynamic diameter with increasing initial sonication time (Fig. 9).

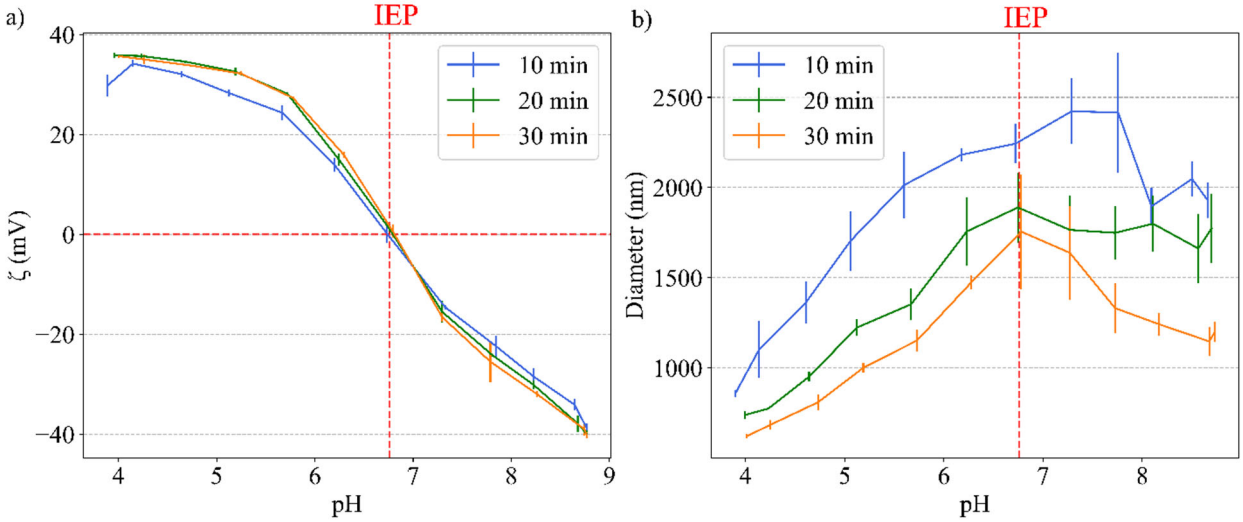

Figure 9*. a) The effect of increasing sonication time on zeta potential of cPANI as a function of pH. b) The effect of sonication on hydrodynamic diameter of cPANI as a function of pH. Blue symbols show 10 min sonication, green shows 20 min, and orange shows 30 min. The error bars at each point represent the standard deviation of triplicate measurements at each pH.*

4.2 K_d experiment

For direct comparison, non-colloidal PANI (PANI), previously synthesized and studied in SERDP project ER18-1052, was tested along with the cPANI and cPOT produced for this study that used various synthesis reaction times. At pH 6.0 ± 0.2 , PANI has Q_e of 101.16 ±0.58 ng_{PFOA} / $mg_{polymer}$, a K_d of 20.72 ±8.12 L mg^{-1}, and a removal efficiency of 99.47 ± 0.18% from a 50 ppb PFOA solution. As the synthesis reaction time decreases, the Q_e, K_d, and removal efficiency of cPANI and cPOT likewise decreased (Fig 10). cPOT performed less effectively than cPANI at its highest

synthesis reaction time of 10 h. cPANI with a 10 h reaction time had a Q_e of 98.34 ± 0.62 ng_{PFOA} / $mg_{polymer}$, a K_d of 4.11 ± 0.79 L mg^{-1}, and a removal efficiency of 97.59 ± 0.42%. The difference in the removal efficiency between the cPANI and PANI is -3.57 ± std%. cPANI with a 10 h reaction time had a specific surface area (SSA) of 29.97 ± 0.22 m^2 g^{-1} which is similar to that of PANI (26.3 m^2 g^{-1}; He et al. 2022) suggesting similar trends between PFOA removal normalized to SSA and those previously found for PANI (adsorption capacity of PFOA on PANI > PAC when normalized to SSA; Olshansky et al. 2022). For cPOT, the removal efficiency was 70.24 ± 5.26 % for the 10 h reaction time and 57.72 ± 8.28% for the 3 h reaction time.

A higher K_d indicates greater adsorption of PFAS onto the polymer at a given aqueous phase equilibrium concentration. Due to the relatively lower size variability, spherical uniformity, and higher removal efficiency of cPANI compared to cPOT, subsequent experiments focused on cPANI.

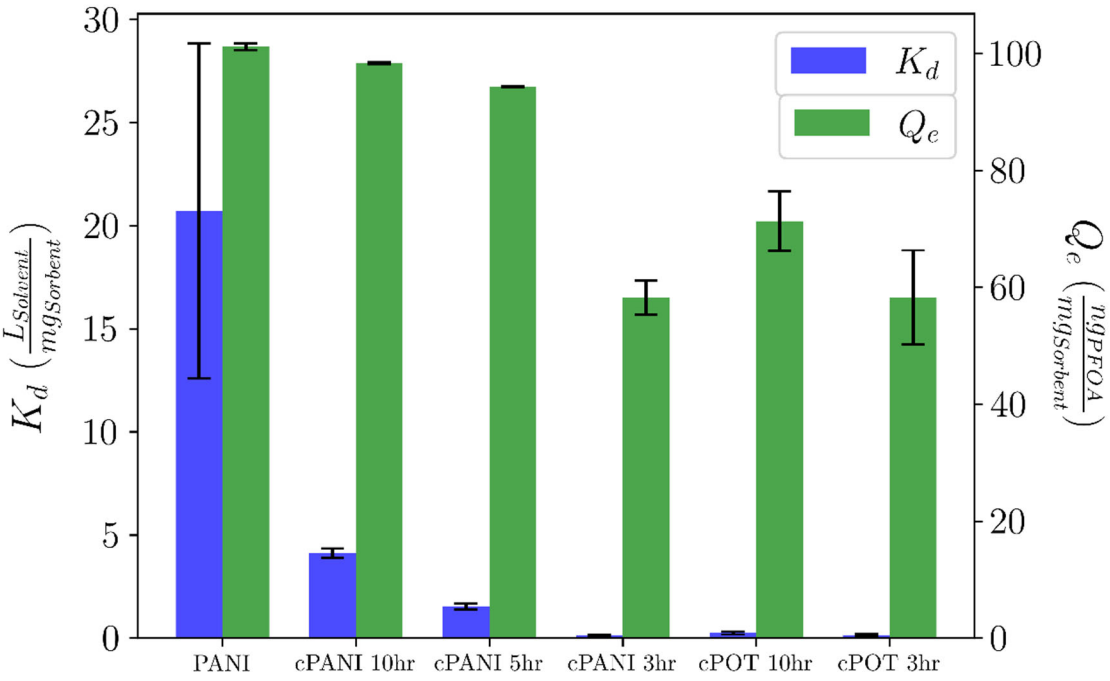

Figure 10. *K_d and Q_e values for PFOA between products of different synthesis reaction times for cPANI and cPOT as compared to PANI synthesized in Olshansky et al. (2022) as part of SERDP project ER 18-1052. The error bars at each point represent the standard deviation of triplicate samples.*

4.3 Zeta potential, hydrodynamic diameter, and aggregation rate

The aggregation rate as a function of pH and zeta potential have a concave down parabolic relationship with the lowest rate measured at pH 9 (ζ ~ -40 mV) and the highest measured rates, near the IEP (pH 6.76), at pH 6 (ζ ~ -15 mV) and pH 7 (ζ ~ -10 mV) over the 30 min measurement

timeframe (Fig. 11). Injectability of cPANI is controlled by the size (< 1 um) and stability of the suspension. A stable suspension of pure polymer depends on the balance between the electrostatic and van der Waals interactions among polymer particles. If the electrostatic repulsion forces are weakened due to lessening of charge in a circum-neutral pH solution, the van der Waals interactions can dominate leading to aggregation and making it difficult for the polymer to be effectively injected and travel between sand grains (DLVO theory). Due to the difference in aggregation rates with pH, the performance of infusions of cPANI at pH 3, 5, 6, 7, and 9 were tested at two different levels of influent concentration.

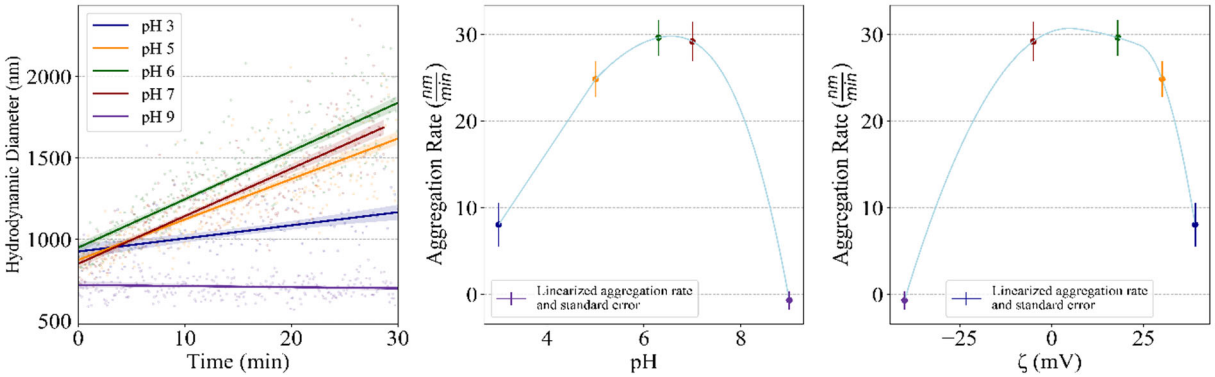

Figure 11. *a) Hydrodynamic diameter of cPANI over time at different pH values, linearized aggregation rate as a function of b) pH and c) zeta potential. The error bars at each point in b) and c) represent the standard error of the slope of each regression line in a).*

4.4 Experiment 1A

The effluent cPANI concentration of each column was averaged with its replicates (n=3) and the average was then normalized to the average influent cPANI concentration for the respective influent suspension pH (pH 4, 6, or 9).The average normalized effluent concentrations of cPANI from columns infused with cPANI suspensions at pH 4, 6, and 9 remain well below 1 indicating no breakthrough of cPANI was achieved (Fig. 12).

The loading of the cPANI showed a declining load trend with distance from the inlet and infusion point of the column for each of the three pH groups. Loading in the pH 4 and 9 columns showed greater loading further into the column compared to pH 6 after common behavior to about 5.5 cm.

Under constant infusion of cPANI over thousands of pore volumes, the average C/C_0 of cPANI in the effluent stayed below about 0.22 for the columns infused with pH 4 and 9 indicating significant retention of the cPANI on the sand medium. The influent concentration of cPANI in each of the three pH groups was intended to be 100 mg L^{-1}. To mitigate aggregation related, the suspensions were constantly and vigorously stirred, but due to the high concentration of the cPANI in the suspension, stirring, and the length of time between changing the influent suspension, some aggregation and settling was observed, which decreased influent concentrations. Average influent

concentrations were measured to be 39.73 ± 12.41 mg L^{-1} for pH 4, 65.27± 23.82 mg L^{-1} for pH 6, and 64.96 ± 21.77 mg L^{-1} for pH 9.

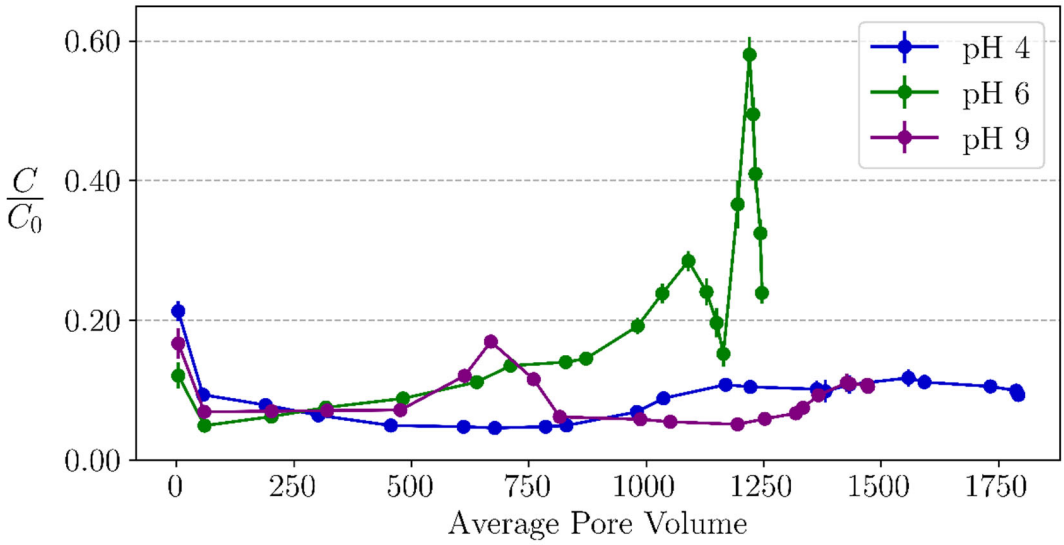

Figure 12. *cPANI average breakthrough for each set of triplicate columns infused with pH 4, 6, or 9 cPANI suspension. The vertical lines at each point represents the standard deviation of mean values of the triplicate columns. The points of each line represent the average of the triplicate columns infused with distinct pH of cPANI suspension.*

Particle aggregation caused some high-pressure problems due to clogging within the columns, but only at the end of the experiment when the columns were already heavily loaded with cPANI especially near the inlet (Fig. 13). Higher magnitude of cPANI surface charge enhanced colloidal stability pH 4 and 9, which decreased inlet aggregation, thereby allowing the cPANI to travel further down the column before adhering to the sand particle surfaces. Longest migration distances were observed for cPANI at pH 4 (ζ = 40 mV, Fig 11c). Sand adhesion resulted in low breakthrough of the cPANI at pH 4 (Fig 12) and the loading of the cPANI at greater distance through the sand column under the pH 4 infusion. The lower loading with distance of cPANI infused at pH 9 is attributable to charge repulsion between the negatively charged sand and cPANI (ζ = -40 mV, Fig 11). The influent suspension at pH 6 was subject to the most aggregation as expected with the comparatively high aggregation and the low magnitude of zeta potential close to the IEP (Fig 10). In order to maintain the 1 mL min^{-1} flow rate, the tubing was changed periodically towards the latter pore volumes and the inlet was cleared of excess cPANI buildup. The spike in cPANI in the effluent at about 1200 latter pore volumes (Fig. 12) is most likely due to some dislodging of cPANI from the column during increased inlet pressure required to maintain influent flow.

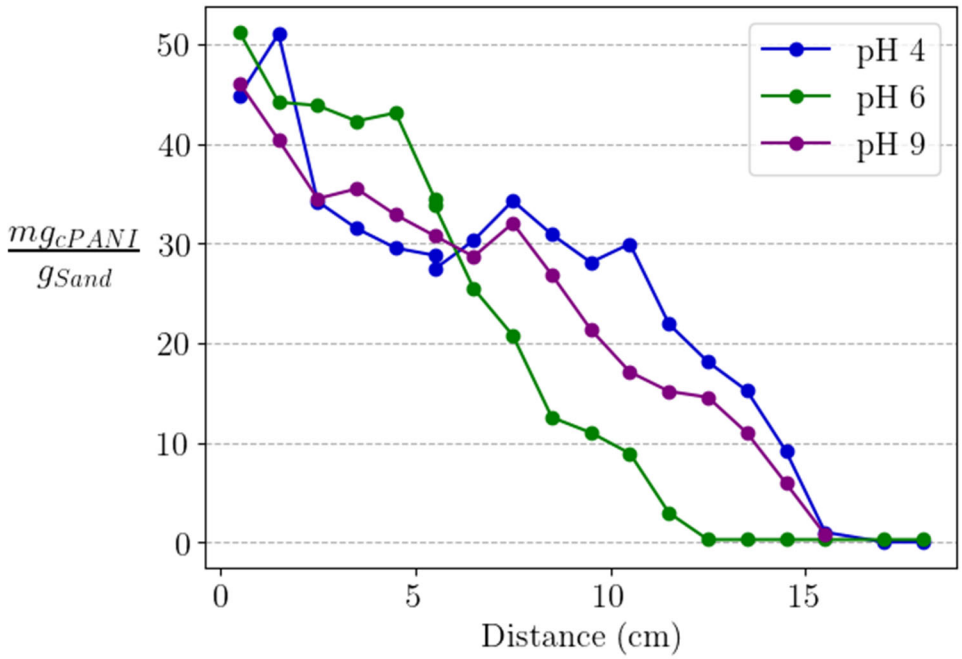

***Figure 13**. cPANI loading on sand at 1 cm increments along the length of one of the triplicate columns to represent the loading with distance for the respective triplicates infused with a pH 4,6 or 9 cPANI suspension of 100 mg L^{-1}.*

Despite pressure issues towards the end of the cPANI infusion experiment, the infusion into cPANI retained columns of cPANI-free background electrolyte solution at the corresponding pH (4, 6, and 9) immediately resolved the flowrate without significant loss of cPANI. The loss of cPANI from the columns during the 5 mM NaCl infusion was minimal (55 ± 1 mg, 43 ± 1 mg, and 66 ± 16 mg for pH 4, 6 and 9 respectively) over >2500 PV.

The average influent concentration for each column was integrated over the total number of PV delivered to the column to calculate the total mass of cPANI injected to the columns. The total cPANI loaded was subtracted from the integrated effluent concentrations for each column to find the total cPANI retained on the sand surface. The calculated retained cPANI was normalized to the amount of sand added to each column and the loadings were averaged between each set of replicate columns. The mass balance calculated loadings showed the highest average loading at pH 9 and a similar average loading between pH 4 and pH 6 infusion, though these differences were likely not significant. The solid phase loading measured by dissection shows the highest average loading at pH 4 and the lowest average loading at pH 6, with overlapping error bars (Fig. 14).

For both loading measurements, the cPANI was shown to be over 10 $mg_{cPANI}\ g_{Sand}^{-1}$ for all three pH columns. The loading at pH 4 seemed underestimated due the low measured average concentration of the infusion suspension, thereby decreasing the amount of PANI introduced to the columns. The solid phase measurement gives a more direct, reliable, and consistent result of the cPANI behavior at each of the pH values.

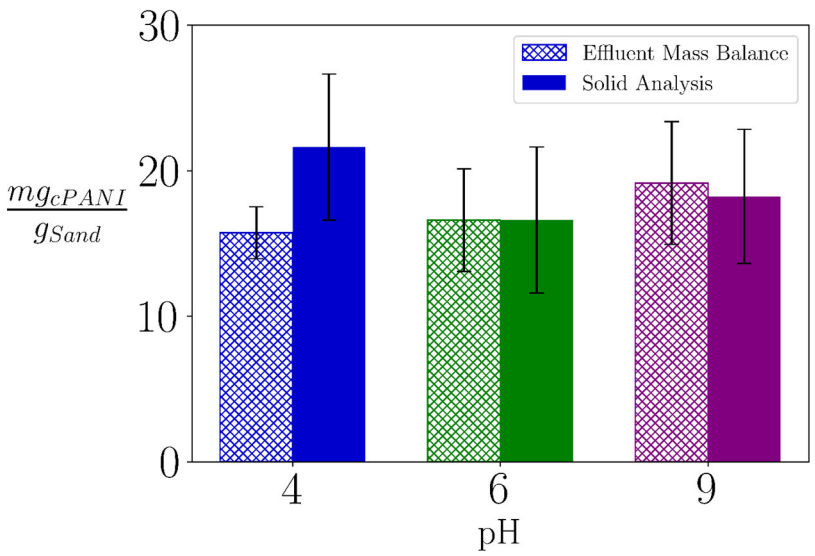

Figure 14*. Comparison of cPANI loading per gram of sand from (i) the average effluent concentration for each group and (ii) the solid phase dissection of a sacrificed column from the triplicates in each group. The error bars for the effluent mass balance values represent the standard deviation of the mean measured from triplicate columns. The error bars for the solid analysis represent the propagated standard error for each column.*

4.5 Experiment 1B

The two undissected columns from experiment 1A were subsequently infused with PFAS solutions to test the efficacy of the polymer in a saturated flow through system. The measured effluent concentrations were normalized to the average influent concentration (1 and, later, 10 µg L^{-1}) for each of the eight PFAS species. PFBA reached complete break through ($C/C_0 = 1$) within in the first 1000 PV whereas the other seven PFAS test species were retained by over 90% in the columns for over 6000 PV. To stress test the polymer capacity, the concentration of each PFAS species was then increased by 10 x. After several hundreds of PV of the 80 ppb total PFAS solution, the effluent concentrations remained well below C_0 for most species except PFBA. Similar to previous studies, the results show that adsorption increases with chain length within each group of PFAS, PFSA, and PFCA, (Olshansky et al. 2022; He et al. 2022) with the exception of PFOA and 6:2-FTS at higher pore volumes. This occurs near the same number of PV as the C/C_0 decrease for PFHxS for each column set's results. The PFSA showed higher adsorption than PFCA with the same chain length, excluding PFOA and 6:2-FTS at later PVs.

It is expected that after cPANI is injected at a targeted pH into a field-site and sorbed to the aquifer material, the pH of the groundwater would buffer to the system back to circumneutral pH. This stage of the experiment was designed to mimic the circumstances of polymer injection in the field by infusing the PFAS solution at pH 6. In the early PV the cPANI showed slight adsorption of PFBA but quickly equilibrated with the influent concentration and PFBA adsorption was diminished. The rest of the PFAS species showed much better adsorption at over 90% across thousands of PV's, even when influent concentrations were increased by ten times C_0. The behavior of PFOA and 6:2-FTS at later PV's can be explained by competitive adsorption.

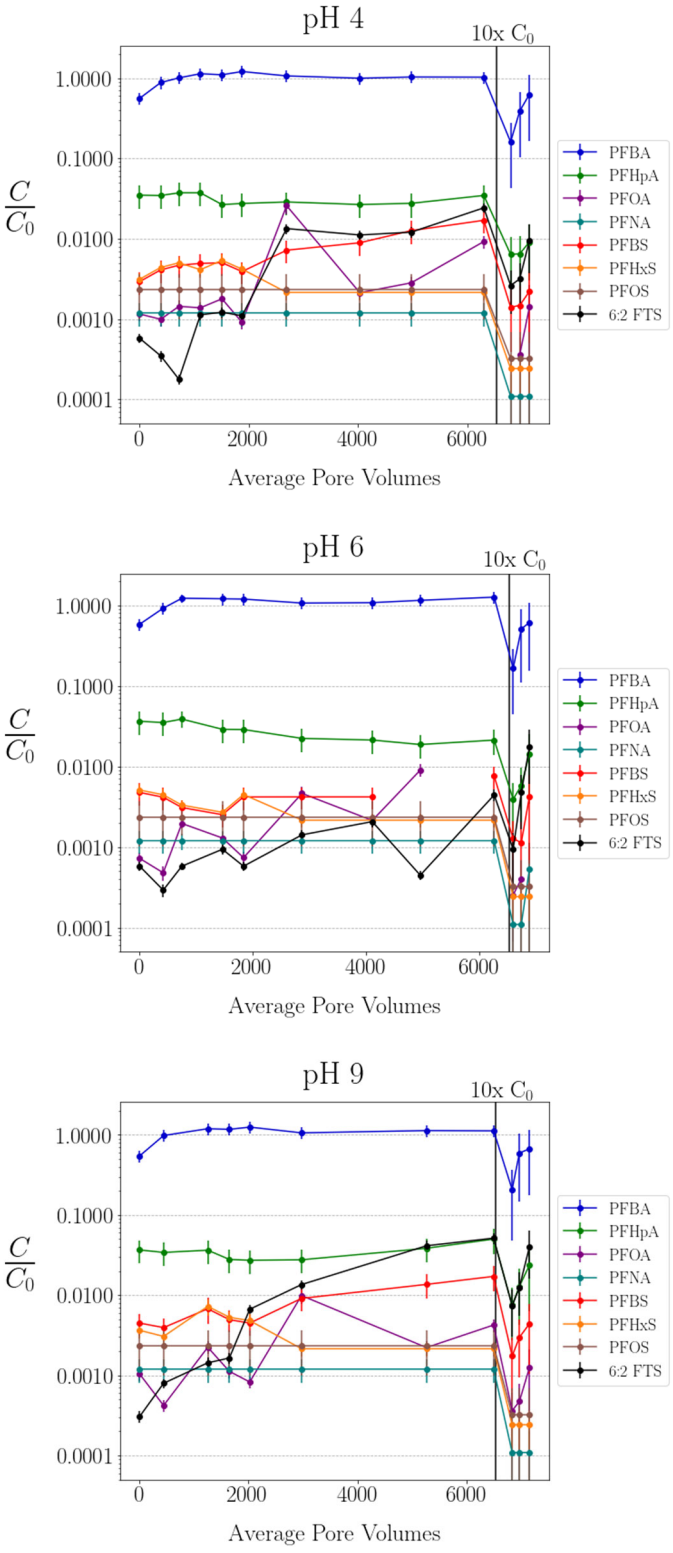

***Figure 15**: PFAS breakthrough following infusion into the a) pH 4, b) group 2 = pH 6, and c) group 3 = pH columns 9 from experiment 1A. The error bars at each point represent the standard deviation of triplicate samples. The vertical line labeled "10x C_0" represents the pore volume when the columns were infused with influent spiked to ten times the original concentration at time zero (8 ng L^{-1} to 80 ng L-1 of total PFAS).*

`

Because the columns were infused with a continuous supply of PFAS, the PFOA and 6:2-FTS were competitively concept. Because the columns were infused with a continuous supply of PFAS, the PFOA and 6:2-FTS were competitively displaced from active sites by more strongly adsorbing PFAS species.

4.6 Experiment 2:

This experiment tested the influence of sand surface charge by employing the Qtz versus Al-Qtz comparison. The effluent sample concentrations (C) are shown normalized to the 10 mg_{cPANI} L^{-1} (C_0) influent suspension concentration for each sample and column. Aqueous cPANI effluent data from the duplicate columns in each pH group and sand type were averaged and standard deviations

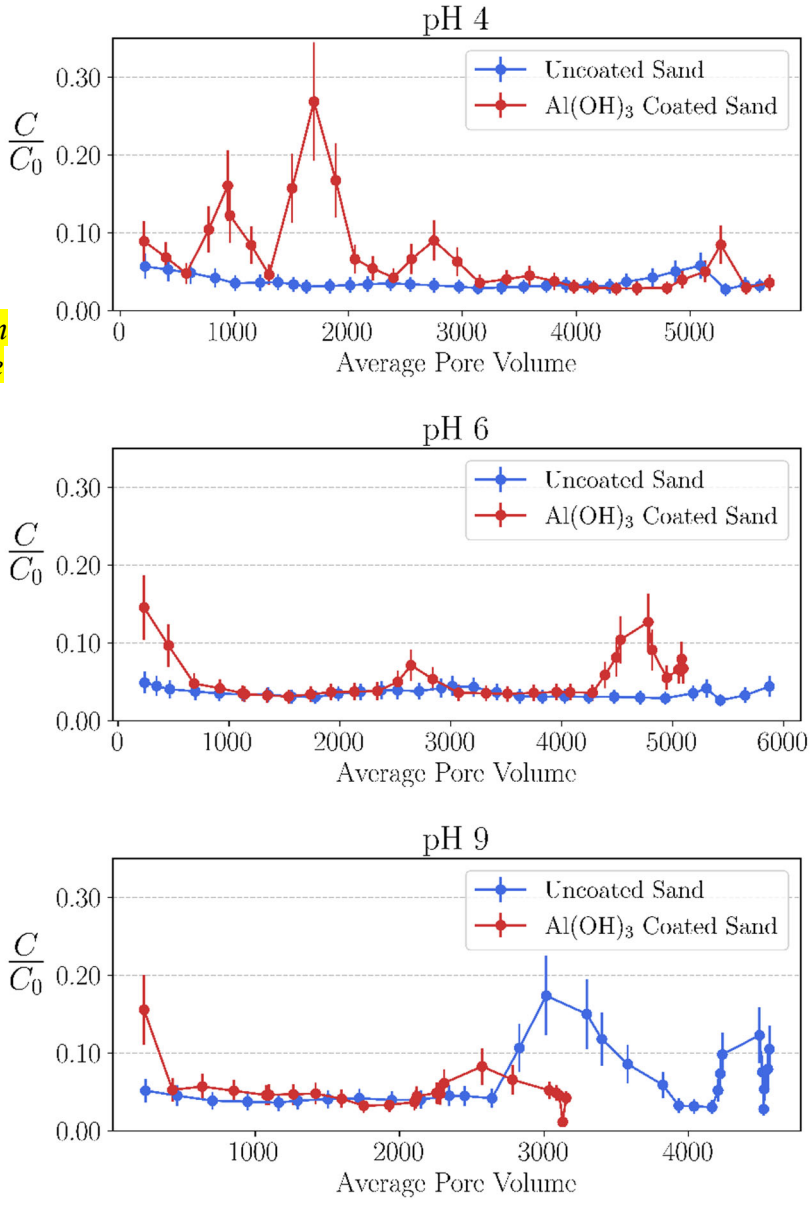

***Figure 16**. Comparison of cPANI average breakthrough from duplicate columns of two types of sand infused at a) pH 4, b) pH 6, and c) pH 9. The error bars at each point represent the standard deviation of measurements from duplicate samples.*

`

of duplicate samples are depicted by the error bars. Experimental progress is shown as PV to compensate for any flowrate differences due to column backpressure. Despite the pH of the influent solution or the charge of the sand matrix, the C does not approach C_0 in either case, which indicates cPANI adhesion to the sands. For columns with influent pH of 4 and 6, the cPANI effluent concentrations were generally lower in the Qtz columns relative to the Al-Qtz columns for the duration of the experiment (Fig. 16).

The mass of cPANI recovered following dissection and forensic analysis of duplicate columns was averaged and plotted as mg of cPANI per gram of sand as a function of distance along the column flowpath. The inlet was assigned distance zero and the outlet was at a distance of 17.5. The 1 cm sections are plotted at their midpoint (Fig. 17). In both sand types, the trend of cPANI adhesion decreases with distance with the highest loading near the inlet and decreased with distance.

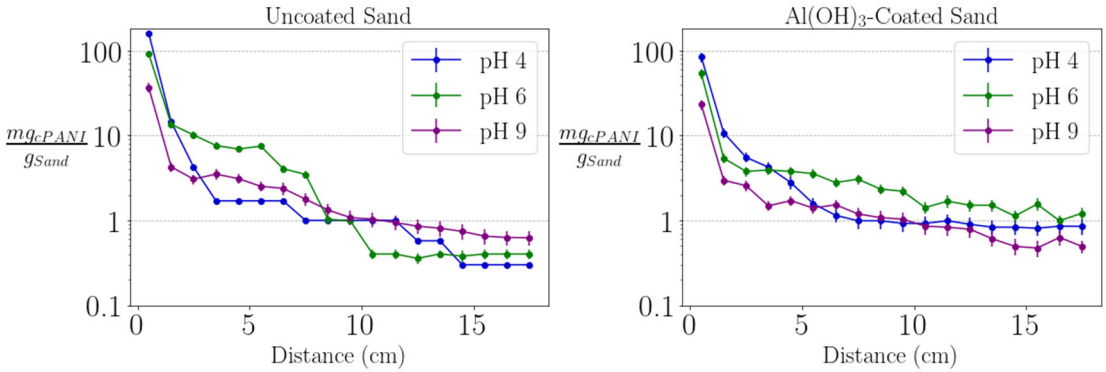

Figure 17*. Comparison of the average loading of cPANI on a) uncoated sand and b) aluminum hydroxide coated sand with distance for the three influent suspension pH's. The error bars at each point represent the standard deviation of duplicate samples.*

Loadings were also calculated by integrating across the effluent data for mass balance retention within the column. Results from the aqueous and solid phase data sets are in good agreement for pH 6 and 9, but pH 4 aqueous measurements yielded a lower average loading than measured in the solid phase (Fig. 18). The average cPANI loading was higher in Qtz than Al-Qtz columns, consistent with higher surface charge repulsion effects in the latter. According to the solid phase data, the average loading of cPANI on both sand types is highest at pH 4 and decreases with increasing pH. The pH 4 suspension yielded around 11.0 mg $_{cPANI}$ g^{-1}_{Sand} loading on negatively charged uncoated sand and around 5.5 mg $_{cPANI}$ g^{-1}_{Sand} loading on positively charged $Al(OH)_3$-coated sand (Fig. 18).

The loading measurements were consistent with the trend observed in experiment 1A (Figs. 14 and 18); however, the average loading in uncoated sand for experiment 2 is less than the average loading for each pH in experiment 1A. This is attributed to the ten-fold reduction in the cPANI in the influent for experiment 2 relative to experiment 1. Nonetheless, the loading of the cPANI onto

`

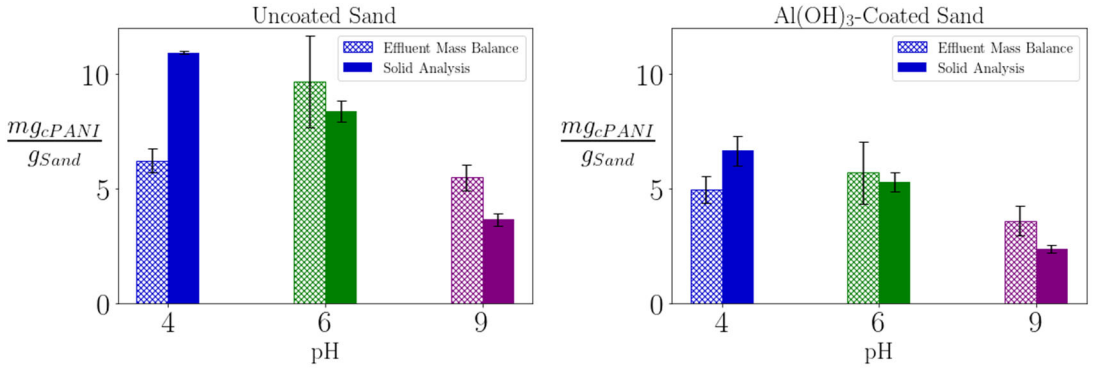

Figure 18. *Average cPANI loading to sand columns calculated from effluent mass balance and solid dissection. The error bars represent the standard deviation of duplicate columns*.

both sand types is efficient and high relative to loadings reported previously for colloidal activated carbon. The trends with pH and sand type are consistent with electrostatic interactions between the charged cPANI and the charged matrices. As shown in Fig. 4a and discussed in previous sections, the IEP of cPANI is around pH 6. Near the IEP, cPANI-cPANI electrostatic repulsion is minimized and cPANI aggregation rate is highest. The higher aggregation of polymer particles may explain why the loading for pH 6 is higher than that of pH 9 in both sand matrices because cPANI-cPANI aggregation may occur within the sand matrix leading to increased cPANI adhesion, even to c-PANI coated sands. At pH 4 the cPANI is positively charged and is attracted to the negatively charged Qtz while being subjected to greater Al-Qtz repulsion. Since the coating of the $Al(OH)_3$ is not complete (Fig. 19), the repulsive effect between sand and polymer would be restricted to the locations of the coating, which was observed to be patchy, but hydrophobic interactions and negatively charged uncoated surfaces would still promote cPANI adhesion, even in the Al-Qtz case.

Significant adhesion of cPANI to Qtz at pH 9, where the cPANI is negatively charged, is not fully explained by electrostatic interactions between the sand and polymer. However, as predicted by XDLVO theory, colloids will adhere to like-charged deposition surfaces because of attractive van der Waals interactions, which can overcome electrostatic repulsion. The slight discrepancy between the loading calculations from aqueous and solid-phase datasets are mostly within the margin of error, and influent solution concentrations may vary with time because of cPANI aggregation in the influent reservoir. In any case, the lower cPANI suspension concentration of experiment 2 relative to experiment 1, along with the lower ionic strength, resulted in a column lifetime that was extended due to promotion of conditions less favorable for cPANI settling and aggregation. This informs on conditions that are likely to be most suitable for *in situ* deployment as well.

`

`

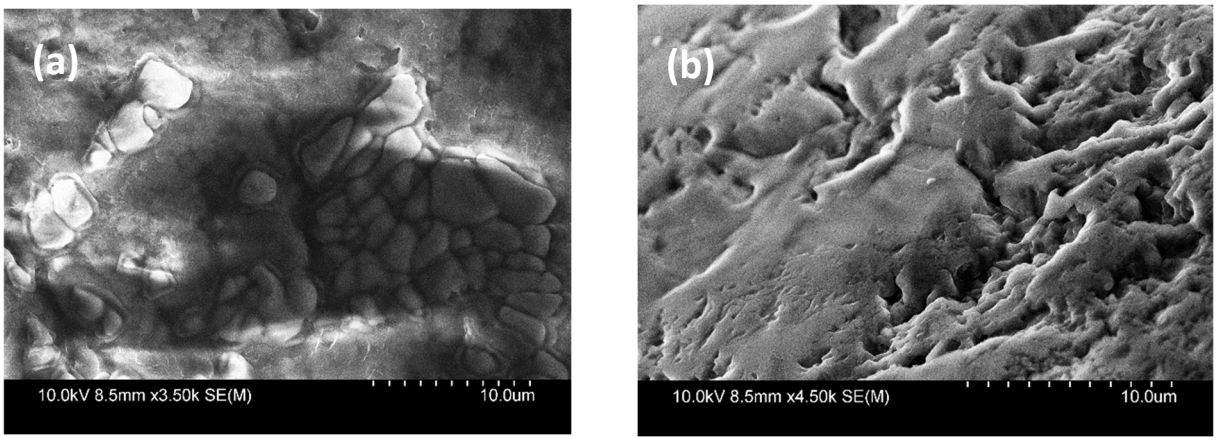

Figure 19*. SEM micrographs of the surface of sand particles on the a) aluminum hydroxide coated sand and b) uncoated sand. The aluminum hydroxide coated sand (a) has nodular texture from the aluminum hydroxide compared to the surface of the plain sand (b). The bright and dark areas in a) are due to charging of the sand surface caused by the patchiness of the aluminum hydroxide coating.*

4.7 Experiment 3A and 3B

The loading with distance in experiment 3A (horiz. flow) and experiment 3B (down flow) in meter long columns show a similar decline of cPANI loading with distance (Fig. 20) as that observed in experiments 3 and 1A (Fig. 17 and Fig. 13). The loading of the cPANI stays above 0.1 $mg_{cPANI}\ g^{-1}_{Sand}$ across the full 1 m distance suggesting a significant amount of cPANI moving through the matrix is still adhering to the sand at greater distances.

Because characterizing and optimizing cPANI mobility in porous sand media were key objectives for this project, the two part experiment 3 aimed to test cPANI mobility and adhesion over a longer injection distance. The 1 m distance mimics the spatial range that cPANI should travel from an injection borehole to prevent a backpressure development that would reduce injection effectiveness. Although the high injection pressures used under field conditions could not be replicated in the laboratory, our findings suggest that with higher injection pressure, and associated sheer force, the cPANI would advect further than in these bench-scale experiments conducted with a flowrate of 1 mL min-1. Despite the lower injection pressures in our experiments, the results from the 1 m columns in both flow regimes show that the cPANI transports and distributes similarly but at greater length scales than in the previously tested 17.5 cm columns.

Experiment 3A revealed a preferential flow path that developed at the top of the horizontally positioned column due to some settling of the sand under gravity. This preferential flow path allowed the cPANI to adhere mostly towards the top of the column and therefore get transported further down the length of the column than expected causing the slight increase in cPANI loading past 50cm.

`

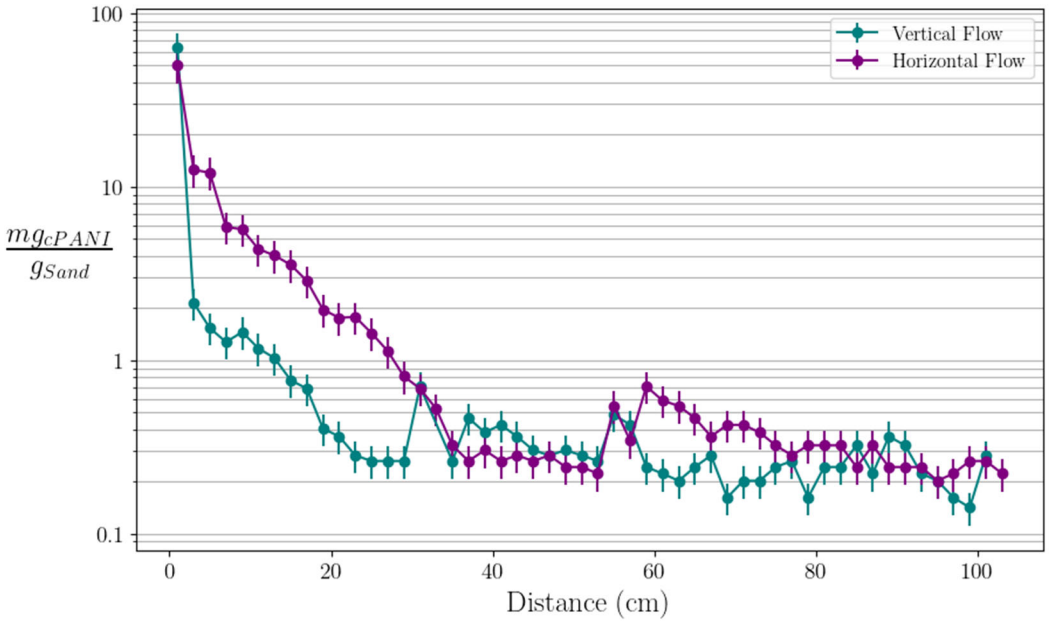

Figure 20. *cPANI loading distribution across a 1 m distance in horizontal and down flow regimes.*

4.8 Experiment 4A and 4B:

The purpose of experiments 4 was to capture the loading of different PFAS species on the cPANI compared to PANI and a colloidal activated carbon (CAC, Filtrasorb, ADA Technologies, USA). Two loadings of cPANI to sand were chosen to capture an average behavior at 20 $mg_{polymer}\ g^{-1}_{sand}$ and a lower behavior at 2 mg polymer g^{-1}_{sand} with two sets of control columns packed with each sand type (n=28). The CAC was delivered from the manufacturer as an aqueous suspension with 150 g kg^{-1} as CAC and 30 g kg^{-1} as sodium carboxylmethlycellulose (CMC) in DI water. Packing of the columns with CAC accounted for the carbon in CMC so as to ensure an equivalent mass of CAC in CAC columns as cPANI and PANI in the PANI columns. To overcome the difficulty in packing columns with an exact amount polymer with uniform mixing, we created a bed of polymer between sections of sand. The columns were saturated with an infusion of 1 mM NaCl solution at pH 6. The data from the duplicate columns were averaged for all the specific polymers, loadings, and sand types. Measurements of the influent and effluent solution showed anomalously high results for C/C_0 ratios for several of the PFAS species over the experiment (Fig. 21 and 22). For all of the polymer treatments and sand types, the columns reached C_0 within ca. 5000 PV. This is a behavior that we attribute to the development of preferential flow paths that may bypass unreacted polymer. The low influent concentrations for PFAS species, specifically PFOS, could

be attributed to insufficient mixing in the influent tanks.The low influent concentrations for PFAS species, specifically PFOS, could be attributed to insufficient mixing in the influent tanks.

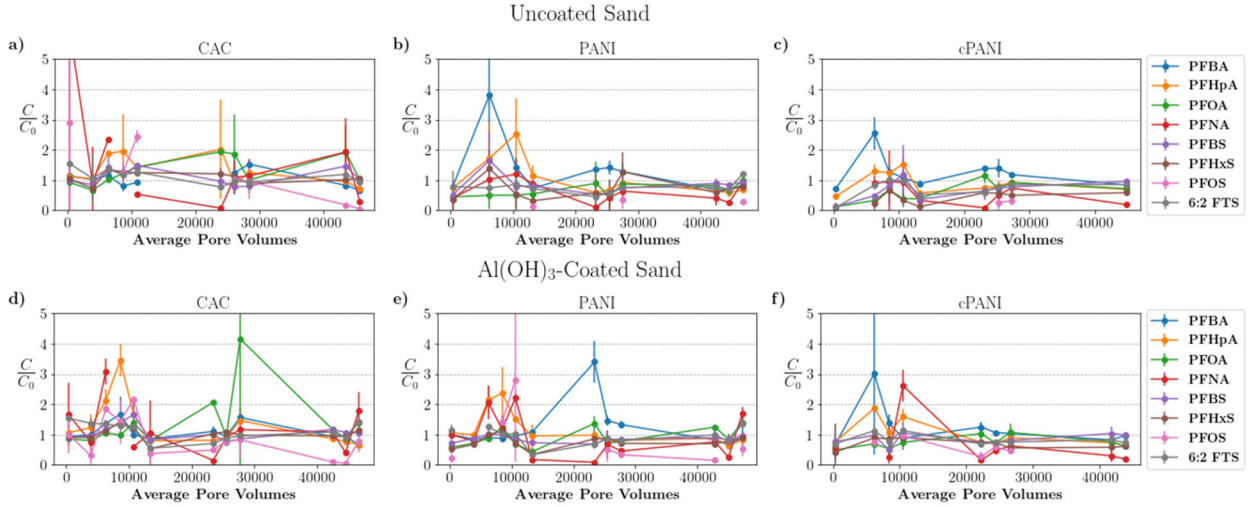

Figure 21*. Column breakthrough data normalized to the influent concentrations for 20 mg of (a, d) CAC, (c, f) cPANI, and (b, e) PANI to g of aluminum hydroxide coated (a-c) and uncoated sand (d - f). The error bars at each point represent the standard deviation of the measurements from duplicate samples.*

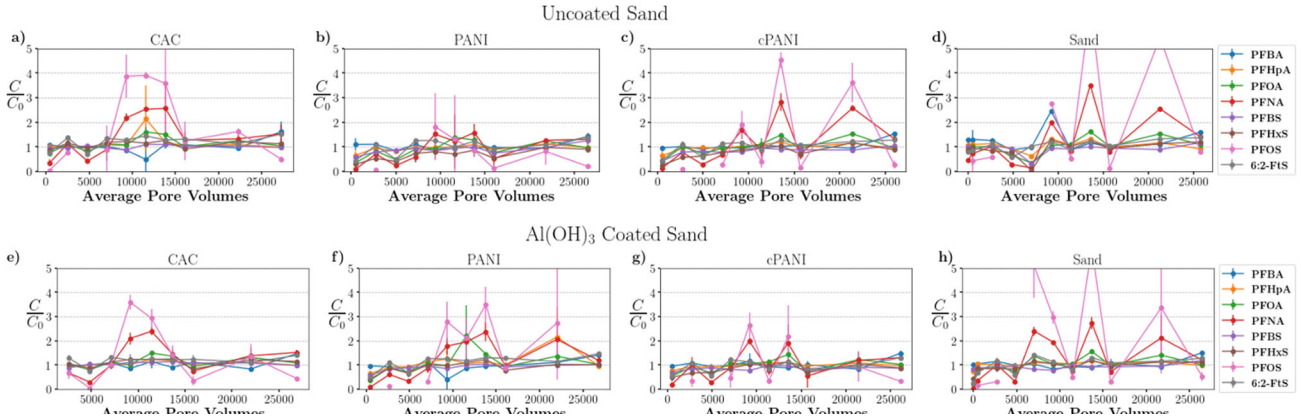

Figure 22. *Column breakthrough data normalized to the influent concentrations for 2 mg of (a, e) CAC, (c, g) cPANI, and (b, f) PANI to g of aluminum hydroxide coated (a-c) and uncoated sand (e, f). The two sands were used as controls for PFAS through aluminum hydroxide coated (d) and uncoated sand (h). The error bars at each point represent the standard deviation of measurements from duplicate samples.*

`

To obtain a more direct measure of PFAS uptake to column materials, the PFAS was extracted from the contents of all 28 columns using a 1% NaCl/MeOH solution, and then measured, and normalized to the mass of polymer added. Duplicates were used to calculate the average adsorbed mass of each PFAS species per unit mass of polymer. The contribution of PFAS in the entrained solution at the end of the experiment was accounted for in all calculations.

For experiment 4A, (20 mg g^{-1} loading) the performance of cPANI was similar to PANI in both sand matrices (Fig. 23 a, b). In the case of experiment 4B (2 mg g^{-1} loading) the cPANI performed similarly to PANI for most of the analytes except PFOS and PFHxS (Fig. 25 a, b). Results show cPANI had a higher capacity for sorbing PFOS and PFHxS in a negatively charged sand matrix.

PFAS uptake to untreated sands was negligible (Fig. 23 a, b). The performance of the CAC was much lower than expected for an activated carbon (Olshansky et al., 2022). However, we note that during the PFAS infusion there was visible CAC loss from both of the sand matrices (i.e., effluent tubing showed discoloration due to CAC loss from the columns). To account for the loss of CAC from the columns, effluent TOC from CAC and the untreated sand columns were compared. The TOC was converted to CAC+CMC by calculating the total weight percent carbon. After accounting for the loss of the CAC from the columns throughout the course of the experiment, and assuming similar loading of PFAS on the mobilized CAC, the PFAS loading performance of the CAC was more similar to that of cPANI and PANI (as expected) for a majority of the species (Fig 24 a, b).

`

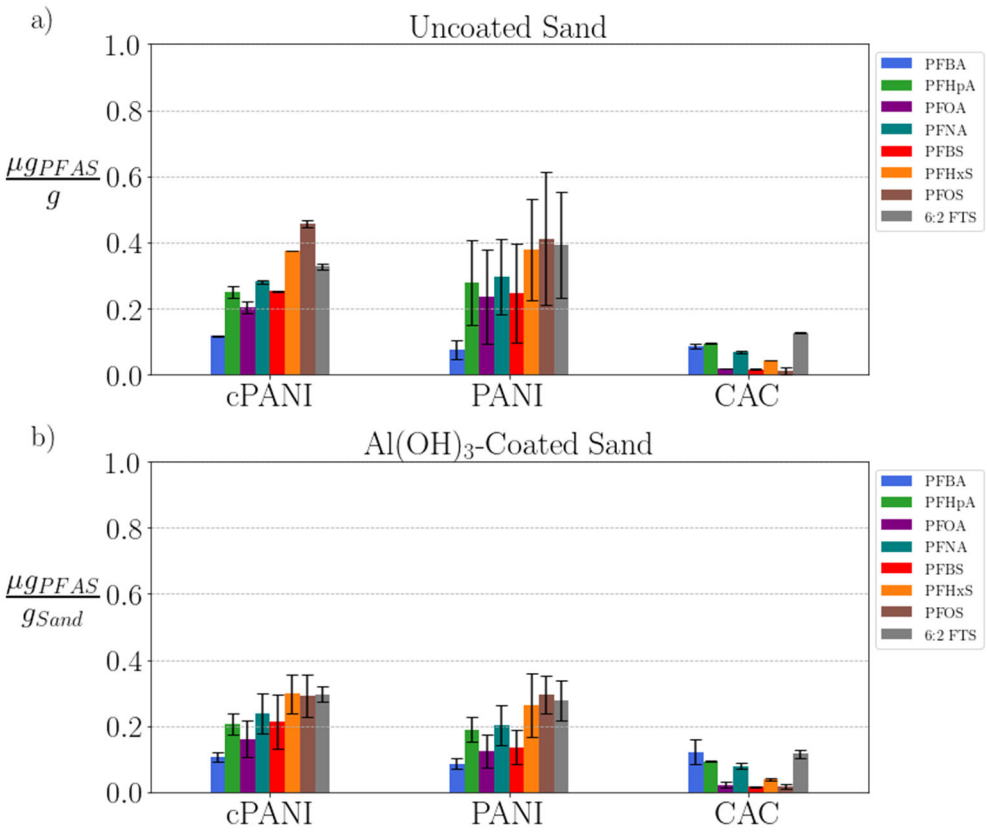

Figure 23. *PFAS loading onto cPANI, PANI, and CAC from the 20 mg g^{-1} loading experiment without accounting for CAC loss. The error bars at each point represent the standard deviation of measurements from duplicate samples.*

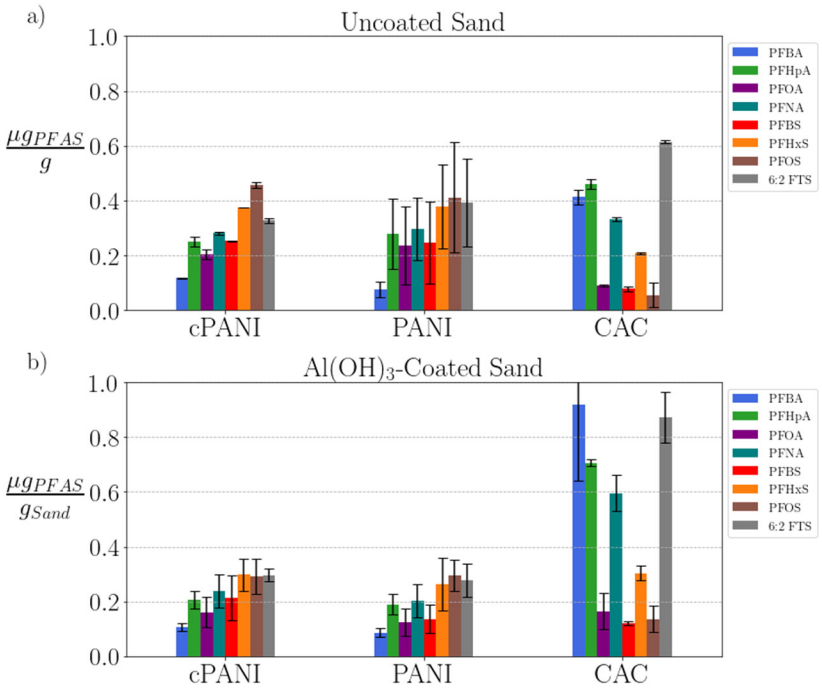

Figure 24. *PFAS loading onto cPANI, PANI, and CAC from the 20 mg g^{-1} loading experiment with accounting for CAC loss (same data from Fig 23 but CAC loss included). The error bars at each point represent the standard deviation of measurements from duplicate samples.*

`

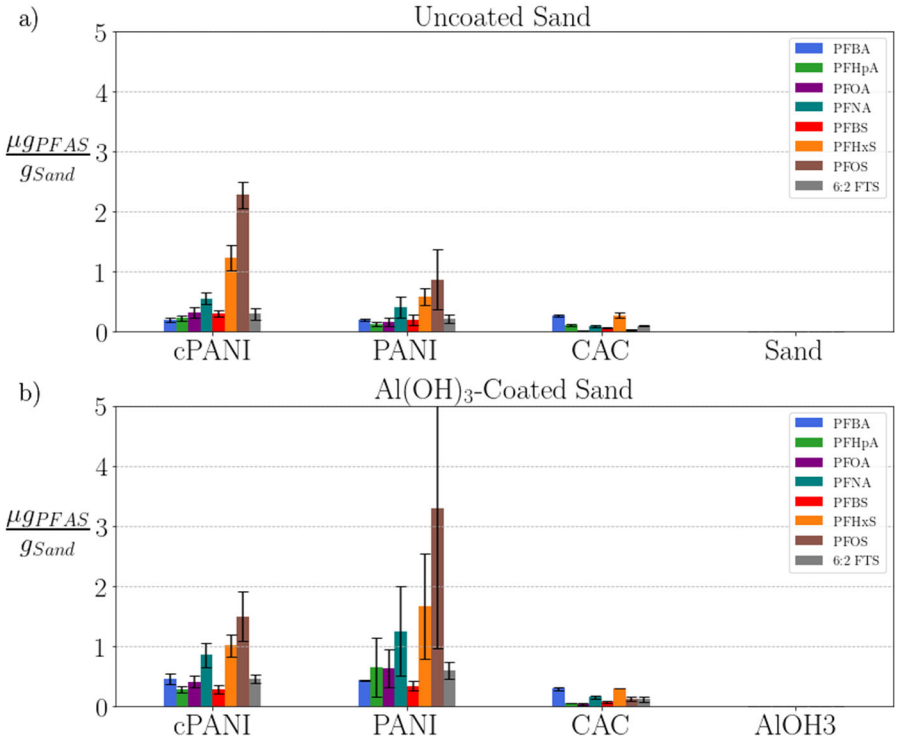

Figure 25. *PFAS loading onto cPANI, PANI, and CAC from the 2 mg g^{-1} loading experiment without accounting for CAC loss. The error bars at each point represent the standard deviation of the measurements from duplicate samples.*

`

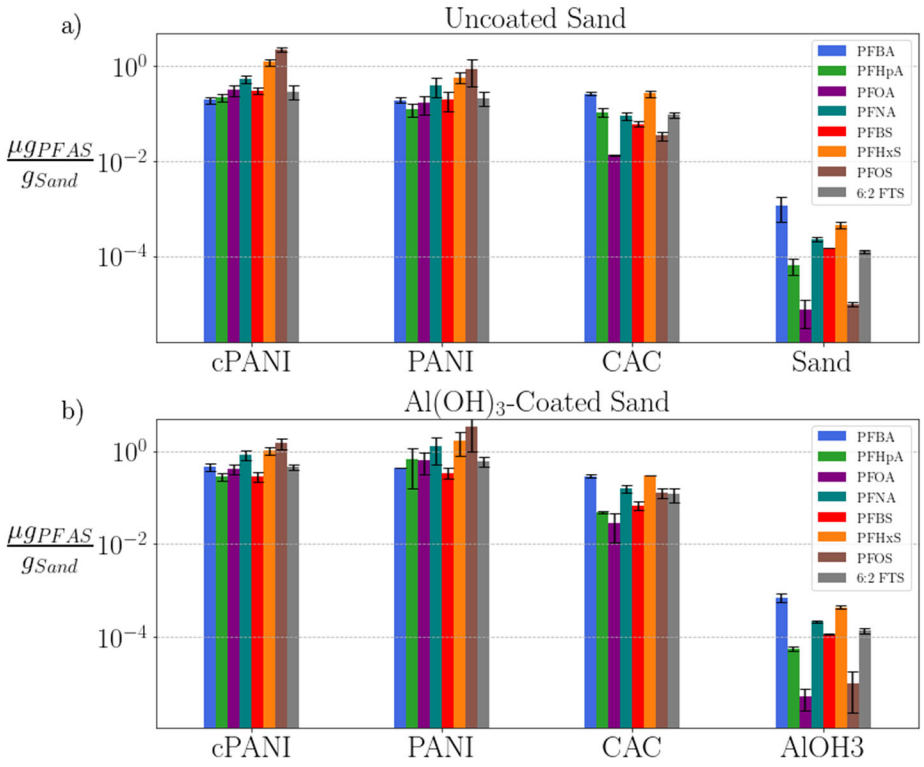

Figure 26*. PFAS loading onto cPANI, PANI, and CAC from the 2 mg g^{-1} loading experiment without accounting for CAC loss (same data in Fig 25 shown log scale). The error bars at each point represent the standard deviation of the measurements from duplicate samples.*

4.9 Experiment 5: The performance of cPANI was tested with three different actual groundwaters with the same packing style as experiment 4A with a loading of 20 $mg_{cPANI}\ g_{Sand}^{-1}$. The pertinent chemical compositions of the groundwater measured by a DoD certified lab are included in Table 6.

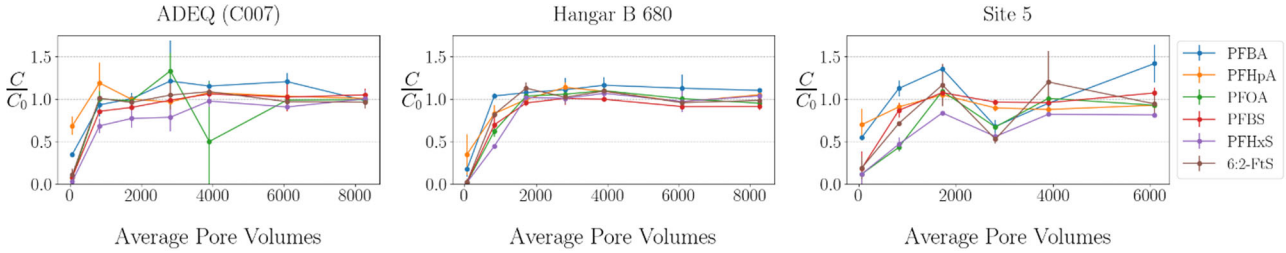

Figure 27: *Breakthrough curves for cPANI columns treating groundwater samples from Willow Grove (Site 5 and Hangar B 680) and Tucson Water (ADEQ) The error bars at each point represent the standard deviation of the measurements from duplicate samples.*

`

Table 6. *PFAS composition of the three groundwaters used to test cPANI performance in natural groundwater.*

	Willow Grove		ADEQ		
	Site 5 composite	**Hanger B composite**	**C007A composite**	**Units**	**LOD**
Measured TOF	5.6 ± 0.21	42.4 ± 0.04	12.500 ± 0.003	ug L^{-1}	5.1
Calculated TOF	3.6 ± 0.1	13.83 ± 0.04	6.66 ± 0.13	ug L^{-1}	
Analyte					
PFBA	500 ± 12	1700 ± 127	2260 ± 77	ng L^{-1}	97.5
PFHpA	102 ± 2	300 ± 28	210 ± 17	ng L^{-1}	2.5
PFOA	3300 ± 65	2300 ± 290	638 ± 9.3	ng L^{-1}	2.5
6:2 FTS	50 ± 1.7	3200 ± 110	2200 ± 100	ng L^{-1}	2.5
PFBS	80 ± 10	1109 ± 116.2	186 ± 1	ng L^{-1}	5.0
PFHxS	600 ± 200	5400 ± 620	1300 ± 110	ng L^{-1}	99.7
PFNA	18 ± 1.1	31 ± 2.9	2.7 ± 0.2	ng L^{-1}	5.1
PFOS	250 ± 5	4010 ± 50	1850 ± 38	ng L^{-1}	2.5
PFPeA	138 ± 9.1	680 ± 14	540 ± 22	ng L^{-1}	7.6
PFHxA	199 ± 8.4	1480 ± 14	760 ± 26	ng L^{-1}	2.5
PFDA	11 ± 3.8	9 ± 1.9	< LOD	ng L^{-1}	1
PFUnA	4.5	3.3	< LOD	ng L^{-1}	2.5
PFDoA	< LOD	< LOD	< LOD	ng L^{-1}	2.5
PFTriDA	< LOD	< LOD	< LOD	ng L^{-1}	5.1
PFTreA	< LOD	< LOD	< LOD	ng L^{-1}	5.1
4:2 FTS	< LOD	26.7 ± 0.6	6 ± 1	ng L^{-1}	2.5
8:2FTS	34 ± 2.5	146.600 ± 0.004	< LOD	ng L^{-1}	5.1
NEtFOSAA	< LOD	< LOD	< LOD	ng L^{-1}	
PFPeS	90 ± 71	850 ± 52	120 ± 30	ng L^{-1}	1.0
PFHpS	13 ± 2.3	700 ± 130	75 ± 5	ng L^{-1}	1.0
PFNS	< LOD	50 ± 4.7	< LOD	ng L^{-1}	5.0
PFDS	< LOD	< LOD	< LOD	ng L^{-1}	5.1
FOSA	< LOD	70 ± 16	500 ± 110	ng L^{-1}	2.5
N-MeFOSA	< LOD	< LOD	< LOD	ng L^{-1}	2.4
NMeFOSAA	< LOD	< LOD	< LOD	ng L^{-1}	10.1
Total:	5400± 200	22100± 700	11000± 200	ng L^{-1}	

The effluent samples were normalized to the average measured concentrations for the pre- filtered groundwaters during infusion (Fig. 27). Similar to experiments 4A and 4B, the effluent samples reached the C_0 concentration within ca. 2000 PV, which is more rapid relative to the observations made in experiment 1A (Fig. 15). Nonetheless, assuming a groundwater flow rate of ca. 0.30 m day^{-1}), 2000 PV can translate to ca. 18 years for each m^3 of treated aquifer.

Precisely why we are seeing earlier breakthrough for impacted natural groundwaters (Experiment 5) than for synthetic groundwaters (Experiment 1B, Experiment 4A, 4B) is a key question that we propose to further address in follow-on research. While we have hypotheses, these need to be tested

`

in the follow on studies that we are proposing for Phase 2 of this project. Several issues are relevant:

1. Total PFAS concentration in the field-contaminated groundwaters were, on average, somewhat higher than in the experimental solutions. Based on the targeted analysis LC-MS/MS data for all 25 PFAS species in Table 6, one finds that the total molar PFAS concentration in solution is 14.5, 59.2, and 31.4 nM for Site 5, Hanger B, and C007A composites, respectively (as compared to the total molar PFAS concentration of 16 nM for the synthetic Experiment 4 solutions).

2. The field-contaminated groundwaters had a higher abundance of TOF (i.e., targeted analytes plus analytes that were not measured by LC-MS/MS) as shown by the comparison between the sum of targeted analyte fluorine and the TOF measured by combustion ion chromatography. That is, for the impacted groundwaters, measured total organic fluorine was significantly higher than that calculated from the LC-MS/MS data, indicating that, in addition to significantly higher targeted PFAS concentrations in the Hanger B and Coo7A composites relative to synthetic groundwaters of Experiment 4, there was also a substantial concentration of PFAS species in the impacted groundwaters that was not captured in the targeted LC-MS/MS analyses (see top two rows of data in Table 6). These would contribute to additional competition for adsorption sites on the adsorbents. This was not the case for the synthetic groundwaters, wherein the TOF was captured quantitatively by the LC-MS/MS analysis.

3. We did not have sufficient time to conduct detailed aqueous geochemical analyses for the impacted groundwaters, which is something that we will focus on in the upcoming Phase 2 work. However, we have measured DOC values for each of them and they fall in the 100-500 ug/L range. These concentrations of DOC are low relative to those where we have previously observed a significant impact on PFAS adsorption (Figure 2, and also see Olshansky et al., 2022). Furthermore, we have found that our synthetic PANI sorbent is less negatively impacted by increased DOC concentration than is granular activated carbon (e.g., see Figure 2).

4. Most importantly, in our view, is the effect of the method whereby cPANI and colloidal activated carbon are introduced into the columns of both Experiments 4 and 5 versus Experiment 1B, wherein the greatest PFAS removals were observed. In Experiments 4 and 5, rather than injecting aqueous suspensions of the colloidal adsorbents, we inserted a layer of colloidal adsorbent between two layers of quartz sand. We are now quite certain that this method of colloidal sorbent introduction to the geomedia was insufficient to provide the most effective, precise and accurate measure of injectable sorbent potential for PFAS removal. This is evident from a comparison of the data from Experiment 1B and Experiments 4 and 5. In the former case, where aqueous suspensions of cPANI were introduced into sand columns in a manner more similar to what would be executed in the field, we observed much greater PFAS removal and over a much longer time frame, than occurred when we prepared the layered media approach. Hence, future work in Phase 2 is designed to emphasize testing aqueous colloidal infusions of polymeric sorbents to better quantify realistic values of PFAS uptake in a system most similar to the field application.

`

5. Conclusions and Implications

This one-year proof-of-concept study had the intent of bridging the gap between our polymer synthesis and PFAS adsorption studies conducted under SERDP project (ER18-1052, *Remediation of Per- and Polyfluoroalkyl Contaminated Groundwater Using Cationic Hydrophobic Polymers as Ultra-High Affinity Sorbents,* PI Sierra-Alvarez) and assessment of *in-situ* application of polymer-based PFAS removal from contaminated geomedia systems.

- This project has shown that cPANI can be developed as a sub micrometer cationic colloidal polymer capable of being stably suspended in aqueous solution for injection.
- Colloidal PANI transport and adhesion in sand columns was found to be a function of suspension aqueous chemistry including pH, polymer concentration, and ionic strength. cPANI at pH 4 has as high positive zeta potential that allows the polymer to stay suspended with minimal aggregation and setting before injection.
- cPANI can function as an injectable sorbent that adheres at high surface concentration to both negative- and positive-charged sand matrix media with minimal subsequent detachment.
- cPANI has a high capacity of removing around 90% of the PFAS concentration from a lab generated mixed water system for over thousands of PVs. It performs similarly to non-colloidal PANI with a high affinity for PFAS at environmentally relevant concentrations ng L^{-1}). The eight chosen PFAS species represented a range of chain lengths and functional head groups.
- cPANI was able to remove a high percentage of PFAS from chemically complex PFAS contaminated groundwater samples for over 1000 PV.

Research that could be addressed following 1-year proof-of-concept study: Based on the results of the current proof-of-concept study, we propose several tasks should be pursued in a subsequent 2-year project:

- Flow-through column data fitting to the advection-dispersion equation with chemical retardation enabling direct quantitative comparison to distribution coefficients determined from the batch experiments conducted in the current work and field scale prediction.
- Further optimization of cPOT to become as effective as it's non colloidal counterpart or cPANI.
- Assessment of the long-term fate of the colloidal polymers in the subsurface, including their susceptibility to microbial biodegradation and potential generation of byproducts as amine based polymers.

`

- Mesocosm scale injection into an lab built aquifer model to test larger-scale injection, mobility, and retention patterns of cPANI as well as PFAS remediation.
- Field scale efficacy testing in a contaminated site by injecting the cPANI downstream of a PFAS plume similar to Figure O1.

`

Literature Citations and Published Products

ADEQ (2018). Arizona's Public Water System Screening for Perfluorooctanoic Acid (PFOA) and Perfluorooctane Sulfonate (PFOS) Final Report. Phoenix, AZ, Arizona Department of Environmental Quality. Report #EQR-18-13.

ADEQ. (2020). "Davis-Monthan Air Force Base." https://www.azdeq.gov/DOD/DavisMonthan ADEQ (2020). Final Work Plan for the Central Tucson PFAS Project. Arizona Department of

Aller, L., T. Bennet, J. H. Lehr, R. J. Petty and G. Hackett (1987). DRASTIC: A standardized system for evaluating ground water pollution potential using hydrogeologic settings: 622 pages.

Andriianova, A. N., Biglova, Y. N., & Mustafin, A. G. (2020). Effect of structural factors on the physicochemical properties of functionalized polyanilines. *RSC advances*, 10(13), 7468-7491.

Brusseau, M. L. (2018). "Assessing the potential contributions of additional retention processes to PFAS retardation in the subsurface." *Science of the Total Environment* 613-614: 176-185.

Brusseau, M. L., R. H. Anderson and B. Guo (2020). "PFAS concentrations in soils: Background levels versus contaminated sites." *Science of the Total Environment* 740. DOI: 10.1016/j.scitotenv.2020.140017.

Campos-Pereira, H., D. B. Kleja, C. Sjöstedt, L. Ahrens, W. Klysubun and J. P. Gustafsson (2020). "The adsorption of per- And polyfluoroalkyl substances (PFASs) onto ferrihydrite is governed by surface charge." Environmental Science and Technology 54(24): 15722-15730.

Campos Pereira, H., M. Ullberg, D. B. Kleja, J. P. Gustafsson and L. Ahrens (2018). "Sorption of perfluoroalkyl substances (PFASs) to an organic soil horizon – Effect of cation composition and pH." Chemosphere 207: 183-191.

Chorover, J., J. Zhang, M. K. Amistadi and J. Buffle (1997). "Comparison of hematite coagulation by charge screening and phosphate adsorption: Differences in aggregate structure." *Clays and Clay Minerals* 45(5): 690-708.

Coston, J. A., C. C. Fuller and J. A. Davis (1995). "Pb^{2+} and Zn^{2+} Adsorption by a Natural Aluminum-Bearing and Iron-Bearing Surface Coating on an Aquifer Sand." *Geochimica et Cosmochimica Acta* 59(17): 3535-3547.

`

Ferrey, M. L., J. T. Wilson, C. Adair, C. M. Su, D. D. Fine, X. Y. Liu and J. W. Washington (2012). "Behavior and fate of PFOA and PFOS in sandy aquifer sediment." Ground Water Monitoring and Remediation 32(4): 63-71.

Gao, X. and J. Chorover (2012). "Adsorption of perfluorooctanoic acid and perfluorooctanesulfonic acid to iron oxide surfaces as studied by flow-through ATR-FTIR spectroscopy." *Environmental Chemistry* 9(2): 148-157.

Guo, X., Fei, G. T., Su, H., & De Zhang, L. (2011). Synthesis of polyaniline micro/nanospheres by a copper (II)-catalyzed self-assembly method with superior adsorption capacity of organic dye from aqueous solution. *Journal of Materials Chemistry*, *21*(24), 8618-8625.

He, J., A. Gomeniuc, Y. Olshansky, J. Hatton, L. Abrell, J.A. Field, J. Chorover, R. Sierra-Alvarez, 2022. Enhanced Removal of Per- And Polyfluoroalkyl Substances by Crosslinked Polyaniline Polymers, Chemical Engineering Journal, 137246. DOI: 10.1016/j.cej.2022.137246

Hoek, E. M. V. and G. K. Agarwal (2006). "Extended DLVO interactions between spherical particles and rough surfaces." Journal of Colloid and Interface Science 298(1): 50-58.

Li, R., C. Wei, H. Cheng and G. Chen (2019). "Adhesion of colloids and bacteria to porous media: A critical review." Reviews of Adhesion and Adhesives 7(4): 417-460.

Liu, C., J. Hatton, W. A. Arnold, M. F. Simcik and K. D. Pennell (2020). "In situ sequestration of perfluoroalkyl substances using polymer-stabilized powdered activated carbon." *Environmental Science and Technology* 54(11): 6929-6936.

Lyu, Y., M. L. Brusseau, W. Chen, N. Yan, X. Fu and X. Lin (2018). "Adsorption of PFOA at the air-water interface during transport in unsaturated porous media." *Environmental Science and Technology* 52(14): 7745-7753.

McGregor, R. (2018). "In situ treatment of PFAS-impacted groundwater using colloidal activated carbon." Remediation Journal 28: 33-41.

McGregor, R. (2020). "Six pilot-scale studies evaluating the in situ treatment of PFAS in groundwater." Remediation 30(3): 39-50.

Olshansky, Y., A. Gomeniuc, J. Chorover, L. Abrell, J.A. Field, J. Hatton, J. He, R. Sierra-Alvarez, 2022. Tailored Polyanilines Are High-Affinity Adsorbents for Per- and Polyfluoroalkyl Substances. ACS ES&T Water. DOI: 10.1021/acsestwater.2c00166

Olshansky, Y., A. Gomeniuc, J. Chorover, L. Abrell, J.A. Field, J. Hatton, R. Sierra-Alvarez, 2021. Synthesis and Characterization of Customizable Polyaniline-Derived Polymers and

Their Application for Perfluorooctanoic Acid Removal from Aqueous Solution, ACS ES&T Water, 1:1438-1446. https://doi.org/10.1021/acsestwater.1c00019

Olshansky, Y.; J. Chorover, L. Abrell, J. A. Field, A. Gomeniuc, J. Hatton, R. Sierra-Alvarez. 2019. Sorption of PFAS by Cationic Hydrophobic Polymers. Abstracts of Papers of the American Chemical Society,Vol. 257. Meeting Abstract: 169. Published: MAR 31 2019. ISSB 0065-7727.

Reilly, T. E., K. F. Dennehy, W. M. Alley and W. L. Cunningham (2008). Groundwater availability in the United States. Reston, VA.

Scow, K. M. and K. A. Hicks (2005). "Natural attenuation and enhanced bioremediation of organic contaminants in groundwater." Current Opinion in Biotechnology 16(3 SPEC. ISS.): 246- 253.

Sierra-Alvarez, R., J. A. Field, J. Chorover, L. A. Abrell and Y. Olshansky (2019). "Remediation of per- and polyfluoroalkyl contaminated groundwater using cationic hydrophobic polymers as ultra-high affinity sorbents." *Interim Report, SERDP Project ER18-1052, July 2019*.

Silva, J. A. K., J. Šimůnek and J. E. McCray (2020). "A modified hydrus model for simulating PFAS transport in the vadose zone." Water 12(10), 2758; doi:10.3390/w12102758

Simcik, M. F., W. A. Arnold and K. Pennell (2019). "Development of a novel approach for in situ remediation of PFC contaminated groundwater systems." Strategic Environmental Research and Development Program (SERDP) and Environmental Security Technology Certification Program (ESTCP), Alexandria, VA. March, 2019.

Tufenkji, N. and M. Elimelech (2004). "Correlation equation for predicting single-collector efficiency in physicochemical filtration in saturated porous media." Environmental Science and Technology 38(2): 529-536.

Vazquez-Ortega, A., S. Hernandez-Ruiz, M. K. Amistadi, C. Rasmussen and J. Chorover (2014). "Fractionation of dissolved organic matter by (oxy)hydroxide-coated sands: Competitive sorbate displacement during reactive transport." *Vadose Zone Journal* 13(7): doi:10.2136/vzj2013.10.0179

Weber, E., Richter, E., & Holze, R. (2022). o-Toluidine in electrochemistry–an overview. *Journal of Solid State Electrochemistry*, 26(4), 1097-1114.

Yu, X., H. Dong and Y. Li (2018). "The deposition characteristics of PAN/PPY on SiO_2 substrate by density functional theory (DFT) calculations." Applied Surface Science 462:890-895.

Zhang, D. Q., W. L. Zhang and Y. N. Liang (2019). "Adsorption of perfluoroalkyl and polyfluoroalkyl substances (PFASs) from aqueous solution - A review." Science of the Total Environment 694: 133606

`

Appendix: Source data for all figures

FTIR comparison of cPANI to PANI and cPOT to confirm compositional changes were minimal.

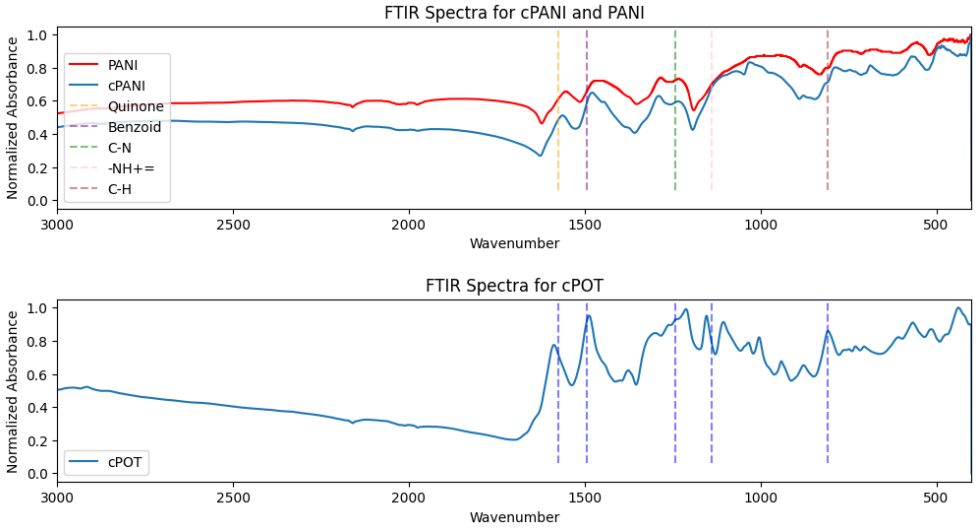

Experiment 1A : Polymer Loading with Distance

pH 4	Distance	PANI mg/g	pH 6	Distance	PANI mg/g	pH 9	Distance	PANI mg/g
4	18	0.05406	6	18	0.300641	9	15.5	0.814669
4	17	0.05406	6	17	0.300641	9	14.5	5.94139
4	15.5	1.043993	6	15.5	0.300641	9	13.5	10.9993
4	14.5	9.165302	6	14.5	0.300641	9	12.5	14.57671
4	13.5	15.23378	6	13.5	0.300641	9	11.5	15.17657
4	12.5	18.1267	6	12.5	0.300641	9	10.5	17.11226
4	11.5	21.92838	6	11.5	2.981177	9	9.5	21.36585
4	10.5	29.9696	6	10.5	8.947123	9	8.5	26.86745
4	9.5	28.1061	6	9.5	11.0294	9	7.5	32.03878
4	8.5	30.91172	6	8.5	12.56206	9	6.5	28.69109
4	7.5	34.28255	6	7.5	20.78326	9	5.5	30.77148
4	6.5	30.31702	6	6.5	25.46267	9	4.5	32.87375
4	5.5	27.44087	6	5.5	33.79312	9	3.5	35.48954
4	5.5	28.81161	6	5.5	34.51262	9	2.5	34.49987
4	4.5	29.54568	6	4.5	43.10518	9	1.5	40.40337
4	3.5	31.50421	6	3.5	42.28195	9	0.5	46.07257
4	2.5	34.21287	6	2.5	43.83765			
4	1.5	51.02537	6	1.5	44.18246			
4	0.5	44.86241	6	0.5	51.18803			

`

`

Experiment 1A: Average polymer loading

Column	Solid	Solid_std	Effluent	Effluent_std
4	21.63	5.02	15.75	1.78
6	16.62	5.02	16.61	3.53
9	18.25	4.61	19.16	4.22

Experiment 1A: CC_o^{-1} cPANI Breakthrough curve

col Group 1	PV_accurate_1	pH4	pH4_Std	Group 2	PV_accurate_2	pH6	pH6_Std	Group 3	PV_accurate_4	pH9	pH9_Std
pH 4	3.572654	0.213162	0.014165	pH 6	3.825441	0.120897	0.018817	pH 9	3.817168	0.166879	0.021879
pH 4	56.36477	0.093483	0.005122	pH 6	59.62102	0.049336	0.003349	pH 9	59.0979	0.069124	0.004941
pH 4	189.6732	0.078824	0.004366	pH 6	202.141	0.062291	0.004099	pH 9	202.4083	0.069979	0.00456
pH 4	301.8192	0.064165	0.003658	pH 6	317.9125	0.075246	0.004966	pH 9	320.7377	0.070834	0.004441
pH 4	456.2845	0.049506	0.002967	pH 6	482.1724	0.088201	0.00598	pH 9	476.6315	0.071688	0.004454
pH 4	611.2683	0.047742	0.00297	pH 6	639.0997	0.111663	0.005927	pH 9	613.2638	0.120641	0.007035
pH 4	677.5663	0.045978	0.003081	pH 6	711.164	0.135124	0.006456	pH 9	669.1583	0.169594	0.008796
pH 4	785.5568	0.047758	0.003604	pH 6	828.5469	0.140228	0.007494	pH 9	760.2028	0.115742	0.006577
pH 4	830.1233	0.049538	0.004259	pH 6	871.8339	0.145332	0.009352	pH 9	815.7405	0.06189	0.004031
pH 4	979.9699	0.068993	0.005492	pH 6	981.7559	0.191906	0.01206	pH 9	987.5136	0.05833	0.003955
pH 4	1036.652	0.088447	0.006549	pH 6	1034.25	0.23848	0.013981	pH 9	1051.337	0.05477	0.003967
pH 4	1168.989	0.107902	0.007602	pH 6	1089.683	0.285054	0.014598	pH 9	1194.452	0.05121	0.004033
pH 4	1221.541	0.10472	0.009177	pH 6	1128.172	0.240739	0.019781	pH 9	1252.363	0.059097	0.004233
pH 4	1363.126	0.101539	0.012158	pH 6	1150.004	0.196425	0.020757	pH 9	1318.283	0.066985	0.004694
pH 4	1381.354	0.098358	0.016197	pH 6	1164.227	0.15211	0.018173	pH 9	1333.515	0.074872	0.005438
pH 4	1432.727	0.108018	0.013277	pH 6	1194.78	0.366276	0.034228	pH 9	1366.528	0.092792	0.008433
pH 4	1558.185	0.117678	0.012181	pH 6	1219.91	0.580442	0.025958	pH 9	1426.878	0.110712	0.013528
pH 4	1592.294	0.111573	0.010689	pH 6	1227.51	0.495168	0.024297	pH 9	1433.091	0.109276	0.010786
pH 4	1732.587	0.105469	0.009342	pH 6	1232.347	0.409893	0.022535	pH 9	1470.568	0.10784	0.008802
pH 4	1787.666	0.099365	0.008143	pH 6	1243.104	0.324619	0.019433	pH 9	1470.568	0.106404	0.007367
pH 4	1792.131	0.09326	0.007098	pH 6	1246.084	0.239345	0.015264	pH 9	1472.277	0.104968	0.006353

`

`

Experiment 1A: cPANI loading calculations from 5mM NaCl infusion

	cPANI Infusion Column Totals								
	4-1	4-2	4-3	6-1	6-2	6-3	9-1	9-2	9-3
Vf (L)	12.61508	11.47708	14.08081	7.569216	8.810754	8.652447	10.26551	9.652047	9.00421
unit pV (mL)	6.964521	7.658556	6.813965	6.330798	6.686751	7.063275	6.438377	6.55148	6.674022
PVs	1811.335	1498.595	2066.464	1195.618	1317.644	1224.991	1594.425	1473.262	1349.143
PANI IN (mg) TOC	498.8504	455.9843	559.4306	494.0427	575.0779	564.7452	666.8473	626.997	584.9135
st dev	40.99722	37.65586	44.4113	54.82085	60.59707	59.48315	64.16916	61.07121	54.69669
PANI IN (mg) TN	421.4698	383.4491	470.4399	395.7186	460.6262	452.3499	542.84	510.4003	476.1426
st dev	52.41	48.33665	57.00822	49.04418	54.21173	53.21519	66.58618	63.37155	56.75693
PANI OUT (mg) TOC	39.25112	38.30128	44.4874	65.65196	69.10939	105.9093	54.40835	45.03438	44.29528
st dev	0.292502	0.304146	0.311477	0.55716	0.503073	0.792695	0.541784	0.366991	0.315816
PANI OUT (mg) TN	14.90266	13.29678	16.81552	6.710254	7.106505	6.258624	10.76851	11.06839	12.77283
st dev	0.108268	0.105473	0.170162	0.053227	0.054374	0.03169	0.110631	0.084989	0.102569
TOTAL PANI in col(mg) TOC	459.599	417.683	514.943	428.391	505.969	458.836	612.439	581.963	540.618
st dev	40.996	37.655	44.410	54.818	60.595	59.478	64.167	61.070	54.696
TOTAL PANI in col(mg)	406.567	370.152	453.624	389.008	453.520	446.091	532.071	499.332	463.370
st dev	52.410	48.337	57.008	49.044	54.212	53.215	66.586	63.371	56.757
Sand (g)	25.594	25.575	25.576	25.577	25.598	25.591	25.601	25.589	25.594
After cPANI in: mg/g	17.958	16.332	20.134	16.749	19.766	17.930	23.923	22.743	21.123
st dev	1.602	1.472	1.736	2.143	2.367	2.324	2.506	2.387	2.137
After cPANI in.: mg/g	15.885	14.473	17.736	15.210	17.717	17.432	20.783	19.514	18.105
st dev	2.048	1.890	2.229	1.918	2.118	2.079	2.601	2.477	2.218
					NaCl Infusion				
Vf (L)	17596.48		18158.07	14741.29		17209.83	17778.09		17987.7
unit pV (mL)	6.964521	7.658556	6.813965	6.330798	6.686751	7.063275	6.438377	6.55148	6.674022
PVs	2526588	0	2664832	2328504	0	2436523	2761269	0	2695182
PANI OUT (mg) TOC	55.88794		54.40786	44.89491		42.64959	54.80037		78.30669
st dev	0.607013		0.540034	0.417586		0.581467	0.530082		0.743539
PANI OUT (mg) TN	9.287907		12.55517	5.049487		8.538116	10.23752		13.66936
st dev	0.0843		0.250125	0.077403		0.07868	0.137663		0.173642
TOTAL PANI in col(mg) TOC	403.711	417.683	460.535	383.496	505.969	416.186	557.639	581.963	462.312

`

`

st dev	40.992	37.655	44.407	54.816	60.595	59.475	64.165	61.070	54.691
TOTAL PANI in col(mg)	397.279	370.152	441.069	383.959	453.520	437.553	521.834	499.332	449.700
st dev	52.410	48.337	57.007	49.044	54.212	53.215	66.586	63.371	56.757
Final: mg/g	15.774	16.332	18.006	14.994	19.766	16.263	21.782	22.743	18.063
st dev	1.602	1.472	1.736	2.143	2.367	2.324	2.506	2.387	2.137
Final: mg/g	15.523	14.473	17.245	15.012	17.717	17.098	20.383	19.514	17.571
st dev	2.048	1.890	2.229	1.918	2.118	2.079	2.601	2.477	2.218

Experiment 1B: CC_o^{-1} PFAS breakthrough curve

col	PV_Avg	PV_Std	PFBA_C	std_PFE	PFHpA_	std_PFH	PFOA_Cco	std_PF(	PFNA_(	std_PFI	PFBS_C	std_PFE	PFHxS_	std_PFH	PFOS_C	std_PF(	62FTS_(	std_62I
pH 4	7.70	**2.11E-01**	5.61E-01	9.42E-02	3.50E-02	1.13E-02	1.16E-03	2.05E-04	1.19E-03	3.81E-04	2.92E-03	9.21E-04	3.13E-03	6.26E-04	2.33E-03	1.33E-03	5.76E-04	7.53E-05
pH 4	393.40	**1.28E+01**	8.83E-01	1.48E-01	3.46E-02	1.12E-02	9.94E-04	1.90E-04	1.19E-03	3.81E-04	4.10E-03	1.30E-03	4.39E-03	8.87E-04	2.33E-03	1.33E-03	3.48E-04	5.44E-05
pH 4	725.20	**1.73E+01**	1.01E+00	1.69E-01	3.74E-02	1.21E-02	1.44E-03	2.85E-04	1.19E-03	3.81E-04	4.68E-03	1.44E-03	5.02E-03	9.78E-04	2.33E-03	1.33E-03	1.78E-04	2.73E-05
pH 4	1118.29	**3.54E+01**	1.14E+00	1.91E-01	3.74E-02	1.21E-02	1.38E-03	2.50E-04	1.19E-03	3.81E-04	4.93E-03	1.53E-03	4.12E-03	8.87E-04	2.33E-03	1.33E-03	1.13E-03	1.64E-04
pH 4	1513.28	**6.80E+01**	1.10E+00	1.85E-01	2.67E-02	8.63E-03	1.79E-03	3.28E-04	1.19E-03	3.81E-04	5.03E-03	1.56E-03	5.39E-03	1.06E-03	2.33E-03	1.33E-03	1.22E-03	1.62E-04
pH 4	1880.22	**8.65E+01**	1.21E+00	2.03E-01	2.75E-02	8.91E-03	9.10E-04	1.61E-04	1.19E-03	3.81E-04	3.91E-03	1.21E-03	4.19E-03	8.25E-04	2.33E-03	1.33E-03	1.10E-03	1.57E-04
pH 4	2694.54	**1.57E+02**	1.07E+00	1.80E-01	2.88E-02	9.32E-03	2.58E-02	5.52E-03	1.19E-03	3.81E-04	7.20E-03	2.21E-03	2.15E-03	4.17E-04	2.33E-03	1.33E-03	1.34E-02	1.90E-03
pH 4	4033.17	**3.13E+02**	1.00E+00	1.68E-01	2.67E-02	8.78E-03	2.13E-03	3.75E-04	1.19E-03	3.81E-04	8.92E-03	2.85E-03	2.15E-03	4.17E-04	2.33E-03	1.33E-03	1.12E-02	1.63E-03
pH 4	4972.32	**4.67E+02**	1.03E+00	1.74E-01	2.76E-02	9.28E-03	2.82E-03	5.37E-04	1.19E-03	3.81E-04	1.26E-02	4.07E-03	2.15E-03	4.17E-04	2.33E-03	1.33E-03	1.21E-02	1.87E-03
pH 4	6300.01	**4.35E+02**	1.03E+00	1.74E-01	3.46E-02	1.12E-02	9.24E-03	1.65E-03	1.19E-03	3.81E-04	1.70E-02	5.22E-03	2.15E-03	4.17E-04	2.33E-03	1.33E-03	2.43E-02	3.31E-03
pH 4	6789.89	**6.60E+02**	1.61E-01	1.18E-01	6.40E-03	4.00E-03			1.09E-04	9.57E-05	1.40E-03	1.01E-03	2.42E-04	1.22E-04	3.22E-04	3.74E-04	2.62E-03	1.45E-03
pH 4	6956.59	**6.95E+02**	3.90E-01	2.86E-01	6.50E-03	4.20E-03	3.57E-04	2.34E-04	1.09E-04	9.57E-05	1.48E-03	1.12E-03	2.42E-04	1.22E-04	3.22E-04	3.74E-04	3.16E-03	1.83E-03
pH 4	7133.66	**7.32E+02**	6.29E-01	4.65E-01	9.12E-03	6.11E-03	1.41E-03	1.22E-03	1.09E-04	9.57E-05	2.21E-03	1.70E-03	2.42E-04	1.22E-04	3.22E-04	3.74E-04	9.46E-03	5.76E-03
pH 6	8.08	**7.00E-01**	5.79E-01	9.71E-02	3.62E-02	1.17E-02	7.21E-04	1.29E-04	1.19E-03	3.81E-04	4.74E-03	1.46E-03	5.08E-03	9.92E-04	2.33E-03	1.33E-03	5.76E-04	7.53E-05
pH 6	424.33	**3.14E+01**	9.16E-01	1.54E-01	3.50E-02	1.13E-02	4.77E-04	9.77E-05	1.19E-03	3.81E-04	4.14E-03	1.27E-03	4.43E-03	8.65E-04	2.33E-03	1.33E-03	2.91E-04	5.32E-05
pH 6	753.07	**#DIV/0!**	1.22E+00	1.44E-01	3.86E-02	8.82E-03	1.95E-03	2.44E-04	1.19E-03	2.69E-04	3.08E-03	6.66E-04	3.30E-03	4.53E-04	2.33E-03	9.41E-04	5.76E-04	5.32E-05
pH 6	1468.70	**5.12E+01**	1.20E+00	2.01E-01	2.88E-02	9.32E-03	1.29E-03	2.33E-04	1.19E-03	3.81E-04	2.51E-03	7.79E-04	2.69E-03	5.30E-04	2.33E-03	1.33E-03	9.35E-04	1.31E-04
pH 6	1841.39	**1.34E+02**	1.19E+00	1.99E-01	2.86E-02	9.26E-03	7.35E-04	1.31E-04	1.19E-03	3.81E-04	4.17E-03	1.28E-03	4.47E-03	8.71E-04	2.33E-03	1.33E-03	5.76E-04	7.53E-05
pH 6	2873.69	**1.91E+02**	1.06E+00	1.78E-01	2.22E-02	7.22E-03	4.61E-03	9.24E-04	1.19E-03	3.81E-04	4.17E-03	1.28E-03	2.15E-03	4.17E-04	2.33E-03	1.33E-03	1.41E-03	2.14E-04
pH 6	4112.99	**5.87E+01**	1.07E+00	1.81E-01	2.12E-02	6.86E-03	2.13E-03	3.75E-04	1.19E-03	3.81E-04	4.17E-03	1.28E-03	2.15E-03	4.17E-04	2.33E-03	1.33E-03	2.06E-03	3.31E-04
pH 6	4960.12	**1.90E+02**	1.15E+00	1.93E-01	1.86E-02	6.03E-03	8.96E-03	1.60E-03	1.19E-03	3.81E-04			2.15E-03	4.17E-04	2.33E-03	1.33E-03	4.46E-04	6.07E-05
pH 6	6264.57	**3.64E+02**	1.26E+00	2.11E-01	2.12E-02	7.17E-03			1.19E-03	3.81E-04	7.56E-03	2.34E-03	2.15E-03	4.17E-04	2.33E-03	1.33E-03	4.41E-03	7.63E-04
pH 6	6599.32	**5.30E+02**	1.64E-01	1.20E-01	3.90E-03	2.37E-03	2.54E-04	1.87E-04	1.09E-04	9.57E-05	1.26E-03	8.49E-04	2.42E-04	1.22E-04	3.22E-04	3.74E-04	9.31E-04	5.81E-04
pH 6	6743.09	**6.06E+02**	5.06E-01	3.96E-01	5.78E-03	3.76E-03	3.99E-04	2.64E-04	1.09E-04	9.57E-05	1.13E-03	9.26E-04	2.42E-04	1.22E-04	3.22E-04	3.74E-04	4.74E-03	3.08E-03
pH 6	6886.07	**7.06E+02**	6.10E-01	4.57E-01	1.42E-02	1.08E-02			5.31E-04	5.96E-04	4.21E-03	3.59E-03	2.42E-04	1.22E-04	3.22E-04	3.74E-04	1.73E-02	1.13E-02
pH 9	7.82	**3.91E-01**	5.47E-01	9.17E-02	3.67E-02	1.19E-02	1.04E-03	1.83E-04	1.19E-03	3.81E-04	4.48E-03	1.37E-03	3.64E-03	7.64E-04	2.33E-03	1.33E-03	3.06E-04	5.33E-05
pH 9	447.00	**1.55E+01**	9.82E-01	1.66E-01	3.41E-02	1.11E-02	4.20E-04	7.50E-05	1.19E-03	3.81E-04	3.94E-03	1.21E-03	3.06E-03	6.19E-04	2.33E-03	1.33E-03	7.95E-04	1.08E-04
pH 9	1256.86	**1.29E+00**	1.19E+00	2.00E-01	3.64E-02	1.18E-02	2.24E-03	3.95E-04	1.19E-03	3.81E-04	6.77E-03	2.44E-03	7.25E-03	1.66E-03	2.33E-03	1.33E-03	1.43E-03	2.18E-04
pH 9	1652.51	**1.86E+01**	1.17E+00	1.97E-01	2.79E-02	9.04E-03	1.12E-03	2.04E-04	1.19E-03	3.81E-04	4.95E-03	1.52E-03	5.30E-03	1.03E-03	2.33E-03	1.33E-03	1.65E-03	2.56E-04
pH 9	2026.05	**3.90E+01**	1.25E+00	2.10E-01	2.73E-02	8.82E-03	8.26E-04	1.46E-04	1.19E-03	3.81E-04	4.48E-03	1.40E-03	4.81E-03	9.54E-04	2.33E-03	1.33E-03	6.67E-03	8.72E-04
pH 9	2975.13	**1.86E+02**	1.06E+00	1.78E-01	2.76E-02	8.94E-03	9.90E-03	2.22E-03	1.19E-03	3.81E-04	9.11E-03	2.82E-03	2.15E-03	4.17E-04	2.33E-03	1.33E-03	1.36E-02	1.81E-03
pH 9	5265.82	**5.71E+02**	1.13E+00	1.90E-01	3.85E-02	1.27E-02	2.22E-03	4.80E-04	1.19E-03	3.81E-04	1.36E-02	4.52E-03	2.15E-03	4.17E-04	2.33E-03	1.33E-03	4.13E-02	6.10E-03
pH 9	6498.37	**1.01E+03**	1.12E+00	1.88E-01	5.01E-02	1.74E-02	4.24E-03	7.78E-04	1.19E-03	3.81E-04	1.72E-02	5.92E-03	2.15E-03	4.17E-04	2.33E-03	1.33E-03	5.14E-02	8.12E-03
pH 9	6836.47	**1.14E+03**	2.07E-01	1.59E-01	7.53E-03	4.80E-03	3.63E-04	2.44E-04	1.09E-04	9.57E-05	1.74E-03	1.25E-03	2.42E-04	1.22E-04	3.22E-04	3.74E-04	7.32E-03	4.31E-03
pH 9	6969.28	**1.21E+03**	5.93E-01	4.45E-01	1.29E-02	8.63E-03	4.72E-04	3.06E-04	1.09E-04	9.57E-05	2.98E-03	2.04E-03	2.42E-04	1.22E-04	3.22E-04	3.74E-04	1.25E-02	7.02E-03
pH 9	7152.91	**1.25E+03**	6.71E-01	4.92E-01	2.37E-02	1.73E-02	1.24E-03	8.88E-04	1.09E-04	9.57E-05	4.39E-03	3.33E-03	2.42E-04	1.22E-04	3.22E-04	3.74E-04	4.01E-02	2.38E-02

`

Raw Data:

c ol	PV_ Avg	PV_ Std	PFB A_C co	std _PF BA	PFH pA_ Cco	std_ PFH pA	PFOA _Cco	std _PF OA	PFN A_C co	std _PF NA	PFB S_C co	std _PF BS	PFH xS_ Cco	std_ PFH xS	PFO S_C co	std _PF OS	62F TS_ Cco	std_ 62F TS
p	7.6	**0.2**	0.5	0.0	0.03	0.01	0.00	0.0	0.00	0.0	0.0	0.0	0.00	0.00	0.0	0.0	0.00	7.53
H	967	**109**	612	941	497	131	1155	002	119	003	029	009	313	062	023	013	057	E-
4	43	**24**	18	6	9	5	49	05	4	81	24	21	4	6	34	31	6	05
p	393	**12.**	0.8	0.1	0.03	0.01	0.00	0.0	0.00	0.0	0.0	0.0	0.00	0.00	0.0	0.0	0.00	5.44
H	.39	**797**	831	483	456	118	0993	001	119	003	040	013	439	088	023	013	034	E-
4	51	**32**	48	14	5	1	646	9	4	81	99	05	4	7	34	31	8	05
p	725	**17.**	1.0	0.1	0.03	0.01	0.00	0.0	0.00	0.0	0.0	0.0	0.00	0.00	0.0	0.0	0.00	2.73
H	.20	**267**	090	693	738	209	1438	002	119	003	046	014	501	097	023	013	017	E-
4	1	**1**	46	37	7	6	403	85	4	81	83	38	9	8	34	31	8	05
p	111	**35.**	1.1	0.1	0.03	0.01	0.00	0.0	0.00	0.0	0.0	0.0	0.00	0.00	0.0	0.0	0.00	0.00
H	8.2	**367**	377	908	736	209	1382	002	119	003	049	015	412	088	023	013	112	016
4	95	**71**	04	97	1	2	573	5	4	81	33	27	4	7	34	31	8	4
p	151	**68.**	1.1	0.1	0.02	0.00	0.00	0.0	0.00	0.0	0.0	0.0		0.00	0.0	0.0	0.00	0.00
H	3.2	**043**	030	851	668	863	1786	003	119	003	050	015	0.00	106	023	013	121	016
4	85	**15**	31	45	8	4	555	28	4	81	28	64	539	3	34	31	9	2
p	188	**86.**	1.2	0.2	0.02	0.00	0.00	0.0	0.00	0.0	0.0	0.0	0.00	0.00	0.0	0.0	0.00	0.00
H	0.2	**479**	119	034	752	890	0909	001	119	003	039	012	418	082	023	013	109	015
4	17	**78**	72	35	8	6	587	61	4	81	07	13	8	5	34	31	7	7
p	269	**156**	1.0	0.1	0.02	0.00	0.02	0.0	0.00	0.0	0.0	0.0	0.00	0.00	0.0	0.0	0.01	0.00
H	4.5	**.53**	678	795	875	931	5842	055	119	003	071	022	214	041	023	013	339	190
4	39	**03**	6	94	8	6	948	15	4	81	98	15	7	7	34	31	8	3
p	403	**313**	1.0	0.1	0.02	0.00	0.00	0.0	0.00	0.0	0.0	0.0	0.00	0.00	0.0	0.0	0.01	0.00
H	3.1	**.09**	004	678	672	878	2129	003	119	003	089	028	214	041	023	013	115	162
4	69	**44**	56	56	5	1	133	75	4	81	24	49	7	7	34	31	4	5
p	497	**467**	1.0	0.1	0.02	0.00	0.00	0.0	0.00	0.0	0.0	0.0	0.00	0.00	0.0	0.0	0.01	0.00
H	2.3	**.12**	349	736	763	928	2824	005	119	003	126	040	214	041	023	013	208	186
4	23	**28**	9	82	2	4	112	37	4	81	25	71	7	7	34	31	4	6
p	630	**434**	1.0	0.1	0.03	0.01	0.00	0.0	0.00	0.0	0.0	0.0	0.00	0.00	0.0	0.0	0.02	0.00
H	0.0	**.91**	304	742	463	121	9237	016	119	003	169	052	214	041	023	013	428	330
4	06	**06**	44	93	8	5	017	51	4	81	82	23	7	7	34	31	7	8
p	678	**659**	0.1	0.1		0.00			0.00	9.5	0.0	0.0	0.00	0.00	0.0	0.0	0.00	
H	9.8	**.79**	606	180	0.00	399			010	7E-	014	010	024	012	003	003	261	0.00
4	87	**89**	06	14	64	9			9	05	01	1	2	2	22	74	8	145
p	695	**694**	0.3	0.2	0.00	0.00	0.00	0.0	0.00	9.5	0.0	0.0	0.00	0.00	0.0	0.0		0.00
H	6.5	**.82**	897	856	650	420	0356	002	010	7E-	014	011	024	012	003	003	0.00	183
4	91	**86**	95	35	1	2	912	34	9	05	8	18	2	2	22	74	316	3
p	713	**732**	0.6	0.4	0.00	0.00	0.00	0.0	0.00	9.5	0.0	0.0	0.00	0.00	0.0	0.0	0.00	0.00
H	3.6	**.13**	291	649	911	611	1409	012	010	7E-	022	016	024	012	003	003	946	576
4	62	**36**	04	93	6	4	975	21	9	05	09	98	2	2	22	74	3	3
p	8.0	**0.7**	0.5	0.0	0.03	0.01	0.00	0.0	0.00	0.0	0.0	0.0	0.00	0.00	0.0	0.0	0.00	7.53
H	796	**002**	788	971	617	170	0720	001	119	003	047	014	508	099	023	013	057	E-
6	9	**93**	13	04	8	3	77	29	4	81	41	6	1	2	34	31	6	05
p	424	**31.**	0.9	0.1	0.03	0.01	0.00	9.7	0.00	0.0	0.0	0.0	0.00	0.00	0.0	0.0	0.00	5.32
H	.32	**376**	155	541	495	130	0477	7E-	119	003	041	012	443	086	023	013	029	E-
6	73	**57**	77	3	2	7	377	05	4	81	36	72	3	5	34	31	1	05
p	753	**#DI**	1.2	0.1		0.00	0.00	0.0	0.00	0.0	0.0	0.0		0.00	0.0	0.0	0.00	5.32
H	.07	**V/0**	155	441	0.03	881	1954	002	119	002	030	006	0.00	045	023	009	057	E-
6	09	**!**	35	94	855	8	672	44	4	69	79	66	33	3	34	41	6	05
p	146	**51.**	1.1	0.2	0.02	0.00	0.00	0.0	0.00	0.0	0.0	0.0	0.00		0.0	0.0	0.00	0.00
H	8.6	**171**	988	011	879	931	1289	002	119	003	025	007	268	0.00	023	013	093	013
6	95	**5**	67	66	2	9	732	33	4	81	09	79	9	053	34	31	5	1
p	184	**134**	1.1	0.1	0.02	0.00	0.00	0.0	0.00	0.0	0.0	0.0	0.00	0.00	0.0	0.0	0.00	7.53
H	1.3	**.46**	888	994	861	926	0735	001	119	003	041	012	446	087	023	013	057	E-
6	89	**59**	65	47	7	3	198	31	4	81	67	81	7	1	34	31	6	05

p	287	**191**	1.0	0.1	0.02	0.00	0.00	0.0	0.00	0.0	0.0	0.0	0.00	0.00	0.0	0.0	0.00	0.00
H	3.6	**.38**	603	780	220	721	4613	009	119	003	041	012	214	041	023	013	141	021
6	88	**41**	12	12	5	8	212	24	4	81	74	77	7	7	34	31	2	4
p	411	**58.**	1.0	0.1	0.02	0.00	0.00	0.0	0.00	0.0	0.0	0.0	0.00	0.00	0.0	0.0	0.00	0.00
H	2.9	**736**	729	806	118	685	2129	003	119	003	041	012	214	041	023	013	205	033
6	86	**39**	29	78	4	8	133	75	4	81	74	77	7	7	34	31	9	1
p	496	**189**	1.1	0.1	0.01	0.00	0.00	0.0	0.00	0.0			0.00	0.00	0.0	0.0	0.00	6.07
H	0.1	**.76**	459	925	864	603	8962	015	119	003			214	041	023	013	044	E-
6	16	**81**	95	8	4	1	259	96	4	81			7	7	34	31	6	05
p	626	**364**	1.2	0.2	0.02	0.00			0.00	0.0	0.0	0.0	0.00	0.00	0.0	0.0	0.00	0.00
H	4.5	**.38**	570	108	115	717			119	003	075	023	214	041	023	013	441	076
6	65	**08**	8	93	8	3			4	81	57	41	7	7	34	31	1	3
p	659	**529**	0.1	0.1	0.00	0.00	0.00	0.0	0.00	9.5	0.0	0.0	0.00	0.00	0.0	0.0	0.00	0.00
H	9.3	**.60**	635	198	390	237	0253	001	010	7E-	012	008	024	012	003	003	093	058
6	2	**64**	69	43	3	1	816	87	9	05	63	49	2	2	22	74	1	1
p	674	**605**	0.5	0.3	0.00	0.00	0.00	0.0	0.00	9.5	0.0	0.0	0.00	0.00	0.0	0.0	0.00	0.00
H	3.0	**.84**	055	955	578	376	0398	002	010	7E-	011	009	024	012	003	003	473	308
6	87	**11**	94	92	2	3	805	64	9	05	33	26	2	2	22	74	9	2
p	688	**706**	0.6	0.4	0.01	0.01			0.00	0.0	0.0	0.0	0.00	0.00	0.0	0.0	0.01	0.01
H	6.0	**.11**	095	568	417	077			053	005	042	035	024	012	003	003	731	134
6	72	**13**	21	7	5	5			1	96	13	93	2	2	22	74	2	1
p	7.8	**0.3**	0.5	0.0	0.03	0.01	0.00	0.0	0.00	0.0	0.0	0.0	0.00	0.00	0.0	0.0	0.00	5.33
H	220	**913**	465	917	668	186	1038	001	119	003	044	013	364	076	023	013	030	E-
9	03	**92**	58	39	8	9	184	83	4	81	84	75	3	4	34	31	6	05
p	447	**15.**	0.9	0.1	0.03	0.01	0.00	7.5	0.00	0.0	0.0	0.0	0.00	0.00	0.0	0.0	0.00	0.00
H	.00	**489**	815	657	412	105	0420	E-	119	003	039	012	305	061	023	013	079	010
9	41	**92**	14	92	9	7	292	05	4	81	37	06	7	9	34	31	5	8
p	125	**1.2**	1.1	0.2			0.00	0.0	0.00	0.0	0.0	0.0	0.00		0.0	0.0	0.00	0.00
H	6.8	**907**	931	001	0.03	0.01	2238	003	119	003	067	024	725	0.00	023	013	143	021
9	64	**77**	77	84	641	178	84	95	4	81	65	41	1	166	34	31	2	8
p	165	**18.**	1.1	0.1		0.00	0.00	0.0	0.00	0.0	0.0	0.0	0.00	0.00	0.0	0.0	0.00	0.00
H	2.5	**583**	716	966	0.02	903	1120	002	119	003	049	015	530	103	023	013	164	025
9	07	**92**	52	9	793	9	988	04	4	81	45	16	1	1	34	31	5	6
p	202	**39.**	1.2	0.2	0.02	0.00	0.00	0.0	0.00	0.0	0.0	0.0	0.00	0.00	0.0	0.0	0.00	0.00
H	6.0	**023**	493	096	725	882	0825	001	119	003	044	014	480	095	023	013	666	087
9	51	**34**	99	25	4	3	529	46	4	81	83	04	6	4	34	31	7	2
p	297	**186**	1.0	0.1	0.02	0.00	0.00	0.0	0.00	0.0	0.0	0.0	0.00	0.00	0.0	0.0	0.01	
H	5.1	**.45**	598	781	763	894	9897	022	119	003	091	028	214	041	023	013	355	0.00
9	33	**66**	04	24	6	3	601	19	4	81	07	2	7	7	34	31	9	181
p	526	**571**	1.1	0.1	0.03		0.00	0.0	0.00	0.0	0.0	0.0	0.00	0.00	0.0	0.0	0.04	0.00
H	5.8	**.26**	315	898	845	0.01	2218	004	119	003	136	045	214	041	023	013	134	609
9	24	**06**	38	5	8	275	766	8	4	81	25	18	7	7	34	31	2	6
p	649	**101**	1.1	0.1	0.05	0.01	0.00	0.0	0.00	0.0	0.0	0.0	0.00	0.00	0.0	0.0	0.05	0.00
H	8.3	**2.8**	233	884	012	744	4244	007	119	003	171	059	214	041	023	013	144	812
9	71	**95**	08	9	3	3	951	78	4	81	58	2	7	7	34	31	8	3
p	683	**113**	0.2	0.1		0.00	0.00	0.0	0.00	9.5	0.0	0.0	0.00	0.00	0.0	0.0		0.00
H	6.4	**8.7**	074	592	0.00	480	0362	002	010	7E-	017	012	024	012	003	003	0.00	431
9	72	**58**	32	67	753	3	643	44	9	05	36	53	2	2	22	74	732	2
p	696	**120**	0.5	0.4	0.01	0.00	0.00	0.0	0.00	9.5	0.0	0.0	0.00	0.00	0.0	0.0		0.00
H	9.2	**9.6**	928	447	286	862	0471	003	010	7E-	029	020	024	012	003	003	0.01	701
9	83	**63**	27	87	8	6	538	06	9	05	76	43	2	2	22	74	248	6
p	715	**125**	0.6	0.4	0.02	0.01	0.00	0.0	0.00	9.5	0.0	0.0	0.00	0.00	0.0	0.0	0.04	0.02
H	2.9	**2.8**	706	917	365	731	1243	008	010	7E-	043	033	024	012	003	003	005	383
9	06	**44**	87	38	3	2	221	88	9	05	88	34	2	2	22	74	6	8

`

Experiment 2: CC_o^{-1} Average cPANI breakthrough curve

PV_accurate	pH4_ UC	pH4_UC_Std	PV_accurate_1	pH4_A	pH4_A_Std	PV_accurate_2	pH6_UC	pH6_UC_Std	PV_accurate_3	pH6_A	pH6_A_Std	PV_accurate_4	pH9_UC	pH9_UC_Std	PV_accurate_5	pH9_A	pH9_A_Std
218.997	0.057	0.02	209.63	0.09	0.03	238.639	0.049	0.01	233.183	0.146	0.04	238.137	0.052	0.02	228.495	0.156	0.04
420.984	0.053	0.02	401.55	0.07	0.02	346.941	0.045	0.01	453.919	0.097	0.03	459.061	0.045	0.01	425.748	0.053	0.02
618.505	0.049	0.01	580.75	0.05	0.01	465.583	0.041	0.01	684.831	0.048	0.01	702.179	0.039	0.01	632.094	0.057	0.02
833.256	0.042	0.01	777.42	0.10	0.03	695.847	0.038	0.01	917.536	0.042	0.01	946.333	0.038	0.01	851.031	0.052	0.01
1009.449	0.035	0.01	944.10	0.16	0.05	912.215	0.035	0.01	1122.617	0.036	0.01	1162.255	0.036	0.01	1076.812	0.046	0.01
1226.963	0.036	0.01	963.25	0.12	0.03	1133.935	0.034	0.01	1142.291	0.034	0.01	1292.478	0.039	0.01	1094.298	0.047	0.01
1383.538	0.037	0.01	1148.97	0.08	0.02	1352.639	0.034	0.01	1344.448	0.033	0.01	1503.190	0.041	0.01	1263.046	0.047	0.01
1521.163	0.034	0.01	1306.67	0.05	0.01	1562.939	0.031	0.01	1537.976	0.031	0.01	1719.498	0.042	0.01	1417.574	0.048	0.01
1632.609	0.031	0.01	1508.21	0.16	0.04	1778.546	0.030	0.01	1735.931	0.034	0.01	1945.570	0.040	0.01	1597.760	0.041	0.01
1838.168	0.032	0.01	1699.67	0.27	0.08	1985.777	0.035	0.01	1920.330	0.037	0.01	2147.270	0.040	0.01	1750.862	0.032	0.01
2016.234	0.033	0.01	1891.19	0.17	0.05	2186.995	0.037	0.01	2130.734	0.038	0.01	2342.953	0.045	0.01	1928.138	0.033	0.01
2171.046	0.034	0.01	2058.79	0.07	0.02	2373.745	0.039	0.01	2336.754	0.038	0.01	2450.834	0.045	0.01	2101.721	0.037	0.01
2371.920	0.035	0.01	2214.56	0.05	0.02	2520.297	0.039	0.01	2521.158	0.050	0.01	2639.709	0.042	0.01	2111.122	0.041	0.01
2543.559	0.034	0.01	2397.14	0.04	0.01	2713.415	0.038	0.01	2641.330	0.071	0.02	2829.438	0.107	0.03	2118.262	0.044	0.01
2752.991	0.033	0.01	2555.25	0.07	0.02	2914.225	0.042	0.01	2837.021	0.054	0.02	3015.027	0.174	0.05	2255.248	0.049	0.01
2972.381	0.031	0.01	2751.62	0.09	0.03	3014.156	0.045	0.01	3070.829	0.036	0.01	3296.244	0.150	0.04	2263.894	0.048	0.01
3138.082	0.029	0.01	2956.57	0.06	0.02	3206.394	0.043	0.01	3318.231	0.035	0.01	3400.472	0.118	0.03	2280.122	0.048	0.01
3343.259	0.030	0.01	3153.55	0.04	0.01	3414.531	0.037	0.01	3511.320	0.035	0.01	3580.374	0.086	0.02	2307.922	0.061	0.02
3537.709	0.031	0.01	3387.68	0.04	0.01	3619.779	0.032	0.01	3747.411	0.036	0.01	3823.615	0.059	0.02	2570.646	0.083	0.02
3737.473	0.032	0.01	3590.18	0.05	0.01	3825.833	0.031	0.01	3953.973	0.037	0.01	3933.772	0.032	0.01	2781.766	0.066	0.02
3908.413	0.033	0.01	3806.86	0.04	0.01	4026.701	0.031	0.01	4077.060	0.037	0.01	4039.286	0.031	0.01	3036.399	0.052	0.01
4098.464	0.033	0.01	3978.91	0.03	0.01	4243.739	0.031	0.01	4277.652	0.036	0.01	4163.905	0.031	0.01	3085.250	0.049	0.01
4293.491	0.032	0.01	4151.72	0.03	0.01	4473.264	0.031	0.01	4390.855	0.059	0.02	4205.712	0.052	0.01	3107.662	0.045	0.01
4439.376	0.037	0.01	4350.14	0.03	0.01	4708.113	0.030	0.01	4492.385	0.082	0.02	4222.169	0.074	0.02	3129.362	0.012	0.00
4670.109	0.043	0.01	4531.69	0.03	0.01	4934.532	0.029	0.01	4530.775	0.104	0.03	4235.922	0.098	0.03	3152.786	0.042	0.01
4870.004	0.050	0.01	4794.98	0.03	0.01	5185.337	0.035	0.01	4780.533	0.127	0.04	4492.937	0.123	0.04			
5089.767	0.058	0.02	4928.78	0.04	0.01	5306.598	0.042	0.01	4814.743	0.091	0.03	4512.874	0.075	0.02			
5307.898	0.027	0.01	5130.48	0.05	0.01	5430.701	0.026	0.01	4947.968	0.055	0.02	4522.436	0.028	0.01			
5479.680	0.033	0.01	5267.30	0.08	0.02	5653.769	0.033	0.01	5053.944	0.066	0.02	4526.286	0.054	0.02			
5607.879	0.032	0.01	5489.23	0.03	0.01	5873.557	0.044	0.01	5081.556	0.079	0.02	4550.829	0.079	0.02			
			5693.097846	0.035884354	0.010761387				5095.788	0.067	0.02	4561.999	0.105	0.03			

Raw data:

PV_accurate	pH4_ UC	pH4_UC_ Std	PV_accurate_2	pH6_ UC	pH6_UC_ Std	PV_accurate_4	pH9_ UC	pH9_UC_ Std
218.997	0.057	0.02	238.639	0.049	0.01	238.137	0.052	0.02
420.984	0.053	0.02	346.941	0.045	0.01	459.061	0.045	0.01
618.505	0.049	0.01	465.583	0.041	0.01	702.179	0.039	0.01
833.256	0.042	0.01	695.847	0.038	0.01	946.333	0.038	0.01
1009.449	0.035	0.01	912.215	0.035	0.01	1162.255	0.036	0.01
1226.963	0.036	0.01	1133.935	0.034	0.01	1292.478	0.039	0.01
1383.538	0.037	0.01	1352.639	0.034	0.01	1503.190	0.041	0.01
1521.163	0.034	0.01	1562.939	0.031	0.01	1719.498	0.042	0.01
1632.609	0.031	0.01	1778.546	0.030	0.01	1945.570	0.040	0.01
1838.168	0.032	0.01	1985.777	0.035	0.01	2147.270	0.040	0.01
2016.234	0.033	0.01	2186.995	0.037	0.01	2342.953	0.045	0.01
2171.046	0.034	0.01	2373.745	0.039	0.01	2450.834	0.045	0.01
2371.920	0.035	0.01	2520.297	0.039	0.01	2639.709	0.042	0.01
2543.559	0.034	0.01	2713.415	0.038	0.01	2829.438	0.107	0.03
2752.991	0.033	0.01	2914.225	0.042	0.01	3015.027	0.174	0.05
2972.381	0.031	0.01	3014.156	0.045	0.01	3296.244	0.150	0.04
3138.082	0.029	0.01	3206.394	0.043	0.01	3400.472	0.118	0.03
3343.259	0.030	0.01	3414.531	0.037	0.01	3580.374	0.086	0.02
3537.709	0.031	0.01	3619.779	0.032	0.01	3823.615	0.059	0.02

`

3737.473	0.032	0.01	3825.833	0.031	0.01	3933.772	0.032	0.01
3908.413	0.033	0.01	4026.701	0.031	0.01	4039.286	0.031	0.01
4098.464	0.033	0.01	4243.739	0.031	0.01	4163.905	0.031	0.01
4293.491	0.032	0.01	4473.264	0.031	0.01	4205.712	0.052	0.01
4439.376	0.037	0.01	4708.113	0.030	0.01	4222.169	0.074	0.02
4670.109	0.043	0.01	4934.532	0.029	0.01	4235.922	0.098	0.03
4870.004	0.050	0.01	5185.337	0.035	0.01	4492.937	0.123	0.04
5089.767	0.058	0.02	5306.598	0.042	0.01	4512.874	0.075	0.02
5307.898	0.027	0.01	5430.701	0.026	0.01	4522.436	0.028	0.01
5479.680	0.033	0.01	5653.769	0.033	0.01	4526.286	0.054	0.02
5607.879	0.032	0.01	5873.557	0.044	0.01	4550.829	0.079	0.02
						4561.999	0.105	0.03

PV_accurate_1	pH4_A	pH4_A_Std	PV_accurate_3	pH6_A	pH6_A_Std	PV_accurate_5	pH9_A	pH9_A_Std
209.63	0.09	0.03	233.183	0.146	0.04	228.495	0.156	0.04
401.55	0.07	0.02	453.919	0.097	0.03	425.748	0.053	0.02
580.75	0.05	0.01	684.831	0.048	0.01	632.094	0.057	0.02
777.42	0.10	0.03	917.536	0.042	0.01	851.031	0.052	0.01
944.10	0.16	0.05	1122.617	0.036	0.01	1076.812	0.046	0.01
963.25	0.12	0.03	1142.291	0.034	0.01	1094.298	0.047	0.01
1148.97	0.08	0.02	1344.448	0.033	0.01	1263.046	0.047	0.01
1306.67	0.05	0.01	1537.976	0.031	0.01	1417.574	0.048	0.01
1508.21	0.16	0.04	1735.931	0.034	0.01	1597.760	0.041	0.01
1699.67	0.27	0.08	1920.330	0.037	0.01	1750.862	0.032	0.01
1891.19	0.17	0.05	2130.734	0.038	0.01	1928.138	0.033	0.01
2058.79	0.07	0.02	2336.754	0.038	0.01	2101.721	0.037	0.01
2214.56	0.05	0.02	2521.158	0.050	0.01	2111.122	0.041	0.01
2397.14	0.04	0.01	2641.330	0.071	0.02	2118.262	0.044	0.01
2555.25	0.07	0.02	2837.021	0.054	0.02	2255.248	0.049	0.01
2751.62	0.09	0.03	3070.829	0.036	0.01	2263.894	0.048	0.01
2956.57	0.06	0.02	3318.231	0.035	0.01	2280.122	0.048	0.01
3153.55	0.04	0.01	3511.320	0.035	0.01	2307.922	0.061	0.02
3387.68	0.04	0.01	3747.411	0.036	0.01	2570.646	0.083	0.02
3590.18	0.05	0.01	3953.973	0.037	0.01	2781.766	0.066	0.02
3806.86	0.04	0.01	4077.060	0.037	0.01	3036.399	0.052	0.01
3978.91	0.03	0.01	4277.652	0.036	0.01	3085.250	0.049	0.01
4151.72	0.03	0.01	4390.855	0.059	0.02	3107.662	0.045	0.01
4350.14	0.03	0.01	4492.385	0.082	0.02	3129.362	0.012	0.00
4531.69	0.03	0.01	4530.775	0.104	0.03	3152.786	0.042	0.01

`

4794.98	0.03	0.01	4780.533	0.127	0.04
4928.78	0.04	0.01	4814.743	0.091	0.03
5130.48	0.05	0.01	4947.968	0.055	0.02
5267.30	0.08	0.02	5053.944	0.066	0.02
5489.23	0.03	0.01	5081.556	0.079	0.02
5693.098	0.035	0.0107	5095.788	0.067	0.02

Experiment 2: cPANI loading comparison bar graph

Column	Effluent mg/L	Effluent mg/L_std	Solid	Solid_std	Column	Effluent mg/L	Effluent mg/L_std	Solid	Solid_std
4	6.24	0.53	10.94	0.07	4_AlOH	4.99	0.59	6.67	0.65
6	9.68	2.01	8.38	0.47	6_AlOH	5.70	1.35	5.31	0.41
9	5.51	0.56	3.66	0.26	9_AlOH	3.61	0.65	2.40	0.16

Experiment 2: cPANI loading with distance

col	Distance	PANImgg	std
1	.5	156.00	0.61
1	1.5	24.65	0.10
1	2.5	5.95	0.02
1	3.5	1.70	0.01
1	4.5	1.70	0.01
1	5.5	0.85	0.00
1	6.5	0.85	0.00
1	7.5	0.30	0.00
1	8.5	0.30	0.00
1	9.5	0.30	0.00
1	10.5	0.30	0.00
1	11.5	0.30	0.00
1	12.5	0.30	0.00
1	13.5	0.30	0.00
1	14.5	0.30	0.00
1	15.5	0.30	0.00
1	16.5	0.30	0.00
1	17.50	0.30	0.00
2	.5	161.10	0.64
2	1.5	4.25	0.02
2	2.5	2.55	0.01

`

2	3.5	1.70	0.01
2	4.5	1.70	0.01
2	5.5	2.55	0.01
2	6.5	2.55	0.01
2	7.5	1.70	0.01
2	8.5	1.70	0.01
2	9.5	1.70	0.01
2	10.5	1.70	0.01
2	11.5	1.70	0.01
2	12.5	0.85	0.00
2	13.5	0.85	0.00
2	14.5	0.30	0.00
2	15.5	0.30	0.00
2	16.5	0.30	0.00
2	17.5	0.30	0.00
3	.5	86.85	0.34
3	1.5	10.04	0.04
3	2.5	9.04	0.04
3	3.5	7.03	0.03
3	4.5	6.02	0.02
3	5.5	7.03	0.03
3	6.5	3.01	0.01
3	7.5	1.00	0.00
3	8.5	0.35	0.00
3	9.5	0.35	0.00
3	10.5	0.35	0.00
3	11.5	0.35	0.00
3	12.5	0.35	0.00
3	13.5	0.35	0.00
3	14.5	0.35	0.00
3	15.5	0.35	0.00
3	16.5	0.35	0.00
3	17.5	0.35	0.00
4	0.50	95.04	8.90
4	1.50	16.99	1.59
4	2.50	11.24	1.05
4	3.50	8.18	0.77
4	4.50	7.82	0.73
4	5.50	7.91	0.74

4		6.50	5.12	0.48
4		7.50	5.93	0.56
4		8.50	1.71	0.16
	4	9.50	1.62	0.15
	4	10.50	0	#DIV/0!
	4	11.50	0.63	0.06
	4	12.50	0.27	0.03
	4	13.50	0.45	0.04
	4	14.50	0.18	0.02
	4	15.50	0.63	0.06
	4	16.50	0.27	0.03
	4	17.50	0.63	0.06
	5	0.50	65.28	6.12
	5	1.50	4.77	0.45
	5	2.50	3.87	0.36
	5	3.50	4.05	0.38
	5	4.50	4.23	0.40
	5	5.50	3.06	0.29
	5	6.50	3.06	0.29
	5	7.50	1.98	0.19
	5	8.50	1.08	0.10
	5	9.50	0.36	0.03
	5	10.50	0.72	0.07
	5	11.50	0.36	0.03
	5	12.50	0.72	0.07
	5	13.50	0.27	0.03
	5	14.50	0.72	0.07
	5	15.50	0.27	0.03
	5	16.50	0.72	0.07
	5	17.50	0.27	0.03
	6	0.50	7.64	0.72
	6	1.50	3.78	0.35
	6	2.50	2.25	0.21
	6	3.50	2.97	0.28
	6	4.50	1.98	0.19
	6	5.50	1.98	0.19
	6	6.50	1.53	0.14
	6	7.50	1.89	0.18
	6	8.50	1.26	0.12

6	9.50	1.89	0.18
6	10.50	1.35	0.13
6	11.50	1.71	0.16
6	12.50	0.99	0.09
6	13.50	1.44	0.13
6	14.50	0.90	0.08
6	15.50	1.08	0.10
6	16.50	0.54	0.05
6	17.50	0.99	0.09
7	0.50	99.98	9.37
7	1.50	4.77	0.45
7	2.50	1.89	0.18
7	3.50	1.35	0.13
7	4.50	0.54	0.05
7	5.50	1.08	0.10
7	6.50	0.54	0.05
7	7.50	0.99	0.09
7	8.50	0.54	0.05
7	9.50	0.99	0.09
7	10.50	0.36	0.03
7	11.50	0.90	0.08
7	12.50	0.54	0.05
7	13.50	0.81	0.08
7	14.50	0.36	0.03
7	15.50	0.72	0.07
7	16.50	0.27	0.03
7	17.50	0.81	0.08
8	0.50	67.97	6.37
8	1.50	16.72	1.57
8	2.50	9.17	0.86
8	3.50	7.10	0.67
8	4.50	4.77	0.45
8	5.50	2.34	0.22
8	6.50	1.53	0.14
8	7.50	1.44	0.13
8	8.50	0.99	0.09
8	9.50	1.44	0.13
8	10.50	0.90	0.08
8	11.50	1.53	0.14

8	12.50	0.99	0.09
8	13.50	1.26	0.12
8	14.50	0.90	0.08
8	15.50	1.35	0.13
8	16.50	0.90	0.08
8	17.50	1.44	0.13
9	0.50	21.04	1.97
9	1.50	7.64	0.72
9	2.50	5.21	0.49
9	3.50	5.21	0.49
9	4.50	5.48	0.51
9	5.50	4.41	0.41
9	6.50	3.51	0.33
9	7.50	3.96	0.37
9	8.50	2.88	0.27
9	9.50	2.79	0.26
9	10.50	1.53	0.14
9	11.50	1.98	0.19
9	12.50	1.35	0.13
9	13.50	1.62	0.15
9	14.50	1.17	0.11
9	15.50	1.71	0.16
9	16.50	1.26	0.12
9	17.50	1.44	0.13
10	0.50	86.23	8.08
10	1.50	3.15	0.29
10	2.50	2.34	0.22
10	3.50	2.61	0.24
10	4.50	2.07	0.19
10	5.50	2.70	0.25
10	6.50	2.07	0.19
10	7.50	2.16	0.20
10	8.50	1.80	0.17
10	9.50	1.62	0.15
10	10.50	1.08	0.10
10	11.50	1.71	0.16
10	12.50	1.53	0.14
10	13.50	1.62	0.15
10	14.50	0.81	0.08

10	15.50	1.62	0.15
10	16.50	0.63	0.06
10	17.50	1.08	0.10
11	0.50	3.24	0.30
11	1.50	1.53	0.14
11	2.50	1.71	0.16
11	3.50	0.99	0.09
11	4.50	1.35	0.13
11	5.50	1.17	0.11
11	6.50	1.17	0.11
11	7.50	0.72	0.07
11	8.50	0.99	0.09
11	9.50	0.63	0.06
11	10.50	1.08	0.10
11	11.50	0.45	0.04
11	12.50	1.08	0.10
11	13.50	0.36	0.03
11	14.50	0.72	0.07
11	15.50	0.18	0.02
11	16.50	0.72	0.07
11	17.50	0.72	0.07
12	0.50	42.89	4.02
12	1.50	4.41	0.41
12	2.50	3.42	0.32
12	3.50	1.98	0.19
12	4.50	2.07	0.19
12	5.50	1.62	0.15
12	6.50	1.89	0.18
12	7.50	1.44	0.13
12	8.50	1.62	0.15
12	9.50	1.08	0.10
12	10.50	1.35	0.13
12	11.50	0.54	0.05
12	12.50	1.26	0.12
12	13.50	0.45	0.04
12	14.50	0.90	0.08
12	15.50	0.18	0.02
12	16.50	0.81	0.08
12	17.50	0.27	0.03

`

Experiment 3A: cPANI loading with distance

Distance	PANImgg_TN	TN_std
1	39.20158	3.67309
3	9.350836	0.87615
5	9.800396	0.918273
7	4.225859	0.395952
9	4.675418	0.438075
11	3.236828	0.303283
13	3.596475	0.336981
15	2.607445	0.244311
17	2.607445	0.244311
19	1.168855	0.109519
21	1.258766	0.117943
23	1.798238	0.16849
25	1.078943	0.101094
27	1.348678	0.126368
29	0.539471	0.050547
31	0.989031	0.09267
33	0.269736	0.025274
35	0.629383	0.058972
37	0.179824	0.016849
39	0.629383	0.058972
41	0.269736	0.025274
43	0.629383	0.058972
45	0.269736	0.025274
47	0.629383	0.058972
49	0.089912	0.008425
51	0.629383	0.058972
53	0.089912	0.008425
57	0.719295	0.067396
61	0.179824	0.016849
63	0.719295	0.067396
65	0.179824	0.016849
67	0.539471	0.050547
69	0.089912	0.008425
71	0.629383	0.058972
73	0.089912	0.008425

`

`

75	0.629383	0.058972
77	0.269736	0.025274
79	0.629383	0.058972
81	0.089912	0.008425
83	0.629383	0.058972
85	0.269736	0.025274
87	0.719295	0.067396
89	0.269736	0.025274
91	0.629383	0.058972
93	0.269736	0.025274
95	0.719295	0.067396
97	0.089912	0.008425
99	0.629383	0.058972
101	0.179824	0.016849
103	0.539471	0.050547

Experiment 3B: cPANI loading with distance

Distance	PANImgg_TN	TN_std
1	51.69933	4.844099
3	1.798238	0.16849
5	1.258766	0.117943
7	1.43859	0.134792
9	0.629383	0.058972
11	0.629383	0.058972
13	1.168855	0.109519
15	0.449559	0.042123
17	0.809207	0.075821
19	0.359648	0.033698
21	0.629383	0.058972
23	0.179824	0.016849
25	0.719295	0.067396
27	0.179824	0.016849
29	0.719295	0.067396
31	0.359648	0.033698
35	0.719295	0.067396
37	0.089912	0.008425

`

`

39	0.269736	0.025274
41	0.629383	0.058972
43	0.359648	0.033698
45	0.629383	0.058972
47	0.269736	0.025274
49	0.809207	0.075821
51	0.269736	0.025274
53	0.719295	0.067396
55	0.269736	0.025274
57	0.719295	0.067396
59	0.359648	0.033698
61	0.629383	0.058972
63	0.359648	0.033698
65	0.719295	0.067396
67	0.359648	0.033698
69	0.809207	0.075821
71	0.449559	0.042123
73	0.629383	0.058972
75	0.269736	0.025274
77	0.809207	0.075821
79	0.359648	0.033698
81	0.809207	0.075821
83	0.359648	0.033698
85	0.809207	0.075821
87	0.359648	0.033698
89	0.719295	0.067396
91	0.359648	0.033698
93	0.629383	0.058972
95	0.359648	0.033698
97	0.809207	0.075821
99	0.359648	0.033698
101	0.719295	0.067396

Experiment 4A: CC_o^{-1} PFAS breakthrough : AC= CAC with AlOH3 coated sand, SC= CAC in uncoated sand P=cPANI, Y=PANI

Col	PV_avg	PFBA_Cco	PFHpA_Cco	PFOA_Cco	PFNA_Cco	PFBS_Cco	PFHxS_Cco	PFOS_Cco	62FTS_Cco	PFBA_std	PFHpA_std	PFOA_std	PFNA_std	PFBS_std	PFHxS_std	PFOS_std	62FTS_std

`

	340.			0.86	1.67	0.89		1.01				0.07	1.03	0.00		0.64	0.03
A	909	0.93	1.07	168	110	562	0.91	007	1.54	0.08	0.33	839	400	886	0.00	078	214
C	1	984	0063	5	1	1	9842	5	6066	92	4526	4	4	6	4274	6	5
	391	0.99		0.79	0.74	0.96		0.31		0.14		0.10	0.26			0.29	0.16
A	9.48	552	1.23	976	867	535	0.90	333	1.37	527	0.42	878	811	0.08	0.00	374	210
C	1	4	0791	5	7	4	1355	9	5702	5	99	8	7	148	3094	7	1
	630	1.36		1.06	3.08	1.16		1.83		0.12		0.00	0.42	0.13			0.02
A	3.73	391	2.14	057	874	457	1.12	847	1.35	385	0.34	369	307	552	0.03	0.00	902
C	4	4	0129	8	8	4	3327	1	2772	6	3942	6	2	3	0778	827	2
	861	1.67		0.98		1.39		1.43		0.58		0.03		0.11		0.73	0.00
A	2.85	937	3.45	377	#VA	793	1.42	367	1.29	214	0.54	954	#VA	695	0.20	103	028
C	2	5	334	8	LUE!	8	2153	4	0329	7	1025	6	LUE!	6	6789	2	9
	107	1.00		1.39	0.60	1.66		2.17		0.06		0.02		0.59		0.10	0.09
A	38.6	213	1.68	319	897	098	1.22	141	1.26	462	0.40	203	0.00	541	0.03	392	936
C	4	4	1569	5	7	5	0993	9	5744	9	8494	6	988	6	1833	2	7
	134	0.85		0.80	1.04	0.83		0.37		0.02			1.09	0.00		0.51	0.27
A	07.6	590	0.80	248	661	399	0.53	487	0.55	816	0.13	0.36	395	980	0.16	944	736
C	3	1	1233	4	8	7	7677	9	0713	8	0092	116	1	3	1614	6	7
	234			2.06	0.15			0.49		0.16		0.00	0.00	0.17		0.04	0.01
A	29.6	1.10	0.81	892	160	1.00	1.03	238	0.71	409	0.01	717	640	876	0.01	551	892
C	3	867	6989	1	4	296	2388	1	0993	8	9251	9	8	3	1416	1	7
		0.95		0.93	0.91	0.75				0.03		0.00	0.07	0.05		0.14	0.07
A	255	954	0.91	423	076	298	1.10	0.79	0.88	286	0.05	980	477	738	0.08	244	166
C	33.2	6	1995	3	8	2	2352	53	5944	6	5942	3	6	8	8181	1	3
	277	1.56		4.16	1.16			0.83		0.01		4.41	0.53	0.08		0.59	0.02
A	41.1	729	1.46	106	686	0.85	0.98	274	0.95	506	0.40	997	387	659	0.04	831	138
C	5	5	6446	2	2	822	4685	1	3626	8	5312	6	9	9	4265	1	9
	424	0.93		1.16		1.17				0.00		0.04	0.07	0.08		0.04	0.01
A	86.7	541	0.86	932	1.09	508	0.96	0.10	1.09	776	0.04	726	354	698	0.06	305	210
C	7	7	2697	7	28	5	4183	217	1574	9	8374	2	6	1	8975	8	8
				0.88	0.40	1.07		0.05		0.01			0.04	0.06			0.06
A	445	0.95	0.77	622	465	113	0.94	891	0.91	759	0.00	0.07	621	667	0.12	0.02	655
C	48.4	432	8581	7	2	8	4862	1	739	5	5633	173	7	5	7242	917	2
	466			1.40	1.79	1.07		0.78		0.04			0.60	0.14		0.38	0.48
A	67.5	0.65	0.67	752	658	007	1.15	926	1.43	929	0.05	0.26	057	463	0.10	325	959
C	9	93	1745	7	8	7	3833	8	4539	9	3417	438	2	5	376	4	8
	340.	1.14		0.93	6.00	0.98		2.89		0.35		0.01	6.83	0.09		3.10	0.02
S	909	196	1.11	076	522	300	1.04	965	1.54	476	0.00	561	242	602	0.05	236	242
C	1	6	0075	1	3	6	3058	7	6699	1	8941	7	5	4	8658	2	4
		1.01		0.66	0.89	0.85				0.08		0.31	1.19	0.10		#VA	0.79
S	393	704	1.04	447	187	133	0.72	#VA	1.05	031	0.14	331	764	922	0.31	LUE	566
C	7.5	1	5873	9	7	9	6928	LUE!	7864	9	9244	8	3	6	9479	!	3
	635	1.16		1.01	2.34	1.41						0.03	0.00	0.35		#VA	0.04
S	4.16	348	1.87	408	421	165	1.34	#VA	1.37	0.09	0.01	644	700	279	0.16	LUE	667
C	7	4	9085	7	5	4	0289	LUE!	5724	289	7713	2	6	6	2398	!	5
	869	0.80		1.21		1.18		1.24		0.18		0.26		0.25			0.17
S	7.10	129	1.95	361	#VA	509	1.27	587	1.16	840	1.20	374	#VA	451	0.02	0.34	952
C	5	1	6407	7	LUE!	7	9244	8	815	6	6937	8	LUE!	2	7406	236	8
	108			1.43	0.53	1.48				0.10		0.02	0.00	0.01		0.20	0.01
S	88.2	0.93	1.41	644	762	655	1.24	2.43	1.26	741	0.11	608	745	215	0.05	283	343
C	6	279	2143	1	9	5	8537	894	339	6	7743	9	3	5	7619	6	5
	239			1.93	0.07	0.95				14.4		0.07	0.06	0.09		#VA	0.01
S	98.4		2.02	993	178	917	1.20	#VA	0.77	537	1.63	884	440	013	0.19	LUE	431
C	9		1793	1	3	9	8403	LUE!	3936	8	2692	4	2	9	1739	!	6
	261	1.24		1.86	1.09	0.78		1.03		0.64		1.31	0.55	0.06		0.17	0.00
S	35.3	042	0.87	135	338	354	1.12	632	0.96	639	0.12	583	281	495	0.06	566	501
C	4	3	8085	4	6	2	1281	7	4899	4	5594	5	6	5	7592	9	2
	283	1.53			1.14	0.80		0.95		0.09		0.11	0.56	0.03		0.57	0.04
S	83.4	118	1.24	1.00	020	030	0.89	238	0.94	563	0.22	090	967	951	0.10	225	684
C	7	8	7868	201	8	5	5412	7	3288	5	3195	5	8	1	105	2	2

	435	0.82			1.93	1.46		0.17		0.03		0.87	1.12	0.09			
S	52.6	645	0.95	1.91	140	605	1.01	964	1.18	320	0.01	797	668	181	0.12	0.06	0.02
C	3	3	3016	779	2	3	2256	1	9543	1	3497	9	3	5	7653	042	826
	457	0.66		1.00	0.29	0.99		0.05		0.05		0.02	0.04			0.00	
S	17.6	135	0.72	158	588	924	1.06	721	0.94	259	0.02	932	941	0.09	0.00	157	0.01
C	7	8	2959	1	8	4	6296	5	48	6	8685	5	5	82	3316	1	809
	328.	0.71		0.11		0.12				0.09		0.05		0.12		#VA	0.12
S	463	921	0.46	762	#VA	153	#VAL	#VA	0.09	636	0.03	407	#VA	464	#VA	LUE	045
P	2	7	1198	5	LUE!	6	UE!	LUE!	4139	2	3752	6	LUE!	9	LUE!	!	3
	624	2.55		0.32	0.90	0.48				0.53		0.16	0.19	0.09		#VA	
S	2.18	121	1.29	933	803	508	0.24	#VA	0.83	445	0.21	846	901	541	0.23	LUE	0.15
P	1	2	2719	8	5	5	3327	LUE!	5012	4	4428	2	3	1	3941	!	747
		1.27		0.68	0.94	0.81				0.15		0.22		0.27		#VA	0.47
S	852	188	1.24	326	678	627	0.67	#VA	1.01	793	0.09	195	1.02	868	0.42	LUE	463
P	0.59	2	1501	1	9	1	1927	LUE!	5629	3	0669	5	323	4	8093	!	4
	106	1.08		0.38	0.92	1.19				0.03		0.09	0.41			#VA	
S	24.4	581	1.52	893	572	336	0.33	#VA	0.97	366	0.29	227	340	0.95	0.24	LUE	0.03
P	3	2	7229	7	8	6	728	LUE!	8556	2	3251	3	8	673	1315	!	354
	132	0.88		0.38	0.33	0.36				0.12		0.12	0.19	0.06		#VA	0.04
S	05.8	083	0.57	643	500	312	0.12	#VA	0.51	816	0.04	103	390	150	0.09	LUE	489
P	8	3	7171	8	4	3	1526	LUE!	6942	4	3176	3	7	4	9351	!	7
	231	1.38		1.15	0.08	0.64				0.04		0.25	0.02	0.14		#VA	0.12
S	26.4	080	0.74	208	388	456	0.58	#VA	0.61	510	0.05	067	107	165	0.22	LUE	180
P	4	4	1213	8	2	7	6339	LUE!	1415	2	866	5	8	9	44	!	8
	252	1.39		0.72	0.50	0.73		0.24				0.11	0.38	0.11			0.05
S	34.5	777	0.80	522	146	239	0.56	906	0.79	0.31	0.17	238	851	115	0.01	0.22	353
P	6	5	2065	9	6	4	8529	2	2739	44	6416	6	2	4	904	37	7
	272	1.18		0.91	0.73	0.77		0.32		0.07		0.11	0.24	0.00		0.16	0.02
S	79.6	066	0.93	767	781	693	0.50	410	0.84	165	0.01	937	751	255	0.00	405	397
P	1	5	2073	6	9	1	0758	2	6047	7	6825	1	9	7	0528	4	7
	448	0.84		0.72	0.19					0.05		0.09	0.06	0.00		#VA	0.02
S	32.6	584	0.69	062	282	0.96	0.58	#VA	0.85	133	0.01	373	468	316	0.00	LUE	419
P	3	9	3633	1	9	189	4265	LUE!	3762	6	2521	8	9	5	0616	!	5
	327.	0.66		0.49	0.57	0.77				0.03		0.35	0.78	0.36		#VA	0.65
A	813	863	0.76	760	314	289	0.42	#VA	0.70	052	0.24	994	635	876	0.27	LUE	959
P	9	4	1793	5	2	6	0728	LUE!	3796	7	2728	5	2	6	4077	!	1
	619	3.01		0.70		0.97		0.76		2.66		0.14		0.07		0.07	0.13
A	3.80	766	1.87	272	#VA	104	0.89	529	1.13	535	0.09	296	#VA	472	0.17	801	653
P	4	5	4988	5	LUE!	3	9882	5	1822	4	8254	6	LUE!	4	907	7	8
	839	1.38		0.53	0.27	0.50						0.32	0.23	0.13		#VA	0.16
A	7.05	131	1.07	346	351	154	0.85	#VA	0.78	0.29	0.29	692	985	667	0.67	LUE	153
P	1	2	3131	3	3	3	7997	LUE!	3132	764	3235	2	8	6	1981	!	6
		0.88		0.74	2.61	1.06		0.96		0.10		0.22	0.53	0.18		0.17	0.24
A	104	627	1.59	719	963	069	0.90	605	1.13	283	0.25	740	123	479	0.31	398	571
P	77.6	1	5152	7	6	2	9706	8	7528	6	8675	9	4	6	2676	3	3
	222	1.25		1.03	0.15			0.27		0.17		0.35	0.00	0.07		0.16	0.01
A	29.7	322	0.74	472	550	0.75	0.73	694	0.69	010	0.02	053	708	812	0.06	976	400
P	8	9	4374	1	5	959	8605	8	7226	3	0028	3	1	9	5717	5	6
	243	1.06		0.72	0.47	0.75		0.60		0.05				0.03		0.07	0.06
A	60.0	702	0.70	298	670	206	0.74	044	0.75	188	0.07	0.03	0.01	973	0.08	705	212
P	5	3	3908	5	6	4	5249	7	5808	9	1335	069	262	6	2276	2	8
	265	1.04		1.07	0.63	0.80		0.45		0.16		0.29	0.01	0.07		0.10	0.02
A	53.3	108	0.89	524	093	595	0.56	928	0.76	668	0.16	334	429	737	0.22	660	867
P	2	1	8361	7	8	5	371	6	0735	1	0986	7	5	5	5418	5	7
	417	0.82		0.76	0.30	1.03				0.08		0.28	0.18	0.24		#VA	0.10
A	44.1	892	0.73	497	375	978	0.58	#VA	0.83	848	0.05	860	887	133	0.16	LUE	931
P	2	4	6644	4	9	2	5414	LUE!	153	9	1186	6	9	4	026	!	7
	438	0.97		0.62	0.19	0.99				0.04			0.01	0.01		#VA	0.11
A	74.6	751	0.64	654	080	317	0.61	#VA	0.73	687	0.01	0.04	844	377	0.07	LUE	955
P	9	9	096	6	7	6	7928	LUE!	5389	1	183	81	7	7	6556	!	4

	335.	0.99		0.58	1.00			0.22		0.15		0.10	0.09	0.12		0.13	0.17
A	227	236	1.06	916	039	0.72	0.52	011	1.14	707	0.20	279	448	003	0.15	935	761
Y	3	1	2881	4	2	299	509	3	3119	2	943	1	1	1	3029	6	1
	385	0.85		0.71	0.78	0.88				0.13		0.00	0.09			#VA	
A	5.60	548	0.99	796	843	204	0.67	#VA	#VAL	147	0.07	439	463	0.07	0.09	LUE	#VA
Y	1	9	3462	1	4	5	7777	LUE!	UE!	6	4923	7	8	058	5803	!	LUE!
	622	0.89		0.87	2.06	1.01				0.04			0.55	0.14		#VA	0.02
A	2.91	199	2.14	896	752	098	0.99	#VA	1.25	664	0.43	0.02	381	225	0.00	LUE	094
Y	7	3	7285	5	2	4	9821	LUE!	9832	9	2135	257	1	8	4519	!	1
	848	0.88		1.25	1.17							0.04	0.42	0.09		0.17	0.03
A	2.54	723	2.36	505	231	0.98	1.11	1.41	1.01	0.06	0.85	279	652	426	0.08	300	868
Y	9	1	7505	3	9	764	4195	924	44	785	7617	7	3	6	2074	7	4
	106	0.96		0.70	2.22			2.80		0.18		0.13		0.01		2.70	0.04
A	07.5	371	1.50	309	254	0.83	0.72	918	1.02	876	0.00	989	0.18	108	0.16	563	612
Y	2	4	2395	3	1	92	4084	4	7463	7	3378	4	133	7	7734	9	5
	133	1.08			0.17	0.73						0.12	0.05	0.05		#VA	0.09
A	22.4	612	0.95	0.43	884	893	0.34	#VA	0.34	0.03	0.37	051	884	333	0.12	LUE	181
Y	4	9	807	731	3	7	4592	LUE!	0773	268	945	6	3	8	1349	!	6
	233	3.40		1.37	0.08	0.68				0.69		0.25		0.14		#VA	0.00
A	87.0	289	0.98	183	981	919	0.86	#VA	0.70	083	0.09	195	0.00	992	0.25	LUE	162
Y	5	4	4906	5	4	1	128	LUE!	3634	1	1273	5	258	8	3156	!	8
	254	1.46		0.71	0.67	0.85		0.51		0.17		0.09	0.45	0.30			
A	76.8	907	0.77	110	535	797	0.86	892	0.86	259	0.09	859	566	013	0.00	0.41	0.10
Y	2	3	1214	2	6	9	9308	9	9707	1	2164	7	1	2	5917	608	592
	277			0.78	0.45	0.84		0.34		0.13		0.03	0.04	0.09		0.10	0.01
A	35.3	1.33	0.81	582	963	736	0.71	151	0.82	570	0.00	231	351	388	0.10	303	598
Y	5	11	2439	2	8	3	477	1	1024	7	4947	2	6	4	713	9	6
	428	0.81		1.25		0.90		0.15				0.00	0.13	0.29		0.01	0.06
A	75.1	987	0.87	341	0.76	069	0.70	315	0.99	0.00	0.09	198	806	058	0.05	042	346
Y	2	2	75	4	123	6	2802	2	4443	355	4675	3	9	1	3996	6	6
	450	0.68		0.83	0.25	0.82				0.07		0.19	0.07	0.18		#VA	
A	21.3	379	0.63	902	566	812	0.78	#VA	0.76	281	0.05	565	892	412	0.18	LUE	0.10
Y	9	7	2249	6	8	2	6395	LUE!	563	3	0599	5	4	4	6131	!	207
		0.88		1.40	1.69	0.96		0.52		0.34		0.18		0.11			0.03
A	472	692	0.83	250	523	826	0.89	630	1.35	551	0.20	368	0.22	402	0.03	0.22	154
Y	42.3	4	5226	3	8	7	81	9	5468	8	588	3	55	2	0757	453	2
	325.	0.78		0.44	0.40	0.51				0.02		0.26	0.40	0.40		#VA	0.50
S	865	881	0.74	610	133	510	0.36	#VA	0.79	122	0.25	726	770	217	0.38	LUE	100
Y	8	5	2268	8	4	5	5983	LUE!	2656	4	9523	4	2	4	4332	!	9
	620	3.81		0.50	1.02	1.65				3.31		0.45	0.68	0.93		#VA	0.41
S	8.87	364	1.72	023	732	146	1.38	#VA	0.73	961	1.15	951	908	242	0.59	LUE	014
Y	4	6	8421	1	8	8	3743	LUE!	8236	6	7072	9	4	4	4187	!	8
	105	1.41			1.20	0.79				0.35		0.43	0.50	0.51		#VA	0.48
S	08.3	640	2.52	0.50	195	117	0.53	#VA	0.85	876	1.16	944	337	607	0.54	LUE	477
Y	6	6	6894	627	5	7	1302	LUE!	777	4	5407	8	5	4	8423	!	1
		0.73		0.54	0.88	0.81		0.12		0.26		0.21	0.10	0.17		0.10	0.07
S	131	005	1.14	911	572	190	0.31	576	0.72	501	0.33	268	203	185	0.22	244	899
Y	60.2	7	6849	1	7	3	8508	2	3313	5	4326	4	1	6	0905	5	4
	232	1.35		0.89	0.09	0.52				0.05		0.71	0.11	0.38		#VA	0.29
S	69.9	664	0.58	547	845	923	0.57	#VA	0.44	963	0.30	689	261	782	0.64	LUE	949
Y	9	6	2446	7	3	1	7127	LUE!	9876	7	3953	7	3	7	293	!	5
	253	1.41		0.47	0.42	0.58				0.23		0.38	0.53	0.27		#VA	0.33
S	75.8	581	0.68	567	753	316	0.49	#VA	0.60	832	0.25	062	648	408	0.53	LUE	796
Y	4	7	6574	9	4	3	9854	LUE!	7761	2	8746	7	2	6	6319	!	8
	275	1.28		0.86	0.63	0.74		0.34		0.28		0.10	0.35	0.08		0.30	0.00
S	93.8	129	0.91	946	589	010	1.27	218	0.76	536	0.04	620	205	421	0.64	150	216
Y	6	3	6869	2	7	4	6134	9	142	9	7386	2	1	4	4337	1	3
	424	0.68		0.82	0.40	0.89				0.05		0.17	0.23	0.01		#VA	0.28
S	59.0	684	0.64	505	743	324	0.59	#VA	0.77	062	0.02	091	282	218	0.07	LUE	663
Y	6	1	3586	9	1	9	0736	LUE!	8018	4	1389	9	6	6	073	!	2

`

	445	0.67		0.64	0.25					0.09		0.19	0.09	0.09		#VA	0.14
S	78.7	295	0.58	619	968	0.84	0.69	#VA	0.70	643	0.00	482	043	658	0.21	LUE	689
Y	1	6	6027	1	4	493	6537	LUE!	2742	1	7015	5	1	7	4879	!	8
		0.83		0.98	0.93	0.94		0.28		0.04		0.12	0.05			0.03	0.01
S	467	906	0.69	635	775	745	0.77	874	1.21	275	0.06	222	427	0.02	0.16	456	288
Y	99	4	1755	6	1	6	9681	5	5977	6	3956	4	2	136	8006	1	6

`

`

Experiment 4A: PFAS loading on polymer

Type	Sample	mg Polymer		PFBA	PFBS	PFHpA	PFHxS	62FTS	PFOA	PFNA	PFOS	PFBA_std	PFBS_std	PFHpA_std	PFHxS_std	62FTS_std	PFOA_std	PFNA_std	PFOS_std
Sand	cP AN I	0.0 428	0.00 3	0. 1 2	0. 2 5	0.2 5	0. 37	0. 33	0. 20	0. 28	0. 6	0.00	0.00	0.02	0.00	0.01	0.02	0.00	0.01
Sand	PA NI	0.0 427 5	0.00 035 4	0. 0 8	0. 2 5	0.2 8	0. 38	0. 39	0. 23	0. 30	0. 4 1	0.03	0.15	0.13	0.15	0.16	0.14	0.11	0.20
Sand	CA C	0.0 419	0.00 8	0. 0 9	0. 0 2	0.1 0	0. 04	0. 13	0. 02	0. 07	0. 1	0.01	0.00	0.00	0.00	0.00	0.00	0.00	0.01
AlOH3 Sand	cP AN I	0.0 423	0.00 028 3	0. 1 1	0. 2 1	0.2 1	0. 30	0. 30	0. 16	0. 24	0. 2 9	0.01	0.08	0.03	0.06	0.02	0.05	0.06	0.06
AlOH3 Sand	PA NI	0.0 424	0.00 014 1	0. 0 9	0. 1 4	0.1 9	0. 26	0. 28	0. 12	0. 20	0. 3 0	0.02	0.05	0.04	0.10	0.06	0.05	0.06	0.06
AlOH3 Sand	CA C	0.0 425	6.88 E-05	0. 1 2	0. 0 2	0.0 9	0. 04	0. 12	0. 02	0. 08	0. 2	0.04	0.00	0.00	0.00	0.01	0.01	0.01	0.01

Experiment 4A: PFAS loading on polymer with calculated CAC loss

Type	Sample	mg Polymer		PFBA	PFBS	PFHpA	PFHxS	62FTS	PFOA	PFNA	PFOS	PFBA_std	PFBS_std	PFHpA_std	PFHxS_std	62FTS_std	PFOA_std	PFNA_std	PFOS_std
Sand	cP AN I	0.0 428	0.00 3	0. 1 2	0. 2 5	0.2 5	0. 37	0. 33	0. 20	0. 28	0. 6	0.00	0.00	0.02	0.00	0.01	0.02	0.00	0.01
Sand	PA NI	0.0 427 5	0.00 035 4	0. 0 8	0. 2 5	0.2 8	0. 38	0. 39	0. 23	0. 30	0. 4 1	0.03	0.15	0.13	0.15	0.16	0.14	0.11	0.20
Sand	CA C	0.0 276	0.00 023 6	0. 1 3	0. 0 2	0.1 4	0. 07	0. 19	0. 03	0. 10	0. 2	0.01	0.00	0.00	0.00	0.00	0.00	0.00	0.01
AlOH3 Sand	cP AN I	0.0 423	0.00 028 3	0. 1 1	0. 2 1	0.2 1	0. 30	0. 30	0. 16	0. 24	0. 2 9	0.01	0.08	0.03	0.06	0.02	0.05	0.06	0.06
AlOH3 Sand	PA NI	0.0 424	0.00 014 1	0. 0 9	0. 1 4	0.1 9	0. 26	0. 28	0. 12	0. 20	0. 3 0	0.02	0.05	0.04	0.10	0.06	0.05	0.06	0.06
AlOH3 Sand	CA C	0.0 224	5.89 E-05	0. 2 3	0. 0 3	0.1 8	0. 08	0. 22	0. 04	0. 15	0. 3	0.07	0.00	0.00	0.01	0.02	0.02	0.02	0.01

`

`

Experiment 4B: CC_o^{-1} PFAS breakthrough: Labels are the same as Experiment 4A

Col	PV_avg	PFBA_Cco	PFHpA_Cco	PFOA_Cco	PFNA_Cco	PFBS_Cco	PFHxS_Cco	PFOS_Cco	62FTS_Cco	PFBA_std	PFBS_std	PFHpA_std	PFHxS_std	62FTS_std	PFOA_std	PFNA_std	PFOS_std
	258	0.89		1.01	0.66	0.89		0.66	1.2	0.06	0.0		0.00	0.13	0.00	0.02	0.22
A	3.7	456	0.96	893	917	024	1.05	358	870	130	116	0.02	330	270	038	662	513
C	66	4	8902	8	1	6	2288	9	22	5	22	4813	8	3	6	5	9
	485			0.80	0.28	1.03		0.03	0.7	0.05	0.0		0.09		0.02	0.03	0.03
A	7.1	1.00	0.98	027	639	231	0.85	994	442	869	037	0.03	059	0.01	873	597	206
C	43	114	7022	3	7	3	996	8	13	6	75	4211	8	645	2	2	3
	709	1.08		1.11	0.97	0.99		1.01	1.3	0.01	0.0		0.06	0.05		0.16	0.06
A	3.5	423	1.03	077	867	889	1.10	966	166	447	682	0.02	015	694	0.10	270	457
C	06	5	7701	5	9	5	7959	5	47	9	55	0949	6	5	963	3	6
	915	0.85		1.00	2.09			3.59	1.1	0.04	0.3		0.07	0.07	0.02	0.24	0.30
A	7.7	271	1.01	532	383	1.10	1.22	085	916	473	397	0.01	352	177	530	278	944
C	65	1	7585	4	1	387	5023	2	54	8	77	4901	7	2	5	6	3
	114	1.14		1.48	2.38	1.10		2.92	1.2	0.28	0.1			0.03	0.00	0.15	
A	15.	056	1.22	995	624	245	1.23	706	439	053	299	0.16	0.10	732	909	230	0.38
C	56	8	8318	5	9	5	403	6	7	4	95	6439	813	8	2	4	658
	136	0.89		1.36	1.45	1.12		1.39	1.2	0.03	0.0		0.03	0.07	0.05	0.19	0.41
A	59.	510	1.16	112	089	980	1.24	452	076	676	064	0.02	835	221	927	571	185
C	88	3	6035	4	9	6	4053	7	91	7	27	3181	4	9	7	5	3
	159	1.10		0.93	0.74	1.07		0.34	1.2	0.05	0.0		0.10	0.16	0.02		0.21
A	05.	892	1.03	911	758	374	0.83	951	309	111	470	0.05	825	948	308	0.08	078
C	98	9	6665	5	1	2	4324	5	11	1	25	5396	5	5	2	987	5
	220	0.83		1.30	1.37	1.07		1.33	1.1	0.03	0.1		0.05	0.14	0.10	0.34	0.52
A	04.	051	1.11	665	750	990	1.21	606	010	666	325	0.03	338	632	032	211	404
C	87	9	6126	6	5	1	2402	5	42	3	06	1369	2	4	7	1	5
	269	1.47		1.07		0.97		0.43	1.3	0.01	0.0		0.02		0.06	0.10	0.10
A	49.	135	0.98	996	1.51	496	1.14	023	931	590	561	0.03	887	0.09	665	099	125
C	92	1	5434	4	29	6	2515	9	16	7	41	6393	3	789	3	7	3
	380	1.07		0.74	0.33	0.94		0.03	0.7	0.01	0.0		0.19	0.14	0.10	0.13	0.01
S	.84	069	1.02	863	796	599	0.84	511	523	040	532	0.01	104	259	739	490	426
C	42	9	1628	4	5	3	9332	8	76	9	84	2946	4	1	2	1	2
	250			1.10		0.94		0.76	1.3	0.03	0.0		0.04	0.08	0.01	0.05	0.07
S	6.1	0.98	0.97	019	1.12	583	1.14	424	695	756	388	0.08	801	125	577	667	498
C	69	622	9062	8	088	8	8765	1	98	7	07	975	7	2	2	8	3
	480	0.94		0.81	0.41	1.04			0.7	0.02	0.0		0.08	0.01	0.01	0.09	#VA
S	6.8	930	1.00	212	928	418	0.93	#VA	124	348	483	0.07	567	327	604	354	LUE
C	18	5	2371	4	9	3	8076	LUE!	86	5	27	5011	8	7	5	1	!
	704	1.01			0.89	0.93		0.87	1.3	0.00	0.0		0.11	0.05	0.15	0.45	
S	7.0	481	1.07	1.11	006	887	1.17	629	385	187	497	0.08	260	894	016	710	1.00
C	78	5	5025	553	5	9	3041	2	8	4	02	1472	3	1	1	1	086
	931	0.85		1.07	2.17	0.87		3.87	1.2	0.06	0.0		0.04	0.04		0.17	0.87
S	8.9	820	1.06	976	996	714	1.22	395	788	031	225	0.02	034	534	0.05	257	997
C	94	9	2927	4	9	3	0177	8	4	6	02	652	1	9	179	9	3
	115	0.48		1.59	2.53			3.90	1.4		0.0		0.14	0.36	0.16	0.06	
S	78.	779	2.13	905	163	1.09	1.14	595	394	0.68	478	1.34	140	539	333	124	0.12
C	73	7	7865	2	8	666	686	1	09	985	26	905	6	7	4	4	456
	138	1.10		1.50		1.09		3.57	1.2	0.18	0.0		0.05	0.05	0.10		2.27
S	34.	519	1.18	455	2.56	299	1.25	862	731	496	515	0.05	417	068	832	0.97	788
C	58	5	1947	4	532	5	7568	7	11	6	93	17	7	5	2	696	2
	160	1.08		0.99				1.23	1.3	0.01	0.0		0.06	0.07	0.05	0.31	0.79
S	86.	092	1.03	615	1.26	1.02	0.90	672	118	070	312	0.04	756	364	256	153	004
C	53	5	4692	7	69	261	5048	8	85	3	45	5322	7	4	3	9	4
	222	0.94		1.25	1.32	1.03		1.61	1.1	0.11	0.0		0.03	0.04	0.05	0.13	0.14
S	65.	797	1.08	243	259	145	1.20	764	201	917	407	0.05	598	240	604	941	177
C	04	9	4309	1	2	2	2414	9	49	6	74	0476	8	1	3	4	1

`

	273	1.61		1.03	1.52	0.96		0.49	1.5	0.41	0.0		0.08	0.17	0.02		0.11
S	12.	384	0.98	052	774	905	1.11	018	180	016	607	0.00	528	045	206	0.35	355
C	64	6	254	5	8	4	8363	2	14	2	71	7028	4	1	2	668	8
	481	0.95		0.36	0.08	0.57			0.4	0.00	0.1		0.15	0.09	0.10	0.06	#VA
A	.33	892	0.64	317	220	638	0.41	#VA	819	184	374	0.11	466	162	538	647	LUE
Y	12	6	7313	4	5	2	7296	LUE!	6	5	53	992	7	7	8	6	!
	269	0.91		0.88	0.59	0.83		0.13	1.1								
A	6.2	135	0.89	794	777	104	0.86	101	065								
Y	66	3	224	2	2	4	37	5	03	0	0	0	0	0	0	0	0
		0.90		0.69	0.32	0.87			0.6	0.01	0.1			0.09	0.02		#VA
A	486	087	0.91	258	673	651	0.65	#VA	823	118	293	0.02	0.15	237	613	0.06	LUE
Y	2.5	6	7412	4	7	8	5506	LUE!	14	9	15	5923	443	3	9	392	!
	707	1.13		1.05	0.85	0.94		0.30	1.2		0.0		0.04	0.09	0.07	0.17	0.05
A	9.3	132	1.12	992	010	235	0.99	296	572	0.08	304	0.10	820	585	738	344	464
Y	83	5	4115	2	1	6	2955	2	54	616	86	0312	7	5	1	9	4
	934	0.39		0.97	1.78	0.84		2.78	1.2	0.55	0.0		0.02	0.08	0.06	0.33	
A	7.4	024	1.24	167	273	848	0.96	502	475	189	767	0.35	773	586	145	069	0.82
Y	03	8	7707	8	3	9	9952	1	66	4	88	2409	6	7	9	2	73
	115	0.86		2.21	1.94	0.98		2.10	1.1	0.02	0.1			0.05	1.24	0.16	0.83
A	87.	469	1.05	179	657	811	1.09	625	696	865	251	0.02	0.13	282	315	811	604
Y	66	7	1427	7	1	5	416	7	79	4	1	0564	003	6	9	5	4
	138	0.94		1.44	2.36	1.03		3.48	1.2	0.01	0.2		0.00	0.02	0.03	0.38	0.75
A	11.	088	1.11	649	551	691	1.22	615	943	812	011	0.02	305	641	003	803	160
Y	69	2	4701	5	5	8	2918	5	04	8	68	9165	2	4	8	1	6
	160	0.97		0.92	0.95	0.91		0.86	1.2	0.01	0.0		0.03	0.00	0.02	0.01	0.07
A	51.	038	1.00	907	634	730	0.77	964	722	182	132	0.08	814	352	118	833	239
Y	95	8	1875	7	6	6	8151	5	55	6	5	4782	7	9	7	9	7
	220	1.10		1.35	2.05	0.98		2.72	1.1	0.00	0.0		0.04	0.14	0.21	0.87	2.34
A	15.	260	2.15	521	036	509	1.02	703	385	889	511	1.23	378	236	266	393	148
Y	5	3	3821	1	9	5	4014	6	99	5	55	5983	6	9	7	6	3
	268	1.39		1.01	1.18	1.00			1.4	0.07	0.1		0.04	0.07	0.08	0.35	#VA
A	30.	911	0.95	352	276	588	1.00	#VA	637	683	072	0.01	135	457	964	242	LUE
Y	09	3	2918	1	4	9	1042	LUE!	19	4	29	6054	8	9	6	5	!
	487	1.09		0.34	0.09				0.4	0.24	0.1		0.11	0.08	0.12	0.04	#VA
S	.82	448	0.65	637	402	0.58	0.29	#VA	410	029	605	0.17	330	619	066	327	LUE
Y	47	8	4915	9	1	104	3106	LUE!	08	2	51	0944	9	5	9	2	!
	274	1.09		0.82	0.70	0.79		0.06	1.0	0.08	0.0		0.10	0.05	0.10	0.05	
S	1.7	920	0.94	710	126	017	0.52	268	565	092	571	0.07	940	020	904	435	0.04
Y	21	7	6519	3	7	2	7127	8	02	6	74	5435	9	8	4	8	764
	498	0.83		0.47	0.23	0.85			0.4	0.02	0.0		0.14	0.03	0.03	0.04	#VA
S	7.8	556	0.81	414	352	692	0.40	#VA	920	580	571	0.03	696	949	468	314	LUE
Y	25	7	8611	6	3	9	1186	LUE!	4	7	52	3416	9	4	6	7	!
	717	1.08		0.90	0.58	0.92			1.2	0.06	0.0		0.32	0.08		0.20	#VA
S	7.4	937	0.98	002	165	964	0.72	#VA	545	879	409	0.04	151	695	0.11	799	LUE
Y	35	4	2678	9	1	9	6505	LUE!	37	4	63	1293	5	8	178	6	!
	938	0.87		0.91	1.51	0.84		1.81	1.2	0.05	0.0		0.30	0.04	0.13		1.35
S	7.0	940	0.96	582	668	055	0.80	800	573	796	518	0.03	640	679	257	0.47	914
Y	67	7	4258	6	1	6	0397	8	29	5	72	9667	1	1	4	697	4
	115	0.99		1.37	1.22	0.93		1.30	0.9	0.25	0.0		0.25	0.27		1.10	1.78
S	78.	892	0.98	827	359	034	0.70	807	878	539	959	0.07	634	226	0.84	111	997
Y	63	7	7833	1	2	5	2209	5	47	9	85	6545	3	1	302	7	2
	137			1.27	1.57	1.00			1.2	0.08	0.0		0.25	0.15	0.05	0.36	0.26
S	66.	0.95	1.08	806	466	549	0.86	0.85	198	360	637	0.00	605	472	580	490	825
Y	45	381	7936	8	4	1	0833	968	79	1	67	7053	9	3	3	3	2
	159	0.97		0.75	0.51	0.73		0.12	0.9	0.03	0.0		0.13	0.13	0.19	0.41	0.13
S	65.	399	0.88	589	659	580	0.53	678	154	047	107	0.08	575	263	576	595	600
Y	8	1	2488	8	5	1	4064	6	71	2	72	5437	2	2	6	3	7
	218	0.94			1.26	0.97			1.0	0.01	0.0		0.06		0.07	0.03	0.52
S	14.	035	1.11	1.23	475	776	0.97	0.81	818	022	455	0.05	379	0.05	976	616	571
Y	39	2	4537	789	5	6	3811	203	54	1	4	8371	6	684	1	7	2

	265	1.42		0.95	1.30	1.25		0.20	1.3	0.11	0.1		0.10	0.17	0.04	0.07	0.06
S	26.	630	0.97	528	457	250	0.89	063	919	457	688	0.00	410	900	796	496	165
Y	38	4	6138	7	6	4	7444	6	97	6	54	2718	9	3	6	8	6
	492	0.94		0.53	0.18	0.68			0.5	0.05	0.2		0.18	0.02	0.10	0.00	#VA
A	.28	220	0.75	285	972	294	0.47	#VA	576	312	205	0.08	037	833	935	141	LUE
P	9	3	9912	9	2	7	7512	LUE!	19	8	05	6168	4	7	7	1	!
	272	1.07		0.91	0.97	0.83		0.32	1.0	0.08	0.0		0.07	0.13	0.05	0.33	0.22
A	8.6	737	0.92	437	325	590	0.66	863	785	928	291	0.06	950	108	977	982	518
P	53	3	8354	1	5	2	515	5	35	8	25	8439	8	6	7	8	9
	491	0.92		0.67	0.27	0.87			0.5	0.11	0.1		0.02			0.08	#VA
A	8.2	644	0.91	119	608	343	0.68	#VA	558	308	097	0.06	405	0.02	0.09	092	LUE
P	63	8	9909	2	4	9	0534	LUE!	07	3	34	3541	4	267	362	1	!
	707	0.96		1.05	0.87	0.81		0.45	1.2	0.01	0.0		0.15	0.01	0.00		0.38
A	0.8	152	0.94	727	432	746	0.86	608	092	716	026	0.02	207	565	032	0.02	881
P	6	5	1952	1	9	9	697	2	09	4	96	9478	1	7	5	416	8
	917	1.15		1.04	1.98	0.77		2.63	1.1	0.31	0.0		0.05	0.00	0.06	0.12	
A	4.4	251	1.04	053	045	248	1.01	573	248	963	856	0.02	126	691	840	952	0.50
P	86	4	2928	2	5	3	2775	7	11	4	24	5177	1	4	9	1	852
	113	0.92		1.12	0.74			0.33	0.8		0.0		0.05	0.00	0.03	0.16	0.10
A	62.	363	1.08	840	993	0.97	0.99	275	331	0.09	114	0.01	033	321	402	915	203
P	15	6	1793	4	3	45	2818	6	95	418	79	7524	7	6	6	2	5
	135			1.42	1.90	0.96		2.17	1.1		0.0		0.02		0.12		1.29
A	13.	0.87	1.10	659	149	537	1.12	169	405	0.00	161	0.05	198	0.09	918	0.75	149
P	77	45	0969	5	1	5	3453	3	06	095	63	9167	7	53	2	696	6
	156	1.00		0.72	0.54	0.78			0.8	0.02	0.1		0.15	0.30	0.29	0.47	#VA
A	68.	008	0.95	857	090	115	0.68	#VA	414	132	533	0.11	113	808	093	661	LUE
P	32	8	1624	3	6	8	2724	LUE!	47	5	51	537	5	3	7	1	!
	214	0.82		1.21	1.18	0.90		0.91	0.9	0.02	0.0		0.11		0.09	0.34	
A	18.	271	1.07	649	859	174	1.02	956	444	582	166	0.01	000	0.06	258	997	0.62
P	78	7	9907	8	9	5	5461	3	24	8	42	8437	9	37	2	1	735
	260	1.48			1.29			0.32	1.2	0.10	0.0		0.06	0.04	0.01	0.02	0.07
A	90.	223	0.96	1.01	457	0.86	0.87	200	990	230	156	0.04	351	192	005	659	695
P	61	2	1898	939	3	022	0993	1	71	6	9	1957	3	9	6	5	7
	493			0.38	0.13	0.41			0.4	0.06	0.1		0.15	0.13	0.19	0.10	#VA
S	.50	0.95	0.63	740	333	734	0.25	#VA	592	944	286	0.22	434	101	000	416	LUE
P	65	646	5425	1	8	1	1115	LUE!	54	5	93	3144	8	1	3	6	!
	271	1.01		1.01	0.77	0.78		0.10	1.0	0.01	0.0		0.04	0.08	0.20		0.03
S	6.2	337	0.93	641	117	324	0.56	453	983	900	513	0.00	891	771	018	0.26	434
P	34	3	6445	9	7	3	7221	6	64	7	39	3348	2	4	6	203	1
	492	0.90			0.27	0.82			0.5	0.16	0.0		0.01	0.00	0.09	0.01	#VA
S	9.2	590	0.96	0.72	963	439	0.62	#VA	897	862	243	0.01	107	831	124	291	LUE
P	21	7	9507	548	2	5	275	LUE!	33	3	99	8976	3	2	4	2	!
	710	1.00			0.67	0.77		0.26	1.1	0.07	0.0				0.03	0.09	0.03
S	1.2	698	0.93	0.94	690	902	0.76	033	257	514	104	0.00	0.03	0.09	676	344	625
P	99	3	7039	049	7	6	2577	9	45	8	81	6126	518	233	6	1	3
	923	0.93			1.67	0.80		1.90	1.1	0.08	0.0		0.06	0.02	0.08	0.35	0.54
S	8.1	285	1.02	0.97	248	065	0.88	057	718	542	570	0.10	059	827	882	689	839
P	22	7	6249	346	7	7	2128	7	04	6	97	9859	8	7	6	3	9
	114	1.06		1.10	0.86	0.94		0.38	0.8	0.08	0.0			0.04	0.22	0.24	0.24
S	16.	646	1.07	974	560	361	0.94	323	960	850	845	0.09	0.26	886	177	219	386
P	04	3	8206	9	7	3	0612	3	77	6	53	4262	722	9	7	7	8
	135	1.01			2.82	0.89		4.53	1.2	0.03	0.0		0.11	0.07	0.06	0.37	0.32
S	17.	583	1.18	1.47	190	678	1.03	327	821	783	364	0.04	090	244	261	812	178
P	18	3	6802	524	1	2	0325	7	82	8	67	0605	9	8	3	9	1
	156	1.06		0.90	0.68	0.87			1.0		0.0		0.01	0.10	0.09	0.20	0.06
S	63.	127	0.97	495	686	381	0.71	0.14	649	0.02	357	0.05	587	756	679	786	752
P	93	4	9319	2	1	1	5707	762	12	477	79	5401	6	4	8	5	2
	214	0.93		1.52	2.58	0.86		3.61	1.2	0.14	0.0		0.08	0.04	0.06	0.11	0.80
S	30.	489	1.14	936	048	771	1.16	262	149	618	022	0.05	869	901	420	785	665
P	17	8	0925	1	1	1	5155	8	64	6	21	2466	9	5	2	1	9

	259	1.52		0.94	1.32	1.04		0.27	1.2	0.01	0.1		0.07	0.06	0.06	0.24	0.16
S	92.	982	0.94	507	864	296	0.87	135	735	553	975	0.00	751	435	214	803	226
P	67	8	2794	6	6	4	4863	5	68	8	5	9301	5	2	5	1	2
	24.	1.01		0.21	0.01	0.82			0.2	0.04	0.0			0.05	0.01		#VA
	107	356	0.74	755	362	256	0.43	#VA	353	876	140	0.02	0.03	005	637	0.00	LUE
A	14	5	5216	2	1	8	5134	LUE!	88	1	5	8259	072	2	8	021	!
	494	1.03		0.78	0.34			0.14	0.6	0.02	0.1		0.03	0.00	0.04	0.10	0.16
	.88	979	1.04	043	923	0.87	0.85	866	741	589	452	0.07	013	470	800	105	213
A	64	4	5705	8	1	234	2143	9	5	4	23	4941	8	2	8	5	3
	273	1.14		0.96	0.99	0.90		0.30	1.1	0.01	0.0		0.12	0.03	0.01	0.30	0.05
	3.1	322	1.00	671	515	767	0.84	676	535	900	180	0.01	188	114	100	416	155
A	98	3	9625	6	7	9	1776	4	54	3	23	9683	6	4	4	2	8
	482	0.98			0.31	0.91			0.5	0.05	0.0		0.05	0.05	0.01	0.02	#VA
	3.4	174	0.94	0.70	935	888	0.82	#VA	890	906	442	0.06	076	273	637	582	LUE
A	58	5	8567	818	3	7	7515	LUE!	65	7	22	2649	6	4	5	1	!
	704	1.02		1.36	2.39	0.81		5.08	1.4	0.00	0.0		0.05		0.04	0.19	1.31
	0.3	929	1.08	391	644	973	1.15	002	164	347	828	0.00	447	0.02	339	115	797
A	41	9	7951	7	5	2	3752	4	55	1	35	8647	9	152	6	2	1
	924	0.82		1.02		0.77			1.1	0.00	0.1		0.00	0.00	0.04	0.02	0.25
	7.4	715	1.07	306	1.93	696	1.04	2.96	284	671	190	0.10	773	712	217	203	749
A	84	3	4068	6	754	7	1137	21	11	7	58	0729	1	8	1	3	4
	114	0.92		1.04	0.74	0.99		0.48	0.8	0.06	0.0		0.02	0.08	0.06	0.13	0.01
	89.	449	1.04	583	565	036	0.89	133	085	541	367	0.03	628	808	954	739	618
A	69	3	4079	5	4	2	2237	8	28	8	85	6766	7	4	6	9	2
	136	0.89		1.55	2.72	0.92		5.87	1.2	0.11	0.0		0.04	0.01	0.05	0.24	0.66
	97.	339	1.15	130	821	099	1.18	923	988	193	890	0.00	897	230	066	248	888
A	97	6	2651	8	4	1	7154	2	39	3	84	5673	5	7	4	1	4
	158	1.08		0.98	0.70	0.91		0.31	1.0		0.0		0.12	0.17	0.16	0.02	0.04
	73.	241	1.04	239	907	730	0.95	689	802	0.02	578	0.05	416	630	239	970	001
A	94	4	2782	8	8	2	9541	6	73	144	12	7213	9	4	1	6	3
	217	0.91		1.39					1.1	0.05	0.0		0.04	0.01	0.11	0.93	2.72
	24.	972	1.12	853	2.11	0.95	1.12	3.36	568	857	598	0.04	086	626	929	950	810
A	08	1	305	8	367	299	2176	521	24	9	35	319	8	1	9	3	9
	264			0.99	1.20	1.17			1.2		0.0		0.01	0.02	0.04		0.18
	37.	1.50	0.97	999	129	909	1.10	0.52	713	0.01	299	0.03	541	459	358	0.09	304
A	91	248	6147	2	7	6	1469	687	31	506	34	1286	5	8	2	313	3
	24.	1.28		0.88	0.45	1.00			0.8	0.02	0.1		0.00	0.01	0.02	0.09	#VA
	350	420	1.08	812	237	230	0.89	#VA	080	438	282	0.04	107	756	485	257	LUE
S	65	7	2549	3	5	8	3962	LUE!	23	5	35	6254	9	9	6	4	!
	448	1.30		0.99	0.72	0.88		0.42	0.8	0.38	0.0		0.03	0.22	0.24	0.47	0.51
	.05	025	1.09	880	240	029	0.94	645	513	081	885	0.12	204	259	597	448	739
S	19	7	31	3	8	6	8536	9	92	9	64	9524	5	7	7	3	9
	265	1.25		1.00	1.00	1.04		0.58	1.0								
	4.2	680	1.12	945	831	527	0.83	204	879								
S	21	4	6103	6	8	7	8331	3	31	0	0	0	0	0	0	0	0
	487	0.86		0.64	0.27	0.92			0.5								
	1.1	650	0.92	694	804	440	0.76	#VA	667								
S	04	8	0565	7	7	5	6927	LUE!	06	0	0	0	0	0	0	0	0
	703			0.34	0.14	0.31			1.0								
	3.4	0.97	0.61	104	180	924	0.03	#VA	244								
S	42	983	9675	3	6	7	2324	LUE!	89	0	0	0	0	0	0	0	0
	921	2.45		1.04	1.99	0.93		2.76	1.1								
	5.2	690	1.32	819	215	486	1.26	562	967								
S	6	7	461	1	4	6	8962	3	41	0	0	0	0	0	0	0	0
	114	0.85		1.11	0.84			0.51	0.9								
	12.	950	1.07	312	016	0.90	1.02	708	054								
S	66	7	5546	7	3	992	4316	8	66	0	0	0	0	0	0	0	0
	135	1.15		1.61	3.50	1.00		6.77	1.2								
	64.	211	1.32	522	798	239	1.23	685	236								
S	94	8	0152	4	3	7	3397	9	71	0	0	0	0	0	0	0	0

`

	157	1.00		1.01	0.78	0.94		0.11	1.0									
	03.	034	0.96	871	373	121	0.92	658	337									
S	9	7	6128	2	4	2	973	8	7	0	0	0	0	0	0	0	0	
	213	1.11			2.54	0.88		5.44	1.3									
	06.	137	1.16	1.52	554	509	1.12	300	217									
S	01	5	4223	968	4	9	0041	5	84	0	0	0	0	0	0	0	0	
	258	1.59		1.08	1.39	1.16		0.79	1.3									
	03.	934	0.91	115	887	741	1.20	120	698									
S	79	7	4753	8	6	1	0605	7	53	0	0	0	0	0	0	0	0	

Experiment 4B: PFAS loading on polymer

Type	Sample	mg	Polymer	PFBA	PFHpA	PFOA	PFNA	PFBS	PFHxS	PFOS	62FTS	PFBA_std	PFHpA_std	PFOA_std	PFNA_std	PFBS_std	PFHxS_std	PFOS_std	62FTS_std
	cPA	0.04	0.00	0.	0.2	0.	0.	0.	1.2	2.	0.3								
Sand	NI	28	0283	20	2	32	55	30	3	28	0	0.03	0.04	0.08	0.10	0.05	0.20	0.22	0.10
	PA	0.04	0.00	0.	0.1	0.	0.	0.	0.5	0.	0.2								
Sand	NI	275	0354	19	2	17	40	20	9	87	2	0.02	0.04	0.07	0.18	0.09	0.14	0.50	0.07
		0.04	0.00	0.	0.1	0.	0.	0.	0.2	0.	0.0								
Sand	CAC	19	0158	26	1	01	09	06	7	03	9	0.02	0.02	0.00	0.02	0.01	0.04	0.01	0.01
AlOH3	cPA	0.04	0.00	0.	0.2	0.	0.	0.	1.0	1.	0.4								
Sand	NI	23	0283	46	8	41	85	28	1	50	6	0.08	0.05	0.10	0.20	0.07	0.18	0.41	0.07
AlOH3	PA	0.04	0.00	0.	0.6	0.	1.	0.	1.6	3.	0.6								
Sand	NI	24	0141	43	5	63	25	34	6	30	0	0.01	0.49	0.32	0.75	0.08	0.88	2.33	0.14
AlOH3		0.04	6.88	0.	0.0	0.	0.	0.	0.3	0.	0.1								
Sand	CAC	25	E-05	29	5	03	15	07	0	13	2	0.02	0.00	0.02	0.03	0.02	0.00	0.03	0.04
AlOH3	AlO			0.	0.0	0.	0.	0.	0.0	0.	0.0								
Sand	H3			00	0	00	00	00	0	00	0	0.00	0.00	0.00	0.00	0.00	0.00	0.00	0.00
	Sand			0.	0.0	0.	0.	0.	0.0	0.	0.0								
Sand				00	0	00	00	00	0	00	0	0.00	0.00	0.00	0.00	0.00	0.00	0.00	0.00

Experiment 5: CC_o^{-1} PFAS breakthrough

Col	Oper_d	PV_esti	PFBA_Cco	PFBS_Cco	PFHpA_Cco	PFHxS_Cco	62FTS_Cco	PFOA_Cco	PFNA_Cco	PFOS_Cco	PFBA_std	PFBS_std	PFHpA_std	PFHxS_std	62FTS_std	PFOA_std	PFNA_std	PFOS_std
		65.	0.3	0.0	0.68	0.03	0.10	0.07	1.29	0.0	#DI	0.0	0.10	0.01	0.07	0.0	0.9	0.0
	0.0	454	471	775	221	053	560	272	003	087	V/0	179	649	547	311	459	102	071
AZ	3	55	82	2	6	4	6	7	8	56	!	92	4	7	7	53	33	13
		829	0.9	0.8	1.18	0.68	1.00	1.00	0.95	0.5	0.1	0.0	0.23	0.08	0.01	0.0	0.0	0.3
	0.3	.09	312	549	831	360	840	077	192	310	369	047	940	531	091	887	524	610
AZ	8	09	62	55	1	4	3	9	2	64	23	57	1	5	2	57	48	55
		172	1.0	0.9	0.99	0.77	0.95	0.97	1.93	0.5	0.0	0.0	0.03	0.10	0.02	0.0	0.0	0.4
	0.7	3.6	024	002	654	037	932	664	900	219	677	897	614	900	111	305	200	252
AZ	9	36	11	6	6	4	5	7	3	88	69	51	2	5	1	97	97	65
		281	1.2	0.9		0.78	1.04	1.33	1.19	0.7	0.4	0.1	0.09		0.16	0.2	1.0	0.4
	1.2	4.5	108	856	0.96	464	562	093	869	795	760	903	706	0.16	747	130	024	444
AZ	9	45	23	72	57	2	4	9	5	31	67	8	7	317	2	61	2	17
		390	1.1	1.0	1.07	0.97	1.08	0.49	4.21	0.6	0.0	0.0	0.02	0.06	0.03	0.7	2.6	0.2
	1.7	5.4	515	587	567	581	597	918	373	255	587	813	397	625	547	034	314	855
AZ	9	55	57	6	9	7	8	2	7	53	47	02	2	1	3	58	43	18
		608	1.2	1.0	1.03		0.96	0.98	1.16	0.8	0.1	0.1	0.00	0.02	0.04	0.0	0.5	0.0
	2.7	7.2	039	218	166	0.90	758	797	073	124	008	711	321	807	542	111	432	108
AZ	9	73	3	16	8	592	4	7	3	19	67	82	1	7	3	92	83	8
		826	0.9	1.0	1.00	1.00	0.96	0.99	1.20	0.9	0.0	0.0	0.01		0.07	0.0	0.1	0.1
	3.7	9.0	808	484	621	214	204	107	433	971	026	716	033	0.09	176	146	881	707
AZ	9	91	62	94	5	3	2	9	4	99	54	88	4	951	5	43	22	07

`

Han		65.	0.1	0.0	0.34		0.02	0.01	11.4	0.0	0.0	0.0	0.23	0.00	0.03	0.0	13.	0.0
gar	0.0	454	725	183	705	0.01	392	661	861	146	859	228	595	531	306	205	909	202
_B	3	55	63	35	5	749	7	1	1	62	91	11	5	1	2	78	21	72
Han		829	1.0	0.6	0.82	0.44	0.81	0.61	0.55	0.0	0.0	0.1		0.02	0.00	0.0	0.0	0.0
gar	0.3	.09	348	955	670	284	846	952	322	675	320	051	0.09	247	602	687	235	193
_B	8	09	43	13	7	2	1	8	4	25	99	4	834	2	8	58	91	76
Han		172	1.0	0.9	0.99	1.01	1.12	1.03	1.09	1.1	0.0	0.0	0.01	0.02	0.07	0.0	0.1	0.0
gar	0.7	3.6	751	531	466	870	692	423	264	159	094	345	108	558	010	168	078	556
_B	9	36	74	01	1	3	2	9	6	47	5	37	2	4	5	86	84	83
Han		281	1.1	1.0	1.13	1.00	1.02	1.05	0.76	0.3	0.1	0.0	0.05	0.06	0.05	0.0	0.0	0.0
gar	1.2	4.5	090	072	697	663	020	596	788	197	383	752	945	035	642	147	864	100
_B	9	45	32	81	8	1	9	3	5	81	59	45	7	5	2	85	93	73
Han		390	1.1	0.9	1.09	1.06		1.09	1.67	2.3	0.0	0.0	0.01	0.08	0.04	0.0	0.0	0.1
gar	1.7	5.4	617	966	004	651	1.09	756	638	452	902	149	719	834	226	072	957	257
_B	9	55	62	45	2	1	347	5	2	08	57	66	7	7	7	2	69	77
Han		608	1.1	0.9	0.96	0.97	0.95	1.00	1.31	1.2	0.1	0.0	0.07	0.12	0.06	0.0	0.1	0.0
gar	2.7	7.2	265	103	648	082	657	359	589	300	578	270	212	621	395	973	091	951
_B	9	73	99	2	4	4	3	5	7	6	92	33	8	1	5	36	69	89
Han		826	1.1	0.9	1.05	1.03		0.94		0.8	0.0	0.0	0.01	0.05	0.04	0.0	0.0	0.1
gar	3.7	9.0	008	119	031	706	0.98	989	1.02	019	095	437	250	236	430	061	876	563
_B	9	91	41	3	5	4	34	5	796	71	17	28	7	4	8	66	42	73
		65.	0.5	0.1	0.69	0.11	0.18	0.11		0.0	#DI	0.2	0.18		0.13	0.1	0.7	0.0
Site	0.0	454	456	825	699	595	881	677	1.24	414	V/0	018	858	0.15	351	511	912	195
_5	3	55	15	65	1	2	4	9	608	63	!	86	2	559	1	72	26	46
		829	1.1	0.8	0.90	0.46	0.71	0.43	0.77	0.0	0.0	0.0	0.04		0.01	0.0	0.2	0.0
Site	0.3	.09	241	663	642	776	229	066	125	087	971	866	800	0.07	739	475	811	054
_5	8	09	32	58	2	8	5	5	1	64	43	82	8	908	3	16	13	88
		172	1.3	1.0	1.04	0.83	1.16	1.09	1.83	5.9	0.0	0.0		0.00	0.25	0.0	0.5	8.0
Site	0.7	3.6	551	749	839	575	492	191	675	585	343	832	0.01	349	139	082	167	924
_5	9	36	79	96	2	1	2	6	2	41	96	01	08	5	6	91	32	24
		281	0.6	0.9	0.89	0.55	0.52	0.67	0.54	0.0	0.0	0.0	0.04	0.04	0.05	0.0	0.0	0.0
Site	1.2	4.5	766	629	458	807	675	010	740	379	761	090	281	235	036	102	409	453
_5	9	45	03	31	5	8	5	4	4	74	44	82	6	3	9	12	86	67
		390	0.9	0.9	0.87	0.81	1.19	1.00	0.84	0.5	0.1	0.0	0.00	0.02		0.0	0.0	0.4
Site	1.7	5.4	496	567	626	991	950	736	348	728	518	920	425	204	0.36	009	675	326
_5	9	55	01	73	8	9	5	7	1	65	76	88	5	3	495	18	44	58
		608	1.4	1.0	0.92	0.81	0.94	0.92	1.47	0.7	0.2	0.0	0.05	0.01	0.13	0.0	0.0	0.0
Site	2.7	7.2	168	707	644	271	230	607	337	099	211	623	270	239	342	312	974	129
_5	9	73	01	33	2	7	4	6	9	46	54	37	5	9	4	44	59	61
		826	1.3	0.7	0.95	1.04	1.49	0.98	1.55	1.2	0.2	0.0	0.01	0.07	0.98	0.0	0.5	0.0
	3.7	9.0	767	426	507	995	060	089	882	887	668	707	020	586	842	804	741	849
	9	91	86	93	1	7	9	5	4	96	54	83	8	2	2	44	26	48

col	dup	PV_Avg	PV_Std	PFBA_Cco	std_PFBA	PFHpA_Cco	std_PFHpA	PFOA_Cco	std_PFO
pH 4	1	7.696743	**0.210924**	0.561218	0.09416	0.034979	0.011315	0.00115549	0.0002
pH 4	1	393.3951	**12.79732**	0.883148	0.148314	0.034565	0.011181	0.000993646	0.000
pH 4	1	725.201	**17.2671**	1.009046	0.169337	0.037387	0.012096	0.001438403	0.0002
pH 4	1	1118.295	**35.36771**	1.137704	0.190897	0.037361	0.012092	0.001382573	0.000
pH 4	1	1513.285	**68.04315**	1.103031	0.185145	0.026688	0.008634	0.001786555	0.0003
pH 4	1	1880.217	**86.47978**	1.211972	0.203435	0.027528	0.008906	0.000909587	0.0001
pH 4	1	2694.539	**156.5303**	1.06786	0.179594	0.028758	0.009316	0.025842948	0.0055
pH 4	1	4033.169	**313.0944**	1.000456	0.167856	0.026725	0.008781	0.002129133	0.0003
pH 4	1	4972.323	**467.1228**	1.03499	0.173682	0.027632	0.009284	0.002824112	0.0005

`

pH 4	1	6300.006	**434.9106**	1.030444	0.174293	0.034638	0.011215	0.009237017	0.0016
pH 4	1	6789.887	**659.7989**	0.160606	0.118014	0.0064	0.003999		
pH 4	1	6956.591	**694.8286**	0.389795	0.285635	0.006501	0.004202	0.000356912	0.0002
pH 4	1	7133.662	**732.1336**	0.629104	0.464993	0.009116	0.006114	0.001409975	0.0012

`